Investigation of high nighttime CO_2-fluxes at the Wetzstein spruce forest site in Thuringia, Germany

Marcelo Zeri

Supervisor: Prof. Dr. Thomas Foken

Jena, October 2007

To my wife Gisleine,
for her love and support.

However much you knock at nature's door, she will never answer you in comprehensible words.
(Ivan Turgenev)

Scientists were rated as great heretics by the church, but they were truly religious men because of their faith in the orderliness of the universe.
(Albert Einstein)

Acknowledgments

I thank **Prof. Dr. Ernst-Detlef** Schulze for giving me the opportunity to work at the Max Planck Institute for Biogeochemitry, in Jena.
I am also grateful to **Prof. Dr. Thomas Foken**, from the Univeristy of Bayreuth, for accepting being my supervisor and for the critical but constructive comments.
I thank specially **Dr. Corinna Rebmann** for the constant support, the confidence in my work, and the helpful discussions about micrometeorology.
I am grateful to **Dr. Werner Kutsch** who always encouraged my progress and also taught me about soil science.
I thank **Dr. Peter Anthoni** for inviting me for a visit at the institute in 2003.

Many thanks to my colleagues at the Max Planck Institute for Biogeochemistry:
Olaf Kolle, **Martin Hertel**, **Karl Kübler**, **Waldemar Ziegler**, and all the field operations staff for the support in the field and for the help dealing with the data.
Fernando Moyano for the recent data about the soil respiration at the Wetzstein site.
Martina Mund for the biomass inventory data.
Annett Börner for her assistance with digital elevation maps.
Kerstin Lohse, **Birgitta Wiehl**, and **Yvonne Hofmann** for the logistic support.
Many thanks go to the people from the **workshop**, the **computer department**, the **library** and the **administration**.

Many thanks to the people who helped me from the University of Bayreuth:
Dr. Christoph Thomas, **Silke Oldenburg**, **Matthias Mauder**, and **Tiina Markkanen**.
I thank **Dr. Stephen Belcher**, from the University of Reading, UK, for providing the code for the modeling of the flow over the hill.
I also thank **Armin Mathes** and **Prof. Dr. Andreas Hense**, from the Univesity of Bonn, for giving me the opportunity to join the COPS Summer School, at the Black Forest, in 2007.

I would like to thank **Youmin Chen**, **Maarten Braakhekke**, **Helena Popa**, and specially **Ulrike Nordkaemper** for helping me learn a little bit of German every week.
I thank my friend José Francisco de Oliveira Júnior, for the valuable comments about the thesis.
I thank my mother **Rachel**, in memoriam, my father **Célio**, my brother **Marco Aurélio**, and my sisters **Ana Carolina** and **Débora Regina** for their love and trust in me throughout my life.

In particular I thank my wife **Gisleine** for her endless love, partnership, and patience during the last years.

Contents

Chapter 1

Introduction

The average increase in Earth's temperature has been caused by the heat being trapped by the so-called greenhouse gases (GHGs) like carbon dioxide and methane (IPCC, 2001). According to recent modeling and observational studies, the anthropogenic emissions of GHGs will lead to an increase of several degrees in the global average temperature in the next decades (Solomon et al., 2007).

In order to have precise annual balances of GHGs one requires to know the strength of natural sources and sinks (oceans, soil, and vegetation) as well as the anthropogenic emissions. The scope of this work is to understand the exchanges of carbon dioxide between the vegetation and the atmosphere in a spruce forest ecosystem (the Wetzstein site), located in Thuringia, Germany. The relevance of the current study relies on the facts that (1) forests account for 30 % of the land use in Thuringia, and that (2) European temperate forests in the same range of latitude are known to be carbon sinks (Ciais et al., 1995; Schulze et al., 2000); however, the Wetzstein site was found to be almost carbon neutral, according to Anthoni et al. (2004). The aim of this work is to investigate the causes of this apparent contradiction.

The specific objective of this work is to clarify whether this contradiction is a result of special properties of the eddy-covariance technique that was used at the Wetzstein site. In particular, the apparent ecosystem respiration is unusually high when compared to similar spruce stands of similar age, leading to annual sums of CO_2 that are not compatible with the biomass inventory (Anthoni et al., 2004). This is a rare situation when compared to the commonly observed underestimation of nighttime measurements, due to factors as lack of turbulence during calm nights and drainage of cold air below the canopy, in sloping terrains (Massman and Lee, 2002; Froelich

and Schmid, 2006). Therefore, the hypothesis developed was that the high apparent respiration results from the position of the tower at the crest of the hill and from medium-scale fluxes that occur in this hilly landscape.

The Wetzstein site is an example for the set up of micrometeorological measurements in so-called "difficult conditions", namely sites where the fundamental assumptions (stationarity and horizontal homogeneity of the flow) of the widely used eddy covariance (EC) technique are not met (Kaimal and Finnigan, 1994). Measurements in non-flat terrains, at sites with inhomogeneous forest cover or under the influence of mesoscale motions are examples of situations when the validity of the standard technique is questioned (Mahrt, 1998). However, since there is a need for annual balances of CO_2 and other greenhouse gases in these ecosystems, it is highly necessary to clarify how the EC-technique works under difficult conditions.

The inspection of data measured at the Wetzstein site can lead to the validation of analytical and numerical flow models that support the existence of horizontal and vertical transport of energy and scalars across the ridge (Kaimal and Finnigan, 1994; Finnigan and Belcher, 2004). According to these models, small hills are subjected to perturbations in the local pressure field that generate horizontal and vertical fluxes of energy and scalars, usually not accounted for by the standard eddy covariance technique (Katul et al., 2006).

The hypotheses proposed to explain the high nighttime fluxes of CO_2 at the Wetzstein site are the following:

- The measurements at the main tower are influenced by the flow passing over the hill, as proposed by Finnigan and Belcher (2004);
- Vortices with time scales on the order of several minutes are associated with the unusually high nighttime CO_2-fluxes;
- Typical micrometeorological conditions associated with high nocturnal fluxes of CO_2 can be used in the gap-filling procedures. As a result, a higher uptake of carbon dioxide should be observed if annual sums of CO_2-flux are calculated.

This thesis is organized in seven chapters, starting by the current introduction. The description of the site and the data used, the weather conditions during the period analyzed, and the methods applied are shown next, in Chapter 2. The influence of the flow passing over the hill on the wind field below the canopy is presented in Chapter 3.

The high frequency data of vertical velocity and CO_2 concentration were inspected in Chapter 4, in order to check for the time scales associated with the high nighttime fluxes of CO_2. The relation between the high nocturnal fluxes of CO_2 and some micrometeorological characteristics as the energy balance and the footprint analysis was analyzed in Chapter 5.

Finally, the main question of this thesis is discussed in Section 5.5, where the situations associated with high nocturnal fluxes of CO_2 are identified and applied in the methodology of calculations of annual sums. The conclusions and main findings of this work are discussed in Chapter 6.

Chapter 2

Experimental Data and Methodology

2.1 Site and Data

The Wetzstein site (50° 27′ N, 11° 27′ E) is located on a plateau, at 785 m above sea level, near the village of Lehesten, Germany. The site is a managed spruce forest with species age around 50 years. Tree species and age classes for the area surrounding the flux tower (red circle) are shown in Figure 2.1. Eddy covariance measurements of energy and scalar fluxes have been performed at the site since 2002 and first results were reported by Anthoni et al. (2004).

The long term temperature and precipitation records for the region surrounding were plotted in Figure 2.2 (measurements averaged monthly from 1961 to 1990). These data were collected by the weather station closest to the Wetzstein site (DWD, 2007), at Teuschnitz-Wickendorf, Bavaria (50° 22′ N, 11° 22′ E, at 568 m above sea level and approximately 7 km distant from the Wetzstein site). The average annual sum of precipitation is 990.5 mm, and it is well distributed during the year.

The average annual temperature over the whole period was 6.2 °C and the highest values ($\approx$ 15 °C) usually occur in July. It should be noted that the actual climatological mean air temperature for the Wetzstein site should be a few degrees lower, since the site is located at an altitude 217 m higher than the weather station at Teuschnitz-Wickendorf. This will be further discussed in Section 2.2.2.

The position of the micrometeorological tower is indicated by the red marks in Figures 2.1 and 2.3. The tower has a homogeneous fetch of 1-2 km in all directions and

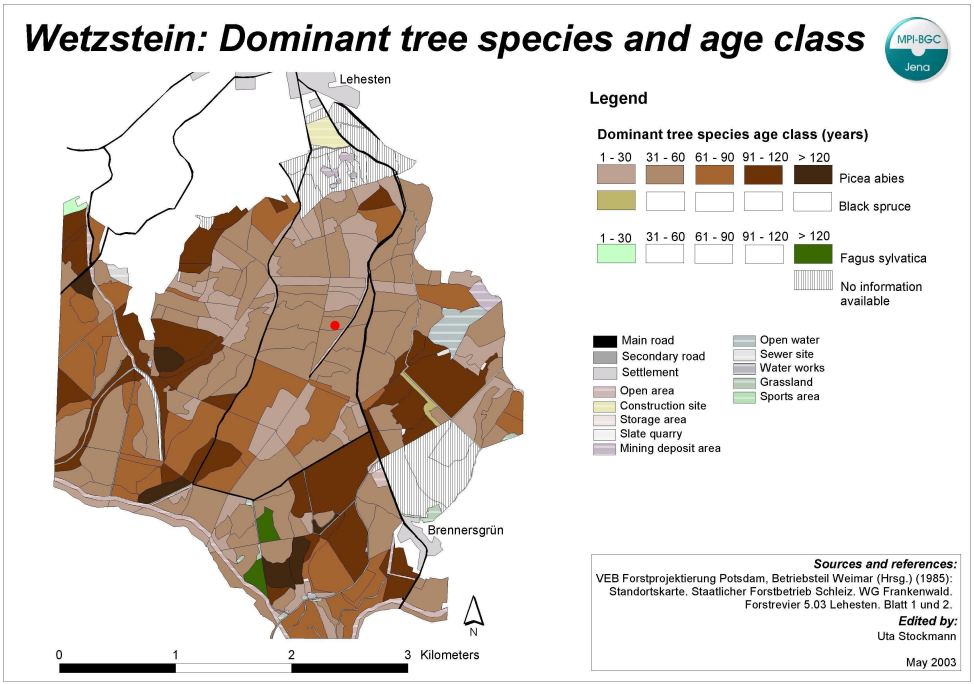

Figure 2.1: Tree species and age classes at the Wetzstein site. Micrometeorological tower located at the red mark. Edited by Uta Stockmann in 2003.

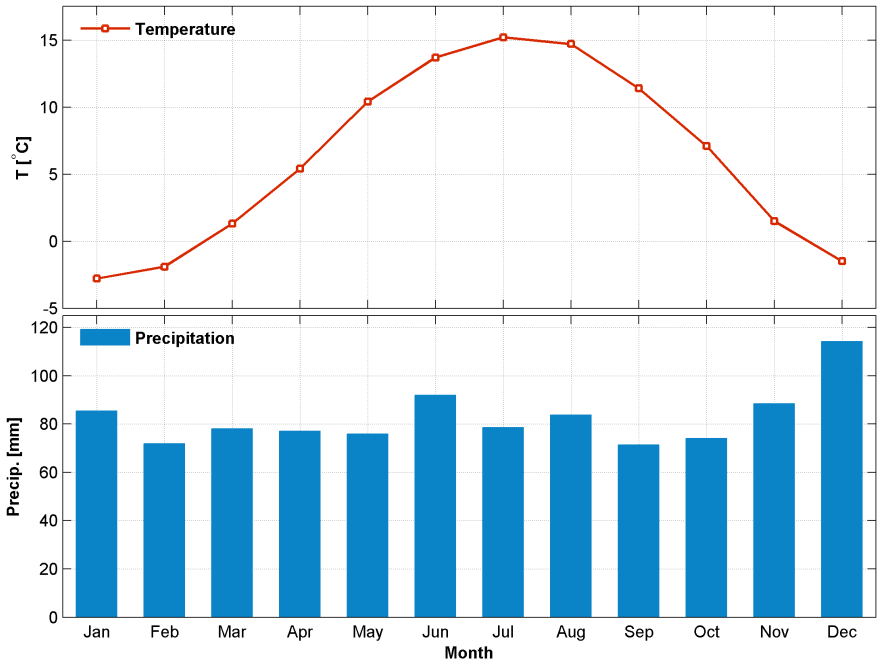

Figure 2.2: Average annual evolution of temperature (top) and precipitation (bottom) at the weather station of Teuschnitz-Wickendorf (Bavaria), distant ≈ 7 km from the Wetzstein site. The measurements were averaged monthly from 1961 to 1990; data gaps were artificially filled as described in DWD (2007) (website).

a 0.5 km^2 clearing to the southwest does not influence the measurements, according to the results from the footprint modeling shown in Section 5.2.

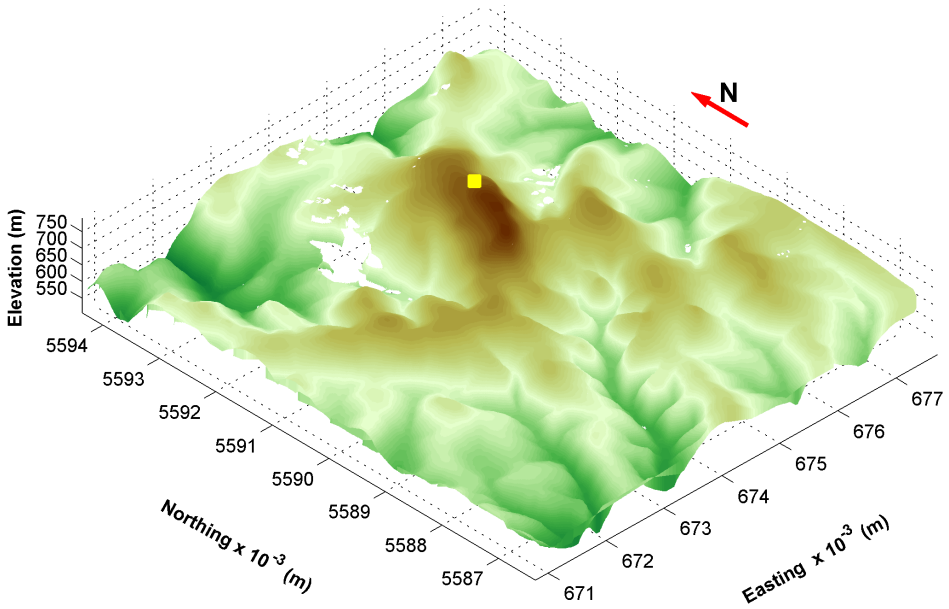

Figure 2.3: Wetzstein site topography. Vertical scale exaggerated five times. Tower position at the yellow square. Horizontal axis marks separated by 1000 m.

The micrometeorological tower is 30 m high and equipped with fast and slow response instruments, placed in several heights above and below the canopy. The eddy covariance technique is used to determine turbulent fluxes, as will be detailed in Section 2.3. Sonic anemometers (model 1210R3, Gill Instruments, Lymington, UK) and infra-red gas analyzers (hereafter referred as IRGA, model Li6262, LiCor Inc., Lincoln, NE, USA) were used to acquire the wind velocity components and CO_2 and water vapor concentrations, respectively. The sampling frequency for both sonic anemometer and IRGA was 20 Hz.

The sonic anemometer is mounted on a boom that is oriented to -41° from the north direction, i.e., 41° in the counterclockwise direction. This offset accounts for the orientation of the boom in relation to the tower (-33°) and the orientation of the tower in relation to the north direction (-8°). The sonic anemometer itself is pointing to north. The inlet of the IRGA is 25 cm distant from the sonic anemometer and oriented to 120° in relation to north.

As the experimental setup described above is oriented approximately to the northwest, the wind flow coming from the opposite direction (≈ southeast) should be disturbed by the tower. Indeed, the footprint and quality control analysis performed at the site (Mathias Göckede, personal communication; and Section 5.2) revealed a low data

quality for winds coming from $\approx$ 100 to 150°. These situations were not taken into account considering that only the high quality data were used in the subsequent analyzes.

A Vaisala HMP35D (Vaisala, Helsinki, Finland) was used to measure air temperature and relative humidity. Wind speed and direction were measured with a cup anemometer and a wind vane (model A100R and W200P, Vektor Instruments, Denbighshire, UK) as well as with a heated 2D sonic anemometer. Shortwave direct radiation components were measured with a Kipp & Zonen CM11 sensor; the diffuse radiation was measured using a CM14 sensor equipped with a shadow ring (Kipp & Zonen, Delft, the Netherlands); long wave radiation components were recorded using a Pyrradiometer (model LXG055, Dr Bruno Lange GmbH, Berlin, Germany).

The measurements of soil temperature were performed with thermistors in several depths (2, 4, 8, 16, 32, and 64 cm); soil moisture was acquired with Delta-T sensors (ML-2x, Delta-T, Cambridge, UK) at 8, 16, 32, and 64 cm depth; soil heat flux was measured with 6 HF3/CN3 heat flux plates (McVan Instruments, Mulgrave, Australia) at 2 to 3 cm depth.

Additional sensors were installed at the site as part of the ADVEX Experiment, conceived to measure advective fluxes in some of the CarboEurope-IP sites (Section 5.4, Feigenwinter et al., 2007). The experimental setup can be seen in Figure 2.4. From April to June of 2006 four additional towers (MP A, MP B, MP C, and MP D) were installed around the existing one (MP BGC). Furthermore, in order to measure the vertical profile of wind velocity below and above the canopy at the slope, an additional tower was installed at $\approx$ 900 m southwest from the main tower (MP 2).

Each tower of the ADVEX experiment was equipped with four levels of measurements, sampling the wind velocity components at 10 Hz and CO_2 concentration and air temperature at 1 Hz. Moreover, the air was sampled in several points along two crossing lines inside the square formed by the towers, in order to measure the horizontal gradients needed to calculate horizontal advection.

Temperature, wind velocity, and wind direction were measured using slow response sensors at the points marked MP 1, MP 3, MP 4, MP 5, and MP 6. Further details about the tower positions and sensor heights are shown in Table 2.1.

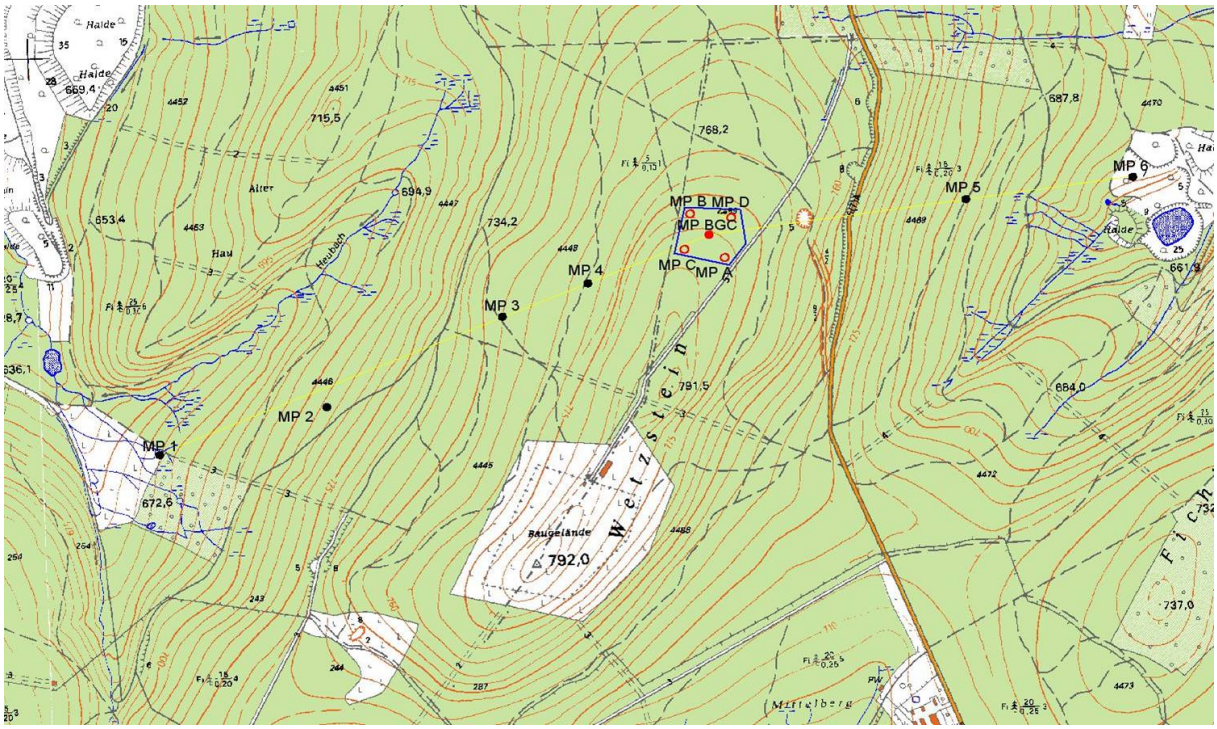

Figure 2.4: Position of the towers during the ADVEX Experiment at the Wetzstein site. Main tower marked with filled red circle and ADVEX towers with open circles. Slope tower at the point marked MP2. Slow response sensors placed at points marked MP1, and MP3 to MP6.

Table 2.1: Turbulence measurements at the Wetzstein site. Towers MP BGC and MP 2 in Figure 2.4 referred as main and slope towers, respectively. Towers MP A to MP D operated only during the ADVEX Experiment (April - June, 2006).

Parameter	Main tower (MP BGC) [sensor (height)]	Towers MP A, MP B, MP D	Tower MP C	Slope tower (MP 2)
Wind speed (3D), air temperature	Gill R3 ultrasonic anemometer (30, 23.8, 3.6 m); Young 81000V ultrasonic anemometer (1.5, 8.8 m)	Young 81000V (23.8, 8.8, 4.4, 1.5 m)	Gill R3 (23.8, 8.8, 4.4 m); Young 81000V (1.5 m)	Gill R3 (35, 8.5, 2 m)
Air temperature (1 Hz)	Thermocouple 75 µm (30, 23.8, 8.8, 3.6, 1.5 m)	Thermocouple 75 µm (23.8, 8.8, 4.4, 1.5 m)	Thermocouple 75 µm (23.8, 8.8, 4.4, 1.5 m)	-
CO_2, H_2O (20 Hz)	LICOR 6262 gas analyzer (23.8, 30 m)	-	LICOR 7500 (30 m)	LICOR 6262 (35 m)
CO_2, H_2O (1 Hz) ADVEX	LICOR 6262, Valve system (23.8, 8.8, 3.6, 1.5 m)	LICOR 6262, Valve system (23.8, 8.8, 4.4, 1.5 m)	LICOR 6262, Valve system (23.8, 8.8, 4.4, 1.5 m)	-
CO_2, H_2O (1 Hz) permanent	LICOR 6262 (30, 23.8, 15, 9, 5, 2, 1, 0.3, 0.1 m)	-	-	-

2.2 Weather in the investigated years

The weather conditions at the Wetzstein site from 2003 to 2006 are presented in the following sections. Daily averages were calculated for air temperature and net radiation, while annual sums were performed for precipitation. Linear interpolation was used to replace values outside the typical range of a given variable (e.g., caused by instrument failures). Gaps in the data availability, caused by power failures, were also filled using linear interpolation (Olaf Kolle, personal communication) before any average or sum computations. Additional micro-meteorological variables were described in Annex A.

2.2.1 Wind speed and direction

Wind speed (U) and direction (θ) were compared for 4 years of measurements. These data were acquired by a 2D heated sonic anemometer placed at 30 m. Histograms of wind direction for 2003, 2004, 2005, and 2006 are shown in Figures 2.5 and 2.6. Bins of 30° width were used for 5 wind speed classes, represented by the different colors in the figures. The sectors are hereafter named as: NE for $0 \leqslant \theta < 90$; SE for $90 \leqslant \theta < 180$; SW for $180 \leqslant \theta < 270$; NW for $270 \leqslant \theta < 360$.

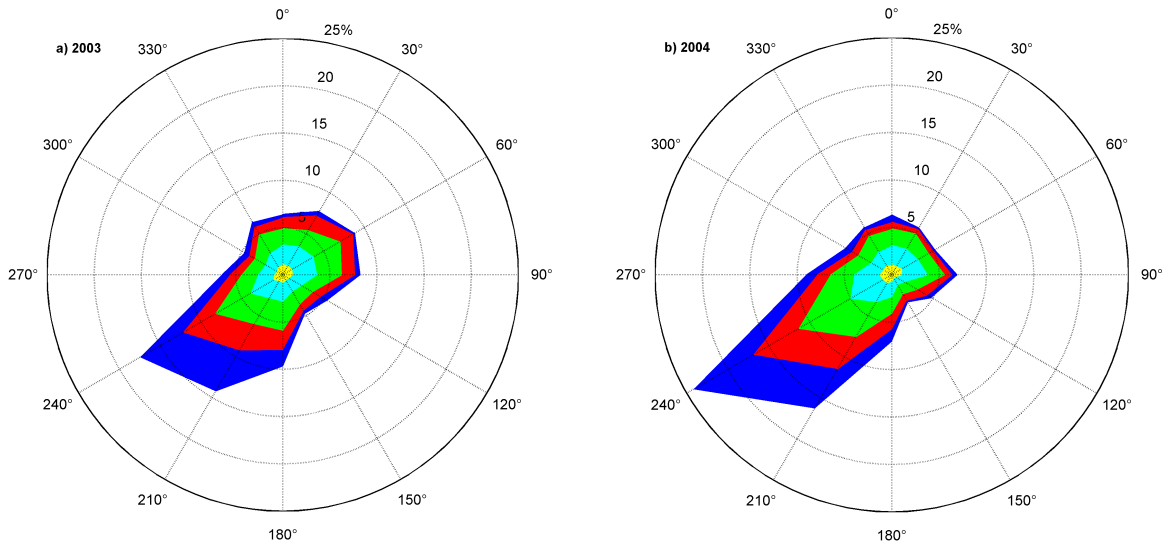

Figure 2.5: Wind direction histograms for a) 2003, and b) 2004. Colors according to the legend in Figure 2.6. Measurement height is 30 m.

All histograms have an elongated part towards southwest, indicating the dominant

wind direction at the site. The overall contribution of the sector SW was ≈ 42, 50, 48, and 50 %, respectively, for the years of 2003, 2004, 2005, and 2006. The second sector regarding the relative contribution is the sector NE, which accounts, on average, for 20 % of all situations.

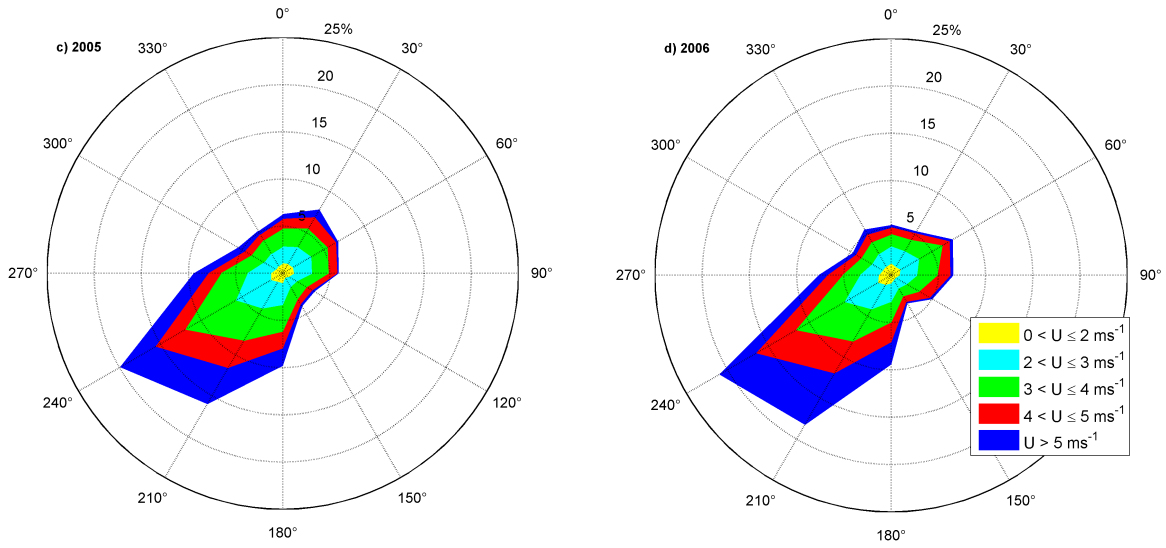

Figure 2.6: Wind direction histograms for c) 2005, and d) 2006. Measurement height is 30 m.

2.2.2 Air temperature

The air temperature in the troposphere (approximately the lower 10 km of the atmosphere) decreases with height. The global-mean value of the lapse rate, or the rate at which the temperature decreases with height, is 6.5 °C km^{-1} (Hartmann, 1994, page 69). For the site area this value should range from 6.1 to 6.2 °C km^{-1} (T. Foken, personal communication). Thus, the climatological mean air temperature for the Wetzstein site should be lower than the value found for the weather station of Teuschnitz-Wickendorf (Section 2.1), as the Wetzstein site is located at a higher altitude (217 m higher).

Using a lapse rate of 6.2 °C km^{-1}, the average air temperature of 6.2 °C found for the weather station of Teuschnitz-Wickendorf should decrease ≈ 1.34 °C at the altitude of the Wetzstein site (785 m). Thus, the climatological average temperature for the Wetzstein site should be approximately 4.9 °C.

Air temperature (T_{air}) measurements at the Wetzstein site have been performed since 2002 using a thermocouple installed at 30 m. The annual cycles for 2003, 2004, 2005, and 2006 are seen in Figure 2.7. The curves are composed of daily averages and the shaded area encloses the daily minimum and maximum temperature range.

The averages of the air temperature ($\overline{T}_{air}$) from 2003 to 2006 are displayed in Table 2.2. $\overline{T}_{air}$ was higher than the approximate climatological mean of 4.9 °C for all the years analyzed, probably influenced by the local weather. $\overline{T}_{air}$ was highest for the years of 2003 and 2006, induced by the hot summer periods observed during these years (second row in Table 2.2).

Table 2.2: Annual average temperature between 2003 and 2006. Units in °C; standard deviations in parenthesis.

	2003	2004	2005	2006
$\overline{T}_{air}$	6.8 (9.0)	5.8 (7.5)	6.1 (8.2)	6.8 (8.4)
$\overline{T}_{air}$ (Jun-Aug)	17.6 (4.1)	14.0 (3.9)	14.0 (4.2)	15.4 (5.1)

The annual averages shown in Table 2.2 outline significant differences between the years compared. The annual average of T_{air} in 2003 was 1 °C higher than the average for 2004 and 0.7 °C higher than 2005. The average for 2006 was the same as 2003, but with a lower standard deviation.

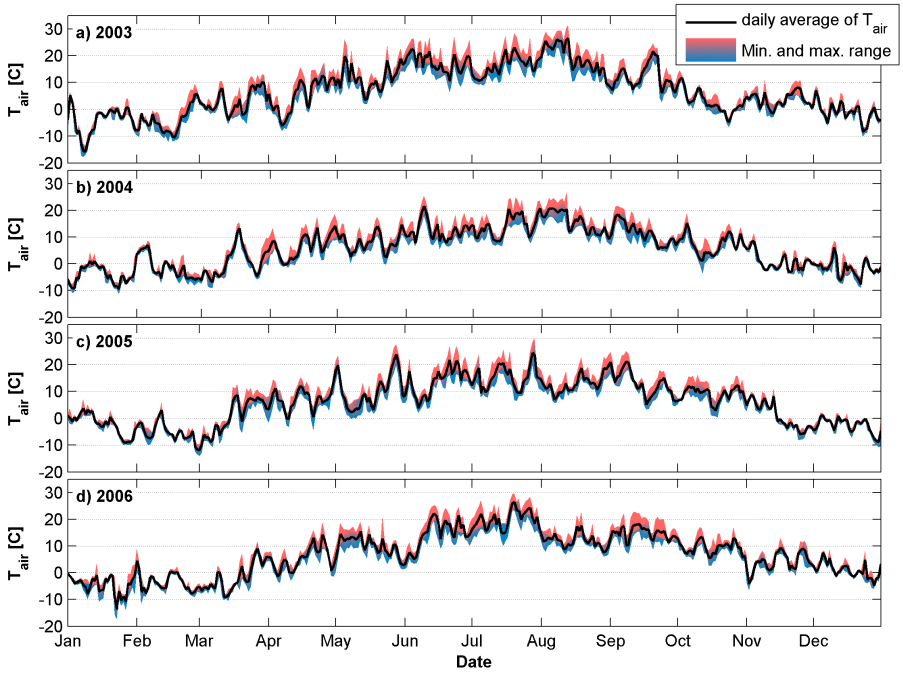

Figure 2.7: Daily averaged air temperatures for 2003, 2004, 2005, and 2006. Shaded areas denote the minimum and maximum range.

The 2003 drought in Europe caused annual precipitation deficits and air temperature means above average in several parts of the continent (Fink et al., 2004; Ciais et al.,

2005). At the Wetzstein site the average of T_{air} between June and August of 2003 was 3.6 °C higher in comparison with the same period in 2004 and 2005 ($\overline{T}_{air} = 14$ °C) and 2.2 °C higher than 2006.

2.2.3 Precipitation

Precipitation is an important processes in the hydrological cycle and it is measured as the amount of water that precipitates on a given surface within a period of time. The climatological mean accumulated precipitation for the region surrounding the Wetzstein site is 990.5 mm, registered at the weather station of Teuschnitz-Wickendorf (Section 2.1).

Given that the Wetzstein site is located at a higher altitude, its precipitation should be higher, induced by orographic rains. According to Koch (1953, page 62) and references therein, the change in altitude in this part of Thuringia (from ≈ 600 to ≈ 800 m a.s.l.) has the effect of increasing the precipitation in approximately 13 %. Thus, it is expected that the true accumulated precipitation at the Wetzstein site should be ≈ 1120 mm.

The annual sums of precipitation at the Wetzstein site for 2003, 2004, 2005, and 2006 are shown in Figure 2.8 (the daily sum of precipitation is plotted together with soil moisture in Figure A.2, Annex A). The year of 2004 had the highest accumulated precipitation of the four years analyzed (1098 mm). It was ≈ 47, 83, and 53 % higher than 2003, 2005, and 2006, respectively, as seen in Table 2.3. However, the value for 2004 was not unusual for the site, as it was the closest to the corrected climatological sum. Rather, the years of 2003, 2005, and 2006 were drier in comparison with the climatological sum.

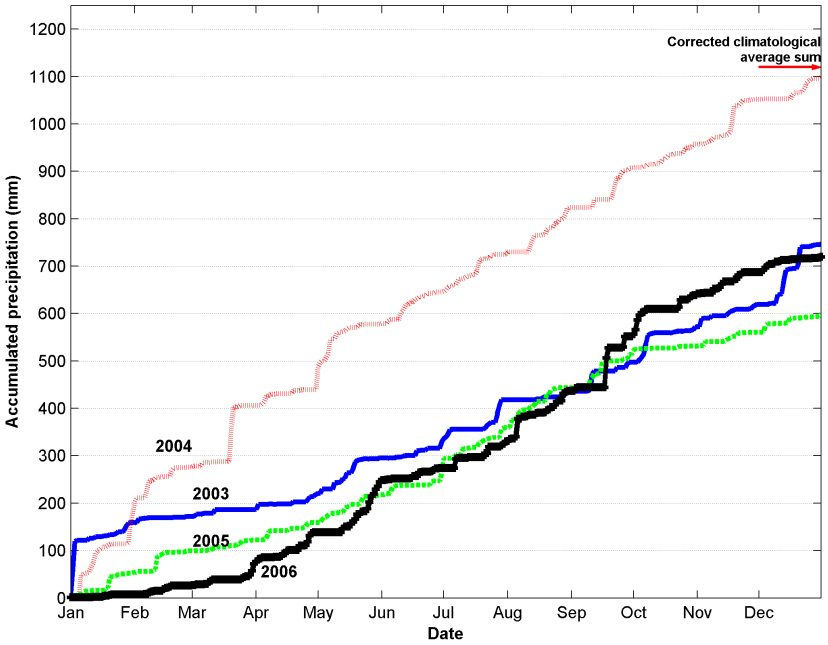

Figure 2.8: Accumulated precipitation between 2003 and 2006. The corrected climatological average sum of 1120 mm is marked with a red arrow.

The drought during the summer of 2003 affected several parts of Europe, including Germany (Ciais et al., 2005). The effects of this severe weather anomaly were detected in different meteorological variables as the precipitation summed over the year and over the summer. The accumulated precipitation between June and August of 2003 was the lowest value registered (both relative and absolute) when compared with the same period for the three following years. The absolute values of precipitation between 2003 and 2006 are seen in the first row of Table 2.3; the relative and absolute values for the *summer* months are shown in the second row.

Table 2.3: Accumulated precipitation between 2003 and 2006. Units in mm; relative contribution during the summer inside the parenthesis.

	2003	2004	2005	2006
Accum. precip.	746	1098	600	720
Accum. precip. – summer	140 (19 %)	246 (22 %)	225 (38 %)	192 (27 %)

2.2.4 Net Radiation

The net radiation (R_{net}) is the difference between the incoming and outgoing radiation at the surface and it is an important component of the energy balance. According to Equation 2.1, it is a balance between the energy absorbed by the visible and longwave radiation (terms 1 and 3), the energy emitted in the infra-red wavelengths (term 4), and the shortwave radiation reflected by the surface (term 2).

$$R_{net} = \quad S\downarrow \quad + \quad S\uparrow \quad + \quad L\downarrow \quad + \quad L\uparrow \tag{2.1}$$

where S↓ is the shortwave incident radiation, S↑ is the shortwave reflected radiation, L↓ is the longwave radiation absorbed by the surface, and L↑ is the longwave radiation emitted by the surface. By definition the downward fluxes are negative and the upward are positive (Stull, 1988).

During the day R_{net} is negative, as the absorption of energy by the surface is higher than its emission (term 1 dominates). Terms 3 and 4 are both large, but with opposite sign; its balance is in general positive, due to the emission of energy from the surface to the atmosphere (Stull, 1988, page 258). At night the incident and reflected solar radiation are obviously zero (terms 1 and 2). As the surface cools down, term 4 dominates and R_{net} becomes positive.

For cloudy nights term 3 becomes more negative, caused by the absorption of the heat that is emitted back to the surface by the clouds. As term 3 contributes negatively, the balance between L↑ and L↓ reduces R_{net}, resulting in a warmer surface. At these conditions the vertical gradient of temperature in the surface layer is small, and the stratification regime is said to be neutral. Neutral stratification is associated with strong winds and intense turbulent activity. For the Wetzstein site it is also associated with high nocturnal fluxes of CO_2, as will be discussed in Section 5.5.

The measurements of R_{net} were taken at the top of the tower using the instrumentation described in Section 2.1. The average daily cycle of net radiation for periods of two months between 2003 and 2006 is shown in Figure 2.9. According to the sign convention, daytime values are negative and nighttime values are positive. As can be seen, the absolute value of R_{net} during daytime is highest from May to August (Figures 2.9-b and -c), implying a higher input of energy. During these months the daytime period is also longer than the nighttime hours.

Some differences in the magnitude of R_{net} were observed between the years compared. In Figure 2.9-b, for May and June, the absolute value of R_{net} is lower in 2004, for both daytime and nighttime periods. In Figure 2.9-c, for July and August, R_{net} was strongly negative during daytime for 2003. Such differences are most probably associated with the cloud cover during the periods averaged.

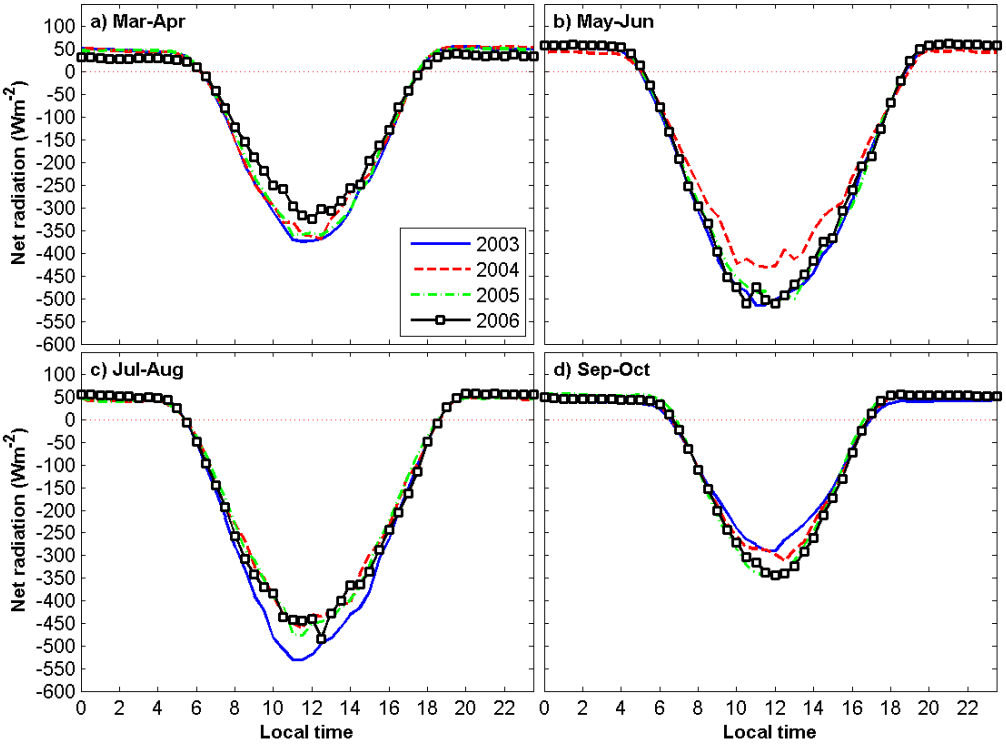

Figure 2.9: Average daily cycle of R_{net} for a) March and April, b) May and June, c) July and August, and d) September and October.

2.3 Methodology

2.3.1 Eddy Covariance Method

The exchanges of momentum, heat, and scalars between Earth's surface and the atmospheric boundary layer (ABL) are described by the equations of motion and conservation of scalars. Considering that no analytical solution exists for this set of equations, they have to be simplified by applying the Boussinesq approximations, assuming the stationarity of the flow, considering the surface to be horizontally

homogeneous, and aligning the coordinate system according to the main wind direction (Stull, 1988). As a result, one obtains the vertical flux F_c of a scalar c, as:

$$F_c = \overline{w\rho_c} \tag{2.2}$$

where w is the vertical wind speed and ρ_c is the concentration of the scalar c.

The instantaneous value of a flow property can be split in an average and a fluctuating part, according to Reynolds averaging (Garratt, 1992; Arya, 2001). Thus, w and ρ_c can be expressed as:

$$w = \overline{w} + w', \tag{2.3}$$

$$\rho_c = \overline{\rho}_c + \rho'_c \tag{2.4}$$

where the overbar denotes time average and prime denotes the fluctuating part.

By applying equations 2.3 and 2.4 in Equation 2.2 one obtains the vertical flux F_c for a given scalar c as:

$$F_c = \overline{w'c'} + \overline{w} \cdot \overline{c} \tag{2.5}$$

where terms involving averages of fluctuations as $\overline{w'}$ or $\overline{c'}$ were already excluded because they are zero according to the definition of Reynolds averaging. The second term on the right hand side of Equation 2.5 is generally neglected as the assumption of horizontal homogeneity of the flow leads to $\overline{w}$=0. However, the validity of this assumption for more general topographies has been questioned in recent years. The implications of this discussion will be commented later in this section.

Direct measurements of $\overline{w'c'}$ can be obtained by using the eddy covariance technique, developed after the works about turbulence spectra of Swinbank, Obukhov, and Montgomery, back in the 1950s (Kaimal and Finnigan, 1994; Arya, 2001; Foken, 2006). In such a technique the wind velocity components and the scalar concentrations (e.g. CO_2 and H_2O) are sampled typically at 10-20 Hz using fast ultrasonic anemometers and infra-red gas analyzers. The following equations show how the vertical fluxes of momentum, heat, and CO_2, are calculated, respectively.

$$\tau = -\rho \cdot \overline{w'u'} \tag{2.6}$$

$$H = \rho \cdot c_p \cdot \overline{w'T'_s} \tag{2.7}$$

$$F_{CO_2} = \frac{\rho}{m_a} \cdot \overline{w'CO'_2} + \int_0^{z_r} \frac{\partial \overline{c}}{\partial z} \mathrm{d}z \tag{2.8}$$

where u' and w' are the departures from the mean of horizontal and vertical wind velocity components, ρ is the air density, c_p is the specific heat capacity of dry air, T_s is the temperature measured by the ultrasonic anemometer, and m_a is the molecular weight of dry air. The second term on the right hand side of Equation 2.8 accounts for the storage of CO_2 below the measurement height z_r.

The eddy covariance technique has been widely used to account for the exchange of momentum, heat, and scalars between the surface and the atmosphere (Goulden et al., 1996; Moncrieff et al., 1997; Aubinet et al., 2000; Lee et al., 2004). It has been used, for example, in the characterisation of turbulent fluxes over forests and wetlands as well as on the calculation of deposition of nitrogen over pastures sites (Araujo et al., 2002; Zeri, 2002; van der Molen et al., 2004; Trebs et al., 2006). During the last decade several networks of micrometeorological measurements have been established (AMERIFLUX, EUROFLUX, LBA, etc.) in order to have long term records of carbon dioxide and energy fluxes in different ecosystems (Baldocchi et al., 2001).

2.3.2 Corrections applied on the turbulent fluxes

Corrections were applied to the turbulent fluxes in order to compensate for experimental and methodological limitations of the eddy covariance technique. These corrections are included in the EDDYFLUX software used in this work (Kolle and Rebmann, 2007) and will be detailed next.

Schotanus correction

The sonic anemometer measures the speed of sound, which can be related to air temperature. Such measurement is affected by the lateral winds that delay the

reception of the ultrasonic pulses between the anemometer transducers. Additionally, the temperature derived from the speed of sound needs to be corrected for the air humidity. The air temperature provided by the sonic anemometer (T_s) was corrected for the effects of side-winds and humidity according to Schotanus et al. (1983).

High frequency losses

The measurement of the concentration of a scalar c (e.g. CO_2 or H_2O) using a closed path gas analyzer requires the air to be pumped via tubes inside the analyzer chambers. However, the transport of air through tubes causes the damping of the high frequency part of the signal, leading to underestimation of the turbulent fluxes. The vertical fluxes of CO_2 and H_2O were adjusted according to Eugster and Senn (1995), that proposed a correction based on the cospectral similarity of vertical fluxes of scalars.

The correction parameters, or the inductances, are regularly checked by comparing the cospectra of $\overline{w'C'}$, for CO_2, and $\overline{w'q'}$, for H_2O, with the cospectra of $\overline{w'T'}$. The value for the inductances is obtained by adjusting the high frequency part of the cospectra of $\overline{w'C'}$ and $\overline{w'q'}$ to the high frequency part of the cospectra of $\overline{w'T'}$.

Lag correction

The transport of air from the inlet close to the sonic anemometer to the gas analyzer takes some time, as the air must be pumped through a certain distance inside the tube. This has the effect of delaying the signals of CO_2 and H_2O in relation to the time series of wind velocity components and temperature, recorded by the sonic anemometer. As a result, the time series of CO_2 and H_2O have characteristic time lags that have to be accounted for in order to keep them synchronized with the sonic anemometer data.

The lags for each half hour were calculated using the EDDYSOFT's EDDYCORR package (Kolle and Rebmann, 2007), which finds the lags between two time series based on the cross-correlation between them. The lags are determined separately for CO_2 and H_2O and are used later when the turbulent fluxes are calculated.

WPL correction

Descending air parcels are denser than ascending ones. Hence, the mass balance forces the ascending ones to move faster, resulting in a non-zero mean vertical velocity. As a result, the second term in the right hand side of Equation 2.5 becomes important and contributes to a substantial part of the turbulent fluxes measured with *open path* gas analyzers. In this case, the fluxes are corrected using the so-called WPL correction, after Webb, Pearman, and Leuning, 1980. This correction takes into account the sensible heat and water vapor fluxes when accounting for the density effects (Webb et al., 1980; Liebethal and Foken, 2003, 2004; Liu, 2005; Kowalski, 2006; Leuning, 2007).

This correction is not applied when closed path gas analyzers are used, because of a different measurement principle: inside the analyzer chambers the temperature and pressure are known at any instant, what makes it possible to calculate the mixing ratios of CO_2 and water vapor (Leuning, 2004). In this case, the turbulent fluxes do not need to be further adjusted using the WPL correction. The WPL correction was applied to data from an open path gas analyzer installed at the top of Tower C during the ADVEX Experiment.

Quality control

Turbulent fluxes measured at the atmospheric surface layer may be affected by instrumental problems and weak stationarity, i.e., time series with changing statistical properties (Wilks, 1995). Examples of instrumental problems are spikes in the high frequency data and discontinuities caused by power failures; weak stationarity in a time series is caused for example by local circulations, gravity waves, or intermittent periods of turbulence (Foken and Wichura, 1996; Vickers and Mahrt, 1997). These situations compromise the basic assumptions of the eddy covariance technique and have to be identified and flagged during the calculations of turbulent fluxes.

In order to quantify the quality of the data, tests for the stationarity and integral turbulence characteristics (Foken and Wichura, 1996) were performed by the software used in this work (EDDYSOFT, Kolle and Rebmann, 2007). Additionally, spikes in the high frequency data were removed from the time series before calculating turbulent fluxes.

Planar fit correction

Measurements of the wind components over sloping terrain or with a tilted sensor result in apparent vertical velocities, caused by the horizontal wind components, and vice versa. To overcome this problem, the three wind components are generally rotated so that the vertical velocity if forced to be $\approx$ zero. Over sloping terrain, however, it is recommended that the coordinate system should be rotated following the flow streamlines that are influenced by the topography (Kaimal and Finnigan, 1994). Such alignment makes it possible to compare the results obtained over sloping terrain with the ones obtained over flat surfaces.

The planar fit correction accounts for the leveling of the coordinate system to the flow streamlines (Wilczak et al., 2001). This correction was applied to the data measured above the vegetation, at 30 and 24 m. As an example, the wind field at 24 m is shown before and after the planar fit rotation in Figure 2.10-a to -c. The topography at the site imposes significant average vertical velocity values, as shown in the original wind field on Figure 2.10-a. After applying the technique using one plane to align the coordinate system, the wind field is still subjected to mean vertical velocities (Figure 2.10-b).

Finally, the result from the sectorized planar fit, used in this work, is shown in Figure 2.10-c. The wind field is homogeneous in this figure and the average vertical velocity (-7.9 10^{-6} m s^{-1}), plotted at the top of the figure, is several orders of magnitude lower than the original value of Figure 2.10-a (-1.1 10^{-2} m s^{-1}).

2.3.3 Wavelet Analysis

The wavelet transform is a mathematical tool that makes it possible to decompose a signal x_i in its frequencies, showing their intensity and variability during time (Daubechies, 1992). It has been used in several studies of geophysical signals, because it provides a useful visualization of non-periodic and intermittent features of a time series (Collineau and Brunet, 1993b; Druilhet and Durand, 1997; Torrence and Compo, 1998; Grinsted et al., 2004; Thomas and Foken, 2005; Baas, 2006).

The wavelet decomposition is calculated as the convolution between the time series x_i and stretched and shrinked versions of a mother wavelet function. A wavelet function $\Psi(t)$ must have a zero mean, must be localized both in time and frequency, and can be

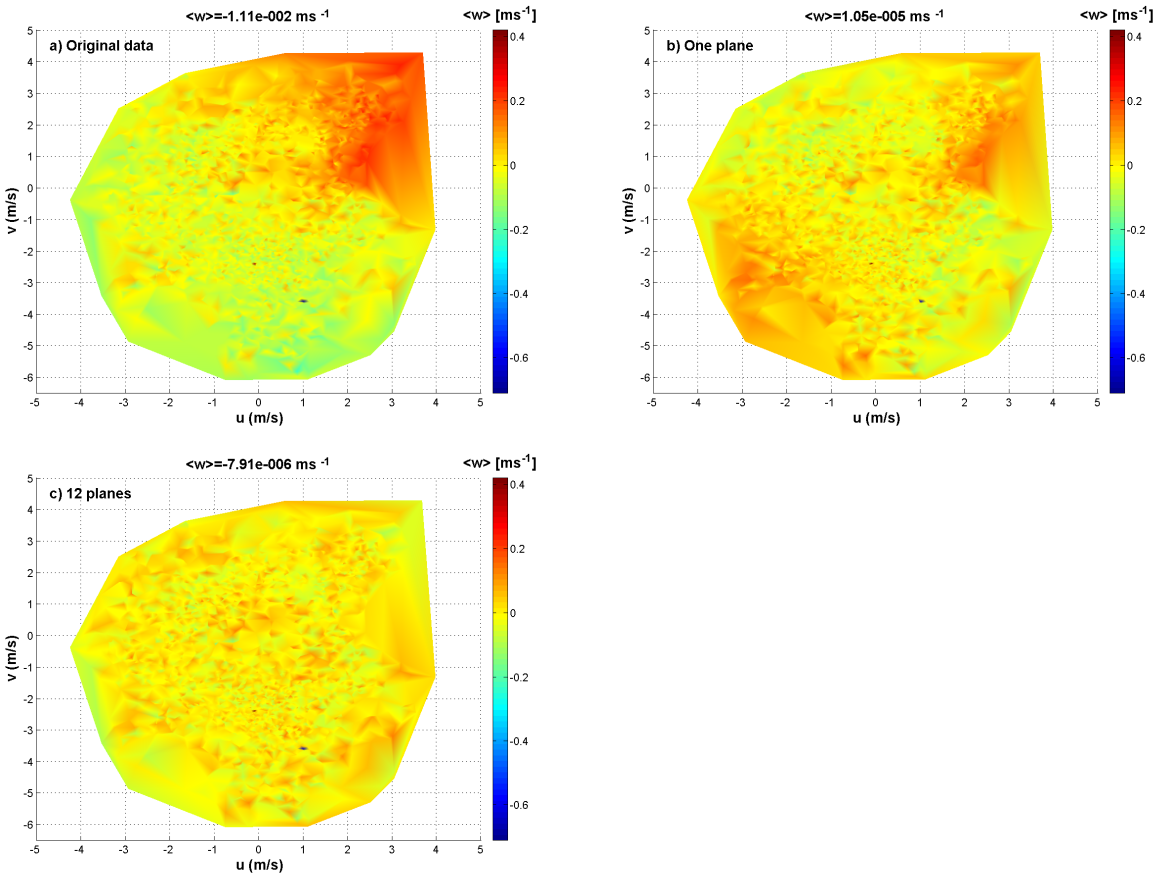

Figure 2.10: Wind velocity components at 24 m before and after the application of the planar fit method. The data is from April to June 2006. The vertical velocity is in the color axis and the global average is indicated at the top of the figure. a) Original data; b) Data fitted to one plane; c) Data fitted to 12 sectorized planes.

continuous or discrete (Farge, 1992; Torrence and Compo, 1998). As an example, the Morlet function, a continuous mother wavelet, is defined as:

$$\Psi(\eta) = \pi^{-1/4} e^{i\omega_0 \eta} e^{-\eta^2/2}, \tag{2.9}$$

where η is the non-dimensional time parameter and ω_0 is the non-dimensional frequency. The mother wavelet should be chosen so that its shape matches the shape of events in the time series. However, according to Torrence and Compo (1998), if one is interested in the wavelet power spectra, the choice of the mother wavelet is not critical. For this work, the Morlet function was used and showed a good performance concerning the identification of spectral properties of known signals.

The wavelet transform is defined as the convolution of the time series x_i with scaled

and translated versions of $\Psi(\eta)$, so that $W(t,a)$, the wavelet coefficient at time t and scale a, is calculated as:

$$W(t,a) = \frac{1}{\sqrt{a}} \int_{-\infty}^{\infty} x(\tau) \Psi \left(\frac{\tau - t}{a} \right) \mathrm{d}\tau \tag{2.10}$$

where t is time, a is the scale parameter, and τ is the integration variable that displaces the scaled versions of the mother wavelet along the time series x_i.

The wavelet analysis applied to a pair of signals x and y is called the wavelet cross spectra analysis (Grinsted et al., 2004). This technique reveals the common characteristics in time *and* frequency of two signals. The cross wavelet identifies an event that occurs at the same time and with the same frequency in both time series.

The cross wavelet analysis was used in Section 4.2 to compare the combined evolution of high frequency data of w and CO_2 for calm and turbulent periods. Moreover, a global cospectrum can be calculated from the cross wavelet analysis if its coefficients are summed up over all scales. In Section 4.3 the wavelet cospectrum between w and CO_2 was calculated for several nighttime periods of two hours, for calm and turbulent conditions.

Chapter 3

Flow over the hill

The well established eddy covariance technique relies on the assumptions of stationarity and horizontal homogeneity of the flow (Stull, 1988; Kaimal and Finnigan, 1994). On practical matters, this means that the choice of the measuring location should be limited to sites with homogeneous vegetation cover and flat terrains. However, the need for reliable estimates about the exchanges of energy and greenhouse gases in forests led to the expansion of the measurement networks over more general topographies (Aubinet et al., 2000; Baldocchi et al., 2001). Thus, it is imperative to understand the characteristics of the flow over topographies that are far from the ideal conditions and that are known to influence significantly the forest-atmosphere interactions (Raupach and Finnigan, 1997; Lee and Hu, 2002; Turnipseed et al., 2003, 2004).

By using an analytical approach Finnigan and Belcher (2004) modeled the flow over a low hill covered with a canopy. They found that as the air passes over the hill a pressure gradient in the streamwise direction caused perturbations in the wind field below the canopy, both at the upwind and lee sides of the ridge. The wind velocity below the canopy in several parts of the hill differed significantly from the no-canopy solution of Hunt et al. (1988), that considered a constant roughness length across the hill, instead of a canopy.

Finnigan and Belcher (2004) obtained the disturbance Δu in the wind field caused by the hill. Vertical profiles of Δu were calculated for several locations across a two dimensional bell-shaped hill (Figure 3.1-a). Additionally, Δu was normalized by a scaling velocity U_{SC}, that depended on the hill dimensions H and L.

As expected, the model results show a speed-up above the canopy at the top of the hill. Most important, though, are the values of Δu below the canopy (light gray area), namely the acceleration ($\Delta u > 0$) at the upwind side of the hill and the deceleration (Δu) at the downwind side. This results will be further discussed next.

The model provided by Stephen Belcher (personal communication) was applied to a height profile obtained from the Wetzstein site topography (Figure 3.1-b). This height profile was obtained from the transect $\alpha \rightarrow \beta$ in Figure 3.2. The model run with parameters derived from the hill dimensions and from the leaf area index (LAI) at the site.

In Figures 3.1-a and b, the light gray area represents the canopy space. The continuous lines are the vertical profiles of Δu if the hill is considered; the dashed lines are the vertical profiles for the solution that considers a constant roughness length, instead of a canopy, as proposed by Hunt et al. (1988).

The two solutions in Figures 3.1-a and b match for several parts of the hill. At the upwind side of the ridge the vertical profiles of Δu are similar for both figures. Also, Δu is strongly positive above the canopy at the top of the hill caused by the commonly expected speed-up of wind velocity at the top of hills (Stull, 1988). The dissimilarities between solutions for the second and third profiles, from right to left, at the lee side of the hill, may be due to the fact that the height profile of the Wetzstein site is not as symmetrical as the bell-shaped curve (S. Belcher, personal communication).

However, the main features of Figure 3.1-a can still be observed on the majority of profiles of Δu in Figure 3.1-b, namely the deceleration at the lee side ($\Delta u < 0$) and the acceleration below the canopy at the upwind side of the hill ($\Delta u > 0$).

The positive value of Δu below the canopy, at the upwind side of the hill, indicates that the wind is accelerated at this part of the ridge. Additionally, the wind speed below the canopy at this part of the ridge is higher than the wind speed below the canopy at the hill top, where Δu is ≈ 0. This difference will be investigated in Section 3.2. At the lee side of the crest the wind speed is lower for the hill solution ($\Delta u < 0$), decelerated by the reversing flow that occurs above the canopy at all levels (Finnigan and Belcher, 2004). Evidence of reversing flow was found in the wind coupling results of Section 5.3.2.

Katul et al. (2006) extended the work of Finnigan and Belcher (2004) by additionally modeling the radiative transfer and eco-physiological processes, both below and above

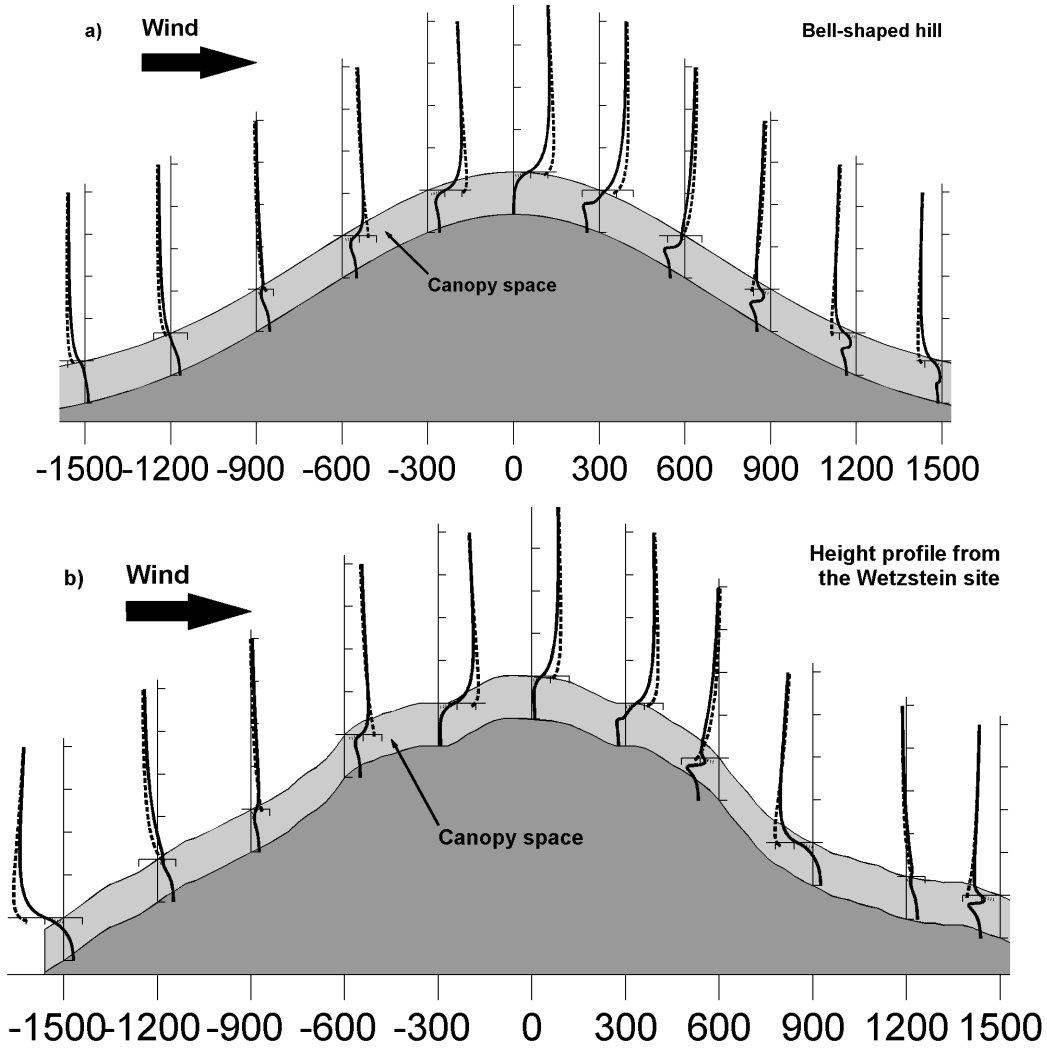

Figure 3.1: **a**: Vertical profiles of the disturbance in the wind velocity caused by the hill (continuous line), as presented by Finnigan and Belcher (2004). The no-canopy solution of Hunt et al. (1988) are presented as dashed lines. **b**: Same as above, for a height profile from the Wetzstein site. Horizontal distance in meters.

the canopy. The authors found that the horizontal and vertical advective fluxes of CO_2 are opposite in sign, but do not cancel each other locally or when averaged over the whole hill. Thus, the total CO_2-flux vary across the ridge.

The Wetzstein site is located on a small hill where unexpectedly high nighttime fluxes of CO_2 are frequently observed (this topic will be detailed in Section 5.5). These high nocturnal fluxes of CO_2 are especially observed during situations of neutral atmospheric stratification and high values of wind speed.

Neutral stratifications are known to enable the flow to pass over the hill, given that the vertical motions of air parcels are not damped, as occurs during stable conditions (Stull, 1988). Thus, if the flow is free to move over the topography, the Wetzstein site is

probably affected by advective fluxes induced by these motions, as predicted by Katul et al. (2006).

The results from Finnigan and Belcher (2004) regarding the wind field below the canopy at several locations across the hill were tested in the current chapter. The model results were tested using data measured at two towers along the main wind direction at the Wetzstein site. A vertical profile of sonic anemometers was installed at the slope tower and the profile at the main tower was improved with two additional sonic anemometers, as already detailed in Section 2.1. The processing of these data and the results obtained will be described next.

3.1 Data and Methodology

Data measured from April to June of 2006 were used to test the results from the modeling work of Finnigan and Belcher (2004). The model considers a two dimensional low hill with H/L < 0.1, where H is the hill height and L the hill width. The dimensions of the height profile at the main wind direction at the Wetzstein site (Figures 3.1-b and 3.2) agree with the definition of a low hill assumed by the model. This height profile was taken from the transect connecting the slope and crest towers in Figure 3.2.

A 30 min average and a 2D coordinate rotation were used in the calculations of horizontal velocity for all heights of measurements. The half-hourly averages were then filtered for stationary conditions (Foken and Wichura, 1996; Vickers and Mahrt, 1997). Finally, given that the model considers a two dimensional hill with the wind blowing from the left in Figure 3.1, it is reasonable to think that only the wind speed components parallel to the transect $\alpha \rightarrow \beta$ in Figure 3.2 would follow the model results.

Thus, only the sectors that have a *positive* component to southwest-northeast (wind direction $\theta = 240°$) were selected, as the transect connecting both towers is oriented according to this direction. Then, the results were filtered for $150 \leqslant \theta \leqslant 330$, as indicated in Figure 3.3. The southwest component of the wind speed, U_{SW}, was calculated as:

$$U_{SW} = U \cdot cos(240 - \theta) \tag{3.1}$$

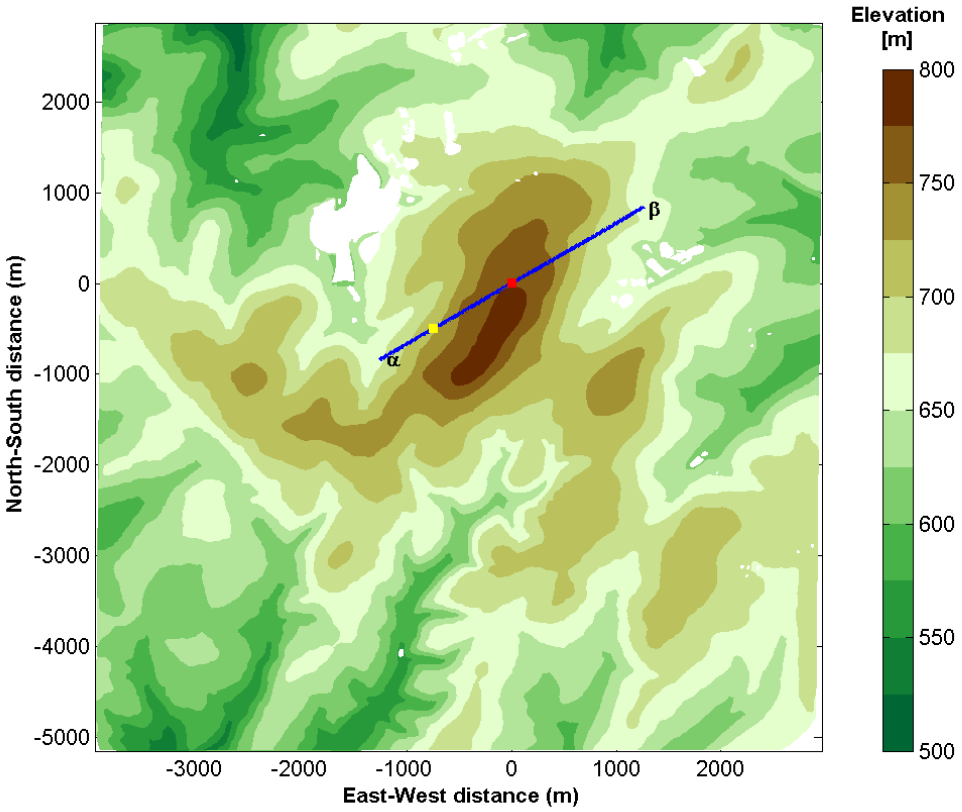

Figure 3.2: Digital elevation map for the Wetzstein site. The white spots are areas of extraction of slate, with no information about the topography. Main tower located at the red square; slope tower located at the yellow square. The height profile of the transect connecting the two towers is shown in Figure 3.1-b.

Additionally, only situations in the neutral range were selected, as this is the atmospheric stratification assumed by the modeling of the flow over the hill. In this work, the neutral range was considered as -0.0625 $\leqslant$ z/L $\leqslant$ 0.0625, where z is the measuring height and L is the Obukhov length.

3.2 Wind speed below the canopy

3.2.1 Average vertical profiles of U_{SW}

The average vertical profile of U_{SW} for the whole period is shown in Figure 3.4-a as triangles. The continuous lines are normalized wind speeds (U_{norm}), derived from the model results presented in Figure 3.1-b: the blue line refers to the hill crest (the 6th

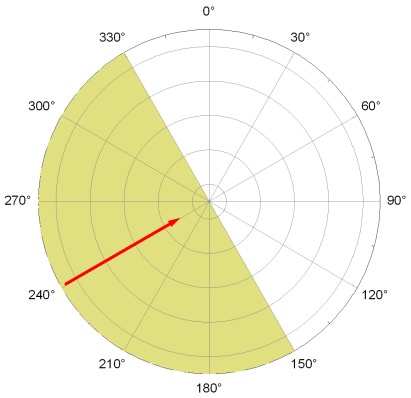

Figure 3.3: Wind direction sectors that have a positive *component* from the southwest ($\theta = 240°$), indicated by the yellow range.

profile from left to right); the green line refers to the slope (3rd profile from left to right). U_{norm} was normalized by the hill dimensions and by the average wind speed of the surface layer (Finnigan and Belcher, 2004). U_{norm} is related to the horizontal axis at the top of Figures 3.4-a and b.

The measurement heights for each tower were normalized by the canopy height, namely 21 m at the crest and 27 m at the slope; the non-normalized heights can be seen in the legends of Figure 3.5. The data in Figure 3.4-a correspond to the average of 30 min means from April 29th to June 5th. The horizontal bars indicate the standard deviation.

On average U_{SW} is higher at the crest, for the measurement height *above* the canopy. This result was expected as the speed-up at the hill top is a common feature of flow over hills (Stull, 1988; Kaimal and Finnigan, 1994). On the other hand, U_{SW} is higher at the slope tower, for the measurement levels *below* the canopy. The tendency of higher wind speeds below the canopy at the slope tower is even stronger in Figure 3.4-b. In this figure, the data were screened for situations when the total horizontal wind speed at the top of the crest tower (30 m) was higher than 6 ms^{-1}. Hence, the difference between the average values of U_{SW} below the canopy increased while the error bars were smaller.

These results agree with the findings from the modeling work of Finnigan and Belcher (2004). According to the authors, the pressure gradient between the crest and the slope disturbs the vertical profiles of wind speed, as shown in Figure 3.1, creating higher wind speeds below the canopy at the upwind part of the hill. However, the difference between U_{SW} at the slope and at the crest for the lowest level was lower than the

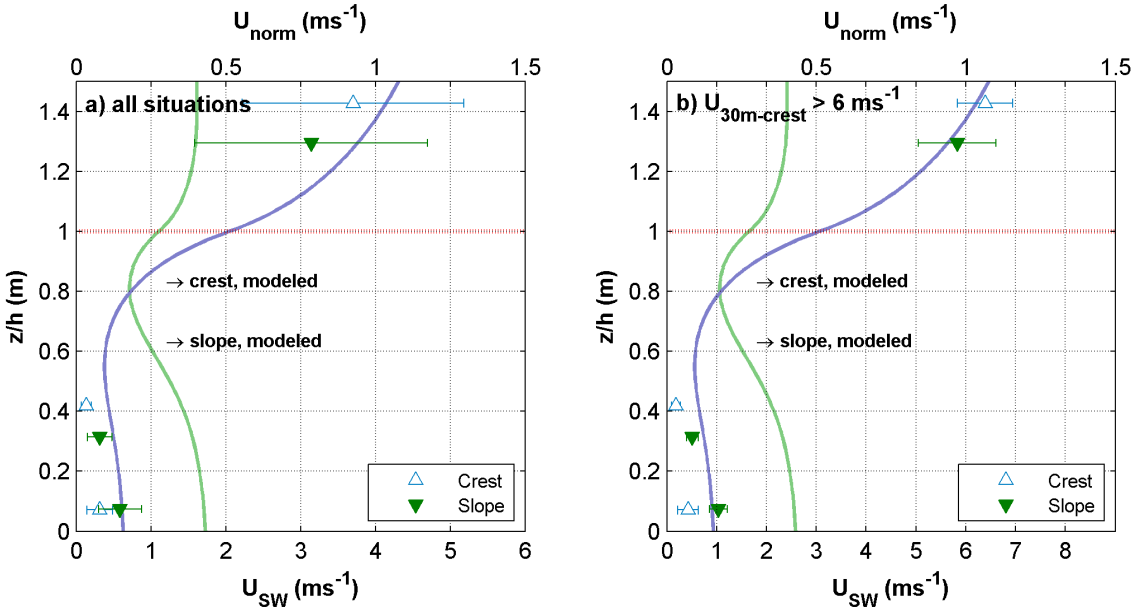

Figure 3.4: Average vertical profiles of U_{SW} and the normalized wind speed (U_{norm}) from the model. U_{SW} was measured from April 29th to June 5th. Vertical axis normalized by the canopy heights: 21 m at the crest and 27 m at the slope. The normalized wind speed (U_{norm}) is related to the horizontal axis at the top. a) All situations; b) Only situations when the average wind velocity at the crest exceeded 6 ms^{-1}.

modeled result. For this level the average of U_{SW} at the slope is approximately 80 % higher than the average at the crest while U_{norm} at the slope is almost three times higher than U_{norm} at the crest. For the data in Figure 3.4-b, the slope/crest ratio of U_{SW} is higher but still lower than the ratio for the modeled wind speed.

This discrepancy between the measured and modeled results can be related to the three dimensional features of the terrain. Also, the model of Finnigan and Belcher (2004) considers a two dimensional hill. This simplification causes the model to not account for all the features of the flow over the Wetzstein site, given its heterogeneous topography.

3.2.2 Time series of U_{SW}

The evolution of the 30 min means of U_{SW} above and below the canopy, for a period of 5 days, is shown in Figures 3.5-a to c. Pairs of slope and crest heights of U_{SW} were compared. The gaps in this figures were caused by the filtering that selected only situations with neutral stratification as well as wind directions that contribute to U_{SW} (Figure 3.3).

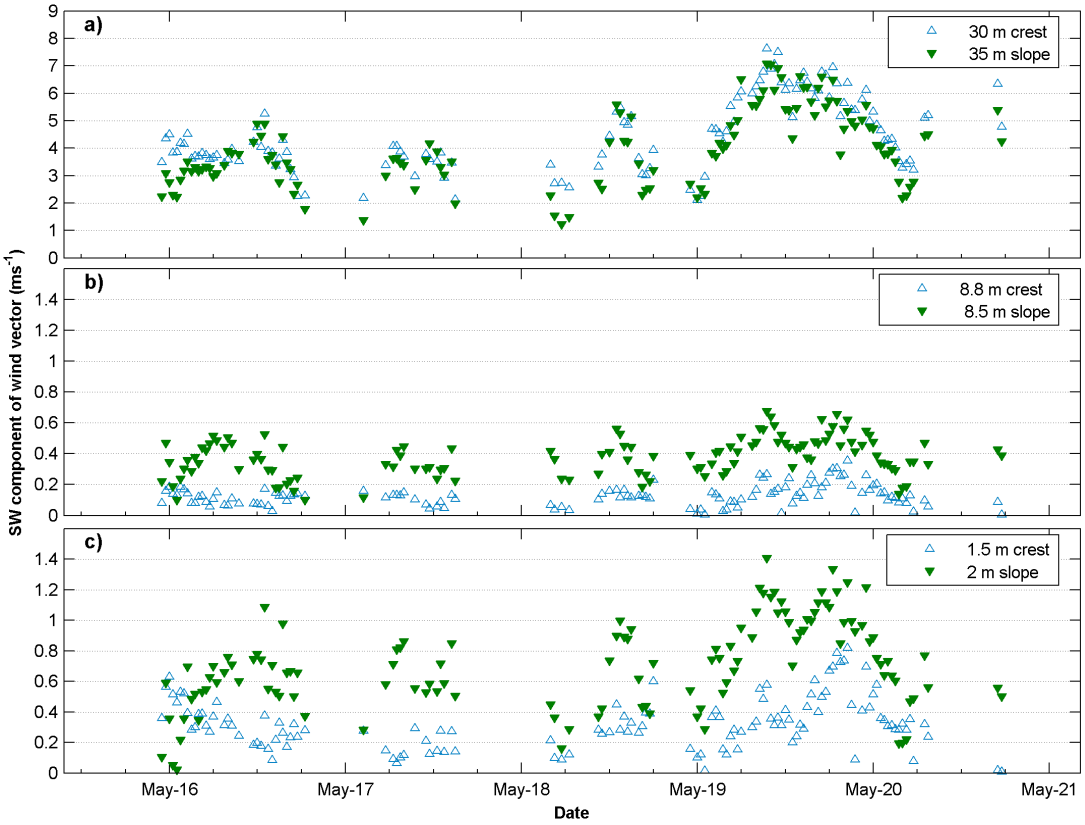

Figure 3.5: Time series of U_{SW} for pairs of slope-crest heights, as indicated in the legends. Gaps indicating periods with non neutral stratification or wind direction outside the yellow range in Figure 3.3. Figure a) *above* the canopy the wind speed is higher at the *crest* than at the slope; Figures b) and c) higher wind speeds below the canopy at the *slope*.

U_{SW} was observed to be higher at the crest, at the levels above the canopy (Figure 3.5-a), as already observed for the average values of Figure 3.4. Similarly, the differences found for the measurement levels below the canopy (Figures 3.5-b and -c) are also in accordance with the average vertical profiles. At these levels U_{SW} is frequently higher at the slope than at crest.

As an example, high frequency data of wind speed below and above the canopy are shown in Figure 3.6. These data were recorded at 20 Hz in April 30th, 2006, from 5:30 h to 6:00 h. This period of data was selected so that the *average* wind direction at each measurement height was limited to the interval between 180 and 270°. A 2D rotation was applied to make w and v components zero and the frequency was reduced from 20 to 1 Hz for clarity. The presented time series are the full streamwise horizontal wind speeds, not only the southwest component as done before.

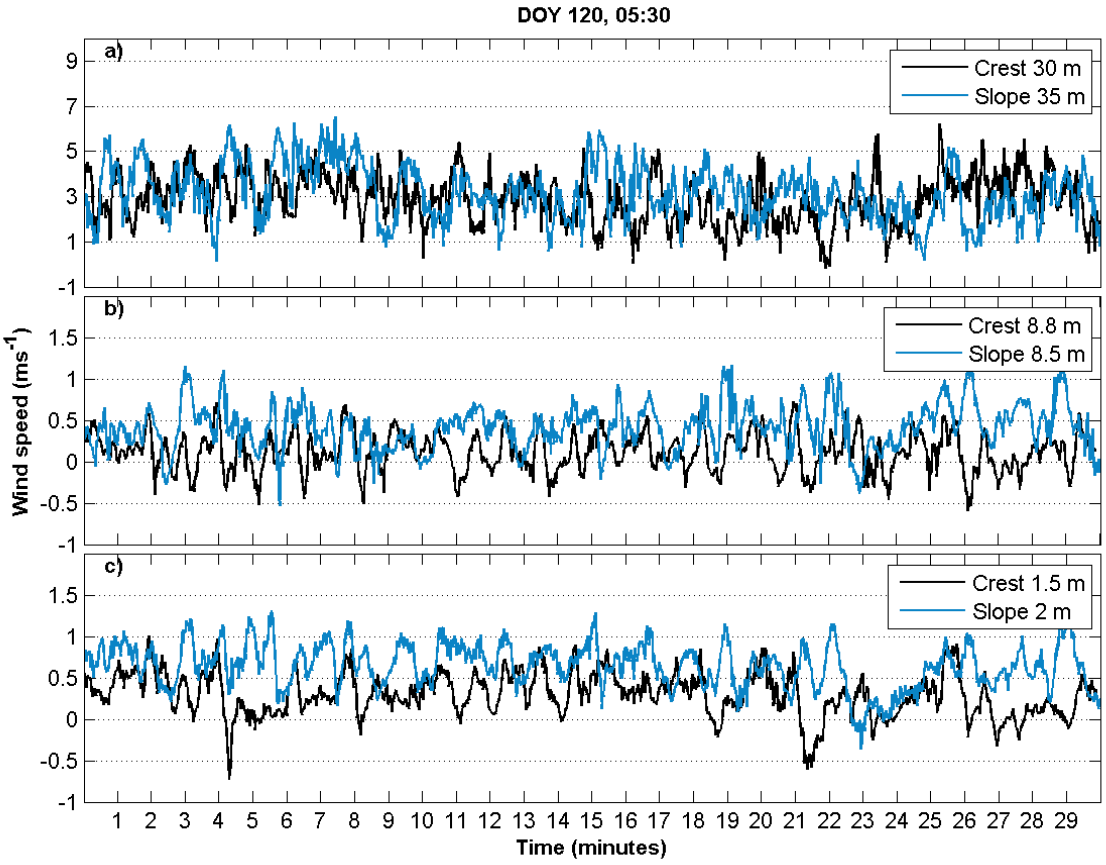

Figure 3.6: High frequency data of streamwise wind speed for April 30th, from 5:30 to 6:00 h. A 2D coordinate system rotation was applied in order to make w and v components zero and the signal frequency was reduced to 1 Hz for clarity.

The wind speed *above* the canopy (at the slope) is higher than the wind speed at the crest during continuous periods of several minutes (Figure 3.6-a). Although this pattern contradicts the average values from Figure 3.4, the large error bars in this figure suggest that for individual half-hours the wind speed can be higher at the top of the slope tower. Indeed, such periods were observed in Figure 3.5-a for May 17th, around 12:00 h. For the measurement levels *below* the canopy, the same pattern of higher wind speeds at the slope are seen in the time series of Figure 3.6-b and -c. This result is consistent with the average values shown in the previous figures.

3.3 Slope-crest linear regression

If the wind is blowing over the hill, it is expected that, for continuity reasons, the wind speed at the slope and at the crest will be significantly correlated. Linear regression

analysis were performed for pairs of slope-crest levels of wind speed to check for any interdependence between these heights. Indeed, the linear regression (not shown) done for the heights over the canopy at the crest and at the slope revealed a good correlation between these levels, with more than 80 % of the variability of the wind speed at 35 m at the slope being explained by the wind speed at 30 m at the crest ($R^2 = 0.84$).

The linear regressions for the levels below the canopy are shown in Figure 3.7-a and -b. The slope-crest pairs of measurements at 2 and 1.5 m and at 8.5 and 8.8 m were analyzed using the data measured from April to June of 2006. Situations with the strongest winds were selected based on the value of U_{SW} at the top of the main tower (U_{30}). The regression analysis for the half-hourly values when U_{30} was higher than 6 ms^{-1} were plotted as red filled squares in Figure 3.7-a and b.

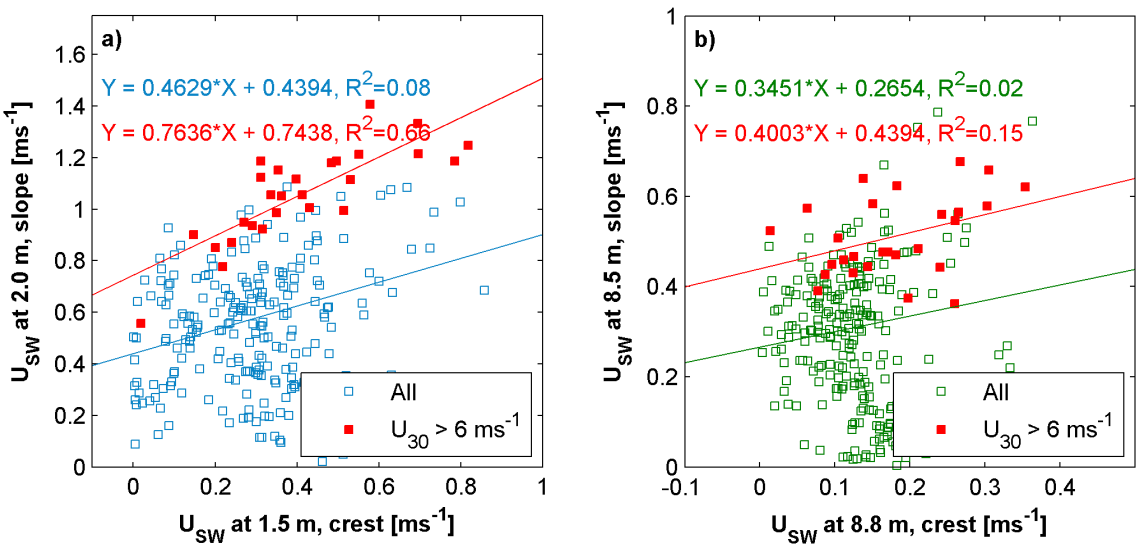

Figure 3.7: Wind speed linear regression between slope-crest pairs of heights, for data as in Figure 3.4. Red points for situations when the wind speed at 30 m at the crest was higher than 6 ms^{-1}. **a)** Southwest component of wind speed U_{SW} at 2 m at the slope versus U_{SW} at 1.5 m at the crest. **b)** Same as a), for the pairs at 8.5 and 8.8 m, at the slope and at the crest, respectively. Note the smaller axis limits in comparison with Figure **a)**.

In fact, a significant correlation was found for the lowest pair of slope-crest heights when $U_{30} > 6$ ms^{-1} (red squares in Figure 3.7-a). This is explained by the balance of forces at these conditions. The high values of U_{30} generate strong inertial forces above the canopy. After being partially absorbed by the canopy drag, these forces are still relevant below the canopy, pushing the air up the hill. Finally, the pressure

force induced by the pressure gradient across the hill (Finnigan and Belcher, 2004) also contributes to push the air in the upslope direction. On the opposite direction, the gravitational force pushes the air downwards. For sufficiently strong winds the upslope forces dominate both above and below the canopy. Such forces blow the air over the hill and promote sub-canopy flows both at the crest and at the slope.

The lack of correlation between the wind speeds at 2 and 1.5 m when $U_{30} \leqslant 6$ ms^{-1} is related to the weak forcing by the pressure gradient between the crest and the slope at these conditions. These two heights are only correlated for values of U_{SW} higher than a threshold for each level of wind speed, as shown in Figure 3.7-a: the points with a good correlation are those when U_{SW} is higher than ≈ 0.8 and 0.2 ms^{-1} at the slope and at the crest, respectively. This indicates the value of wind speed when the balance of forces below the canopy at the slope is reversed, being dominated by the uphill components.

For the levels above 8 m in Figure 3.7-b the correlations are not significant. The high absorption of momentum by the canopy imposes lower values for U_{SW} (note the smaller axis limits) and dump the correlations between the crest and the slope even when $U_{30} > 6$ ms^{-1}.

It should be noted, however, that the correlation between the red squares in Figure 3.7-a does not imply causation between these two levels. As can be seen in this figure, the wind speed below the canopy at the crest and at the slope is lower or ≈ 1 ms^{-1}. In this case the air would take approximately 15 min to travel from one tower to the other ($\approx$ 900 m distant). This delay would obviously compromise any correlation between the half-hourly values. Instead, the wind speed at the sub-canopy spaces at the crest and at the slope are most probably indirectly related, influenced by the large-scale features of the flow passing over the hill.

3.4 Discussion

The analysis of vertical profiles of wind speed for the Wetzstein site has confirmed for the first time experimentally the results from the modeling work of Finnigan and Belcher (2004). According to the model, the flow below the canopy at the upwind side of the ridge should be accelerated, as a result of the pressure gradient induced by the flow passing over the hill. Indeed, this result was confirmed by observing that the wind speed at the sub-canopy space was consistently higher at the tower located at the upwind side of the hill.

Additionally, it was found that the wind velocities, at the sub-canopy space, at the crest and at the slope, were significantly correlated for strong southwesterly winds, for values of U_{SW} at the slope higher than a threshold. This result suggests that sub-canopy flows take place simultaneously at several parts of the hill during these conditions, contributing to advective fluxes of scalars, as found, for example, by Katul et al. (2006).

The results from the current chapter confirm the existence of sub-canopy flows at the Wetzstein site. Such transport of scalars as CO_2 is most probably associated with advective fluxes, as supported by the modeling works of Finnigan and Belcher (2004) and Katul et al. (2006) and measured by Feigenwinter et al. (2007). The existence of sub-canopy flows at this site emphasizes the importance of advective fluxes of CO_2 for forests over complex topographies.

Chapter 4

Wavelet Spectral Analysis

The Wetzstein site is subjected to weather conditions that impose strong wind speeds and neutral stratification regimes during whole nights. Unusually high nocturnal fluxes of CO_2 are frequently observed during these situations (Section 5.5). In this chapter, the wavelet transform was applied to time series of w and CO_2-concentration, for nights characterized by neutral stratification and high values of friction velocity u*.

The wavelet analysis was performed using high frequency data of w and CO_2 concentration, in order to check if the high nocturnal fluxes of CO_2 are characterized by any specific spectral frequency or phenomena, such as local circulations or coherent structures. For a matter of comparison, the analysis was applied as well to data measured during stably stratified nights with lower values of CO_2-fluxes and u*.

The turbulent flow in the Atmospheric Boundary Layer (ABL) is composed of motions of several frequencies or time scales (Panofsky, 1969; Kaimal and Finnigan, 1994). The spectra of wind components and scalars measured over flat and homogeneous terrain generally present a distinct gap separating the boundary layer turbulence from synoptic (or mesoscale) motions (Panofsky and Dutton, 1984; Stull, 1988). In the Convective Boundary Layer (CBL), such a gap is found between 10^{-3} and 10^{-4} Hz (Panofsky, 1969; Kaimal and Finnigan, 1994). Below this gap, turbulence in the form of short-lived vortices transport energy and scalars between the surface and the atmosphere.

Events with time scales higher than the spectral gap (the mesoscale motions) are associated with the mean flow. According to Raupach et al. (1996), these motions contribute little to the vertical fluxes of energy and scalars. On the other hand, some

authors have reported that these nonturbulent motions contribute to 20 to 30 % of the turbulent fluxes of heat and scalars (Sakai et al., 2001; Von Randow et al., 2002). However, according to Sun et al. (1996) and Saito et al. (2007), the mesoscale flux can be positive or negative for single half-hour values. Consequently, its global contribution is reduced when averaged over long periods.

McNaughton and Brunet (2002) proposed that mesoscale motions, part of the so-called inactive turbulence, initiate ejection and sweep events at the surface. According to these authors, such interaction between scales may be caused by pressure fluctuations above the Atmospheric Surface Layer (ASL), generating regions of subsidence and uplift. In each of these regions, the sheer generated by the faster air streams passing over slower streams creates roll and horse-shoe like vortices.

These vortices create ejection and sweep movements close to the surface. The ejection and sweep movements, also called coherent structures, are generally recorded as ramp-like patterns in measurements of scalar and wind speed and are associated with a significant fraction of the turbulent fluxes above the surface (Finnigan, 2000; Krusche and De Oliveira, 2004; Cooper et al., 2006; Thomas and Foken, 2007b,a).

Coherent structures dominate the turbulent exchanges of energy and scalars above forests and have in general time scales on the order of 10^1 s (Gao and Li, 1993; Chen et al., 2004; Thomas and Foken, 2005, 2007b). In contrast, larger-scale circulations or gravity waves are generally characterized by time scales in the order of several minutes (Sakai et al., 2001; Turnipseed et al., 2004; Thomas et al., 2006; Zhang et al., 2007).

Spectral analysis makes it possible to find individual contributions of different time scales to the total energy of a time series. This decomposition can be performed by Fourier or Wavelet transforms, among other techniques. The latter has the advantage of providing information about the evolution in time of distinct time scales of a signal.

Additionally, a global spectrum is obtained if the contributions by scale are summed. In this chapter, the cospectra of turbulent signals from the Wetzstein site were investigated using the wavelet analysis, described in Section 2.3.3. The cross wavelet transform of w and CO_2 was calculated using the MATLAB® scripts provided by Grinsted et al. (2004).

4.1 Data and Methodology

The data selected for this task was measured in August 2005, the period of the year when the highest nighttime fluxes of CO_2 are generally observed. Continuous periods of two hours were used to ensure that several events with time scales up to several minutes could be enough sampled. On the other hand, a linear trend was removed from the composed signals, in order to filter out diurnal trends occurring at time scales that could not be resolved by the limited period of two hours.

After that the original sampling frequency of 20 Hz was reduced to 1 Hz to speed up the spectra computations. Additionally, the time lag introduced by the measuring system between the measurements of wind components and scalar concentrations (Section 2.3.2) was removed for every half hour before compounding the two hours signal.

Finally, in order to relate the nighttime CO_2-fluxes with cospectral characteristics, the turbulent fluxes were also calculated using an averaging period of two hours (C. Rebmann, personal communication). The resulting CO_2-fluxes were plotted respectively in each global spectrum presented in Section 4.3.

In the next section two examples of nighttime periods with high and low CO_2-fluxes, respectively, were compared using the cross wavelet analysis. In Section 4.3 this comparison was extended to several periods with similar conditions; the wavelet cospectrum was used to compare the turbulent and calm nocturnal periods. The Morlet function was used as the mother wavelet in both cross wavelet and cospectra analysis since this function provides a good localization in time and frequency of events in a time series (Torrence and Compo, 1998; Grinsted et al., 2004; Thomas and Foken, 2005).

4.2 Cross wavelet transform of w and CO_2-concentration

An example of a nighttime period with strong turbulent activity and high CO_2-flux is shown in Figure 4.1. The CO_2-flux for this period was estimated to be 12.1 $\mu molm^{-2}s^{-1}$, while the friction velocity u* was 0.74 ms^{-1}. The time series in the two topmost plots are the departures from the mean of w and CO_2 concentration. These two signals were

used in the calculation of the wavelet cross spectra (Grinsted et al., 2004), which is shown in the periodogram at the bottom.

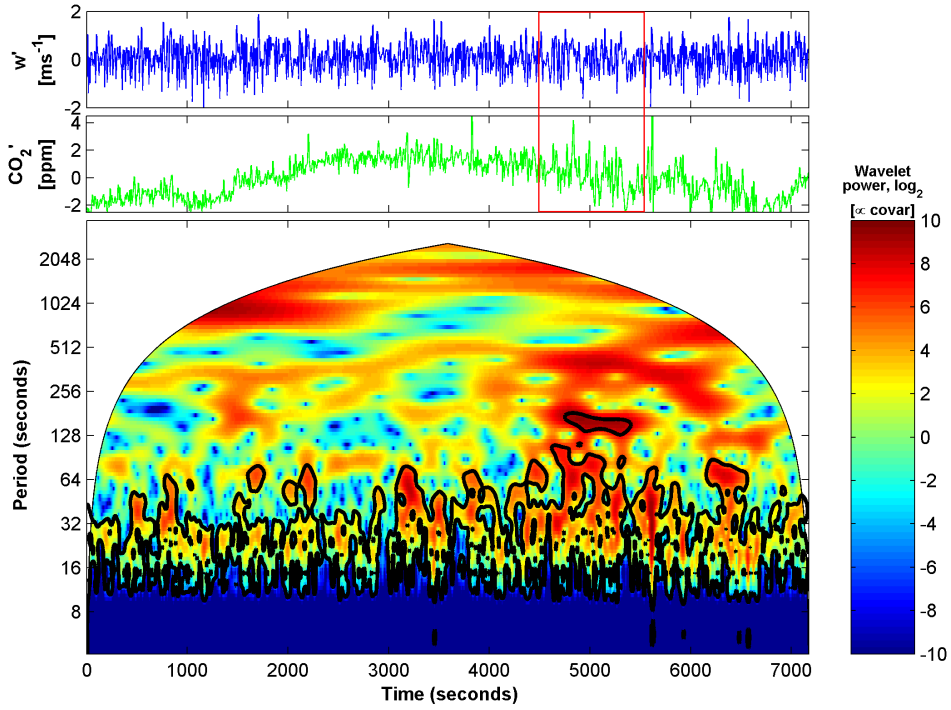

Figure 4.1: Departures from the mean of w and CO_2 concentration (top) and periodogram (bottom) for a turbulent period at DOY 224, from 20 to 22:00 h. Sampling time in the horizontal axis and time scale of events in the vertical axis of the periodogram. The colors denote the wavelet power, which is proportional to the covariance $\overline{w'C'}$. The black contours enclose the areas where the wavelet power is higher than a red noise background, with a confidence level of 95 %. The region enclosed with the red line at the top is zoomed in Figure 4.3-left.

A periodogram makes it easier to check the evolution in time of specific frequencies (or time scales) of a signal. In such a figure, the time scales are decomposed along the periodogram's vertical axis. The periodogram shows the decomposition of the combined evolution of the signals of CO_2 concentration and vertical velocity w. The color axis represent the wavelet power, which is proportional to the covariance $\overline{w'C'}$

In the periodogram of Figure 4.1 the most significant contributions to the wavelet power are enclosed by black contours. These are the regions of the periodogram where the wavelet power is higher than a red noise background with a confidence level of 95 %. Two patterns are seen inside the contours: an almost periodic portion of the wavelet power below $\approx$ 32 s; and intermittent patches above 32 s, as seen by the scattered occurrence of coherent episodes above this time scale. Additionally, the

contribution to the covariance is higher for time scales above 32 s, according to the higher wavelet power (dark red) for the non-periodic events.

Thomas and Foken (2007b) analyzed the wind vector, the sonic temperature, and the CO_2 concentration, among other variables, and found the temporal scales associated with the organized motions in a tall spruce canopy at the Weidenbrunnen-Waldstein site, in Bavaria, Germany. The authors found that the time scale of coherent motions for the vertical velocity signal above the canopy ranged from 20 to $\approx$ 24 s. The organized motions for CO_2 concentration ranged from 26 to $\approx$ 32 s, depending on wind direction and height above the canopy.

The duration of the events below 32 s in Figure 4.1 agree with the typical time scales of coherent structures above forests (Collineau and Brunet, 1993a; Thomas et al., 2006; Thomas and Foken, 2007b). However, the dominant time scales in the periodogram of Figure 4.1 are the result of the *combined* evolution of the vertical velocity w and the CO_2 concentration. Thus, it follows that the organized motions in these signals have a similar duration, as can be seen in the zoomed region of Figure 4.3-left.

Events with time scales on the order of several minutes are most probably associated with the strong mechanical turbulence created by motions such as roll vortices. Such roll-like motions are commonly observed in the flow above forests during conditions of high turbulence.

These vortices are caused by dynamical instabilities in the flow and generate strong mixing at the surface layer. The interaction with lower time scales occurs by the initiation of ejection and sweep patterns that penetrate the canopy, contributing to the turbulent exchanges of energy and scalars (Raupach and Thom, 1981; McNaughton and Brunet, 2002; Cooper et al., 2006). The non periodic occurrence of such motions cause the time series to become non stationary, causing uncertainties in the turbulent fluxes calculated for these periods.

The importance of these time scales to the turbulent fluxes of CO_2 will be discussed in detail in the next section, where the cumulative cospectrum (the ogive function) was calculated for several nighttime periods of two hours measured at similar conditions as in Figure 4.1. The evolution of the ogive function for these periods revealed the relative importance of the motions with time scales of several minutes to the CO_2-fluxes calculated for the Wetzstein site.

A situation with a lower level of turbulence as well as lower CO_2-flux was selected

for comparison (Figure 4.2). This example is from day of year 216, from 20 to 22:00 h, when u* was 0.30 ms^{-1} and the CO_2-flux F_C was 4.3 $\mu molm^{-2}s^{-1}$.

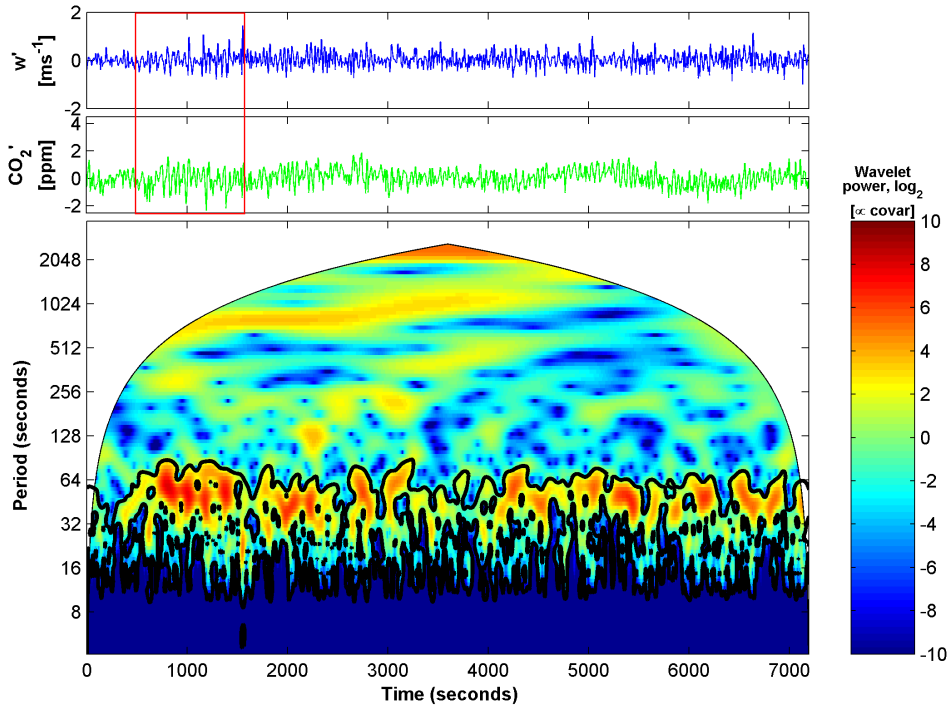

Figure 4.2: Same as Figure 4.1, for a calm nocturnal period at DOY 216, from 20 to 22:00 h. The region enclosed with the red line at the top is shown in detail in Figure 4.3-right.

The level of turbulence for the period shown in this figure is much lower, as indicated by the smaller amplitude of the fluctuations in the high frequency data. As a consequence, the lower covariance between w and CO_2 concentration leads a lower wavelet power.

The highest contributions to the wavelet power in Figure 4.2 are periodic, in contrast to the intermittent features observed for the turbulent period in Figure 4.1. Moreover, these periodic contributions are restricted to time scales between 32 and 64 s. The different turbulent motions for the calm and turbulent periods are shown in detail in the excerpts zoomed in Figures 4.3-left and right.

Discussion

The turbulent regime for nighttime periods is modulated by the intensity of the stable stratification (Cava et al., 2004). The vertical transport of scalars is dominated by

organized motions as the nocturnal conditions are closer to neutrality. Indeed, the period in Figure 4.1 was neutrally stratified (ξ = 0.017), leading to the strong turbulent fluctuations observed for both w and CO_2 in the topmost graphs. Large departures from the mean are seen for both w and CO_2 in the zoomed region of Figure 4.3-left.

Slightly stable surface layers also cause the vertical transport of scalars to be dominated by organized motions. This is evident by the occurrence of periodic patterns in the periodogram of Figure 4.2 or in the ramps observed in the zoomed region of Figure 4.3-right. Indeed, the period shown in these figures was characterized by a moderate value for the stability parameter (ξ = 0.3). However, the ramps observed in Figure 4.3-right have lower amplitudes than the figure to the left, resulting in lower turbulent fluxes.

The comparison performed in the current section has shown that the higher CO_2-flux observed for the neutrally stratified period is caused by a higher level of turbulence, in comparison with the calm and stable period. Although this is an expected result regarding the nocturnal turbulent regimes, it does not explain the source of the CO_2 exchanged vertically by the coherent patterns. This topic will be further discussed in the next section.

Additional stable and neutral periods will be investigated in the next section, in order to better characterize the different turbulent regimes at the Wetzstein site. The analysis will be performed by comparing the general shape of the wavelet cospectrum for turbulent and calm nighttime conditions. The influence of turbulent and non turbulent motions during situations with high CO_2-fluxes will be discussed.

4.3 Wavelet cospectra of nocturnal CO_2-fluxes

Wavelet cospectra (Section 2.3.3) of nighttime w and CO_2 signals were calculated for different periods of two hours to check if the patterns observed in Figures 4.1 and 4.2 are generally observed for similar conditions. Data from nights with high turbulent activity were selected based on the micrometeorological situations typically associated with high nighttime fluxes of CO_2 (Section 5.5). The wavelet cospectra obtained from these data were compared with cospectra from calm nights.

The cospectra for several turbulent periods of 2 h from nights with high values of CO_2-flux are shown in Figure 4.4. The selection of these situations was based on

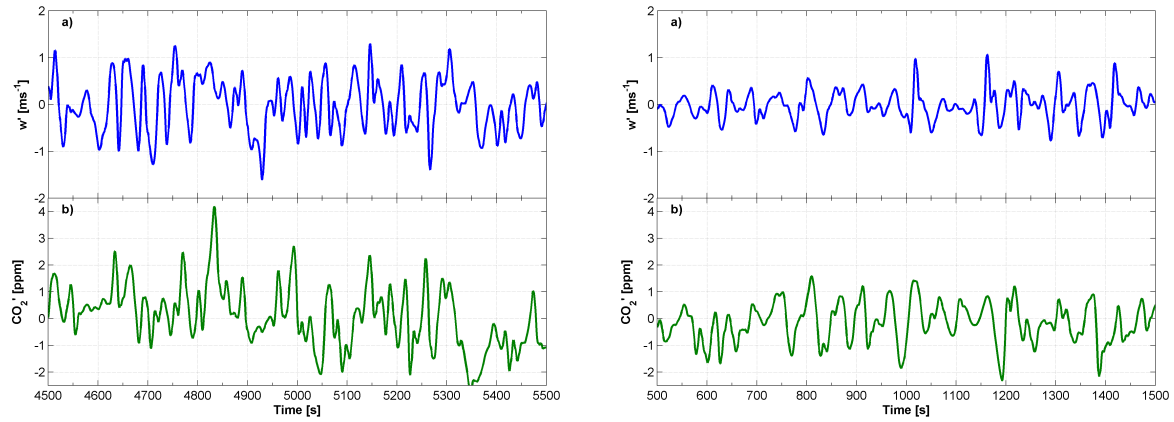

Figure 4.3: Left: Excerpt from Figure 4.1, from 4500 to 5500 s. Turbulent fluctuations observed in the signals of w and CO_2-concentration are stronger than the fluctuations observed during calm conditions (figure to the right); **Right:** Excerpt from Figure 4.2, from 500 to 1500 s. Turbulent fluctuations have lower amplitude when compared with the neutral period the figure to the left.

the following criteria: shortwave incident radiation S$\downarrow \leqslant 10$ Wm^{-2}; friction velocity u* higher than 0.6 ms^{-1}; and wind direction θ according to $180 \leqslant \theta \leqslant 280$ or $0 \leqslant \theta \leqslant 60$.

In every sub-figure the blue curve represents the wavelet cospectrum, calculated by summing up horizontally the wavelet cross spectrum as, for example, the ones displayed in the periodograms of the previous section. The dashed green line is the ogive function, i.e., the cumulative sum of the wavelet cospectrum (Sun et al., 2006c; Foken et al., 2006; Mauder et al., 2007). In this work the sum was performed on the absolute value of the cospectrum, in order to have a relative measure of the total sum by time scale. The time scale at which the sum reaches 90 % is marked with a red square.

The time scale is shown in *seconds* at the lowest figures and in *minutes* at the top axis of the topmost sub-figures. The commonly used averaging period of 30 min is marked with a red vertical line in both axis. Additionally, the CO_2-flux F_C, the friction velocity u*, and the stationarity test ST are shown in every graph. These values were calculated for each run using an averaging period of 2 h (C. Rebmann, personal communication).

The value of ST depend on the inner variability of the time series of turbulent flux. It is determined according to Foken and Wichura (1996) (variability inside parenthesis): 0 for stationary flux (0-30 % allowed), 1 for moderate non stationarity (30 to 50 % allowed), 2 for high non stationarity (variability higher than 50 %).

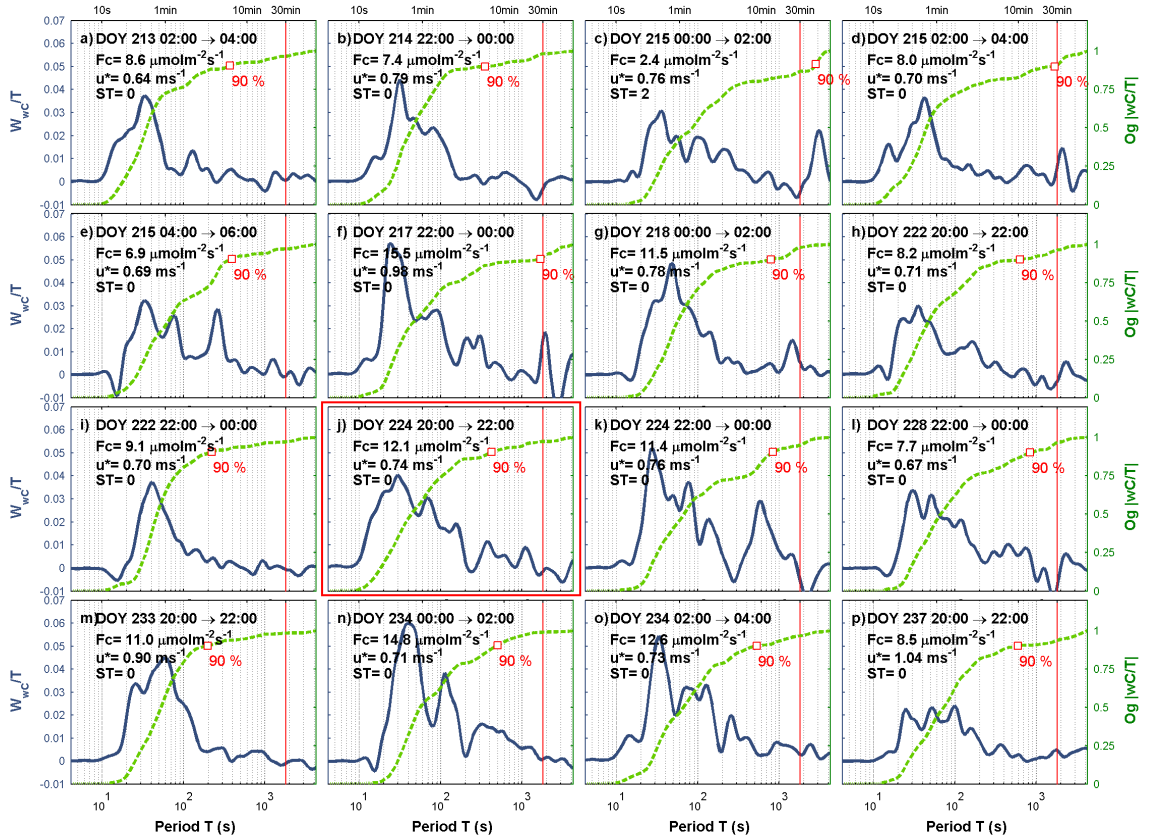

Figure 4.4: Wavelet cospectra of $\overline{w'C'}$ for nighttime periods when u* > 0.6 ms^{-1}. The highlighted cospectrum corresponds to the periodogram in Figure 4.1. The horizontal axis shows the time scale of events in seconds at the bottom and in minutes at the topmost graphs. The vertical axis to the left is related to the wavelet power spectrum (logarithmic scale); the additional vertical axis to the right relates to the cumulative cospectrum (ogive function). The values of the CO_2-flux F_C, the friction velocity u*, and the stationarity test ST were calculated for each 2 h period.

The general pattern observed for all cospectra in Figure 4.4 is the occurrence of a broad peak ranging from 20 to ≈ 100 s. Although some of the cospectra are characterized by a single peak, as in sub-figure **i**, the majority of the curves in Figure 4.4 present a superposition of two or more maxima below 100 s, as in sub-figures **b** and **j**. The ogive function reached the sum of 90 % around 500 s on average.

Peaks between 100 s and 30 min were also frequently observed, as in sub-figures **e** and **k**. This indicate the presence of slow moving vortices with time and length scales larger than the turbulent ones. These motions are caused by dynamical instabilities in the mean flow and initiate pairs of coherent events as sweeps and ejections at smaller time scales (Moeng and Sullivan, 1994; McNaughton and Brunet, 2002; Hogstrom et al., 2002; Thomas et al., 2006).

However, the majority of the CO_2-flux measured during turbulent conditions is caused by events with time scales up to $\approx$ 5 min, as evident by the evolution of the ogive function. Additionally, according to the ogive function more than 90 % of the fluxes are accounted at the time scale of 30 min. This is observed for the majority of the cospectrum in Figure 4.4.

The averaging period used in the calculation of turbulent fluxes for the Wetzstein site is 30 min. Thus, this result indicates that the averaging time usually used in the calculation of CO_2-flux for this site is appropriate, as it includes the majority of the time scales of the turbulent flow.

The existence of large vortices at time scales ranging from the spectral peak of 100 s up to 30 min makes it difficult to identify a clear spectral gap in the graphs of Figure 4.4. The spectral gap separates the turbulent motions from the mesoscale events that are associated with synoptic time scales. At this gap, the spectral contribution usually drops to zero, indicating the maximum time scale of turbulent motions (Vickers and Mahrt, 2003).

The spectral gap for the Wetzstein site during neutral conditions is approximately located around 30 min. The mesoscale contributions above this time scale were observed to be positive and negative (sub-figures 4.4-c and k, respectively). The amplitude of these events was small in comparison with the turbulent scales, contributing little to the high nocturnal fluxes of CO_2. However, few of these events can be sampled in a two hours period, introducing large uncertainties regarding its estimation.

The cospectra and ogive functions for calm nighttime situations are rather different from the ones in Figure 4.4. These nocturnal situations were selected for $u^* \leqslant 0.35$ ms^{-1} and shortwave incident radiation $S\downarrow \leqslant 10$ Wm^{-2}.

The resulting cospectra in Figure 4.5 show narrow and single peaks between 50 and 60 s only, instead of a superposition of time scales as observed for the turbulent cases. Also, on average the ogive function reaches a level of slow increase around 200 s, approximately half the time observed for the cospectra of Figure 4.4.

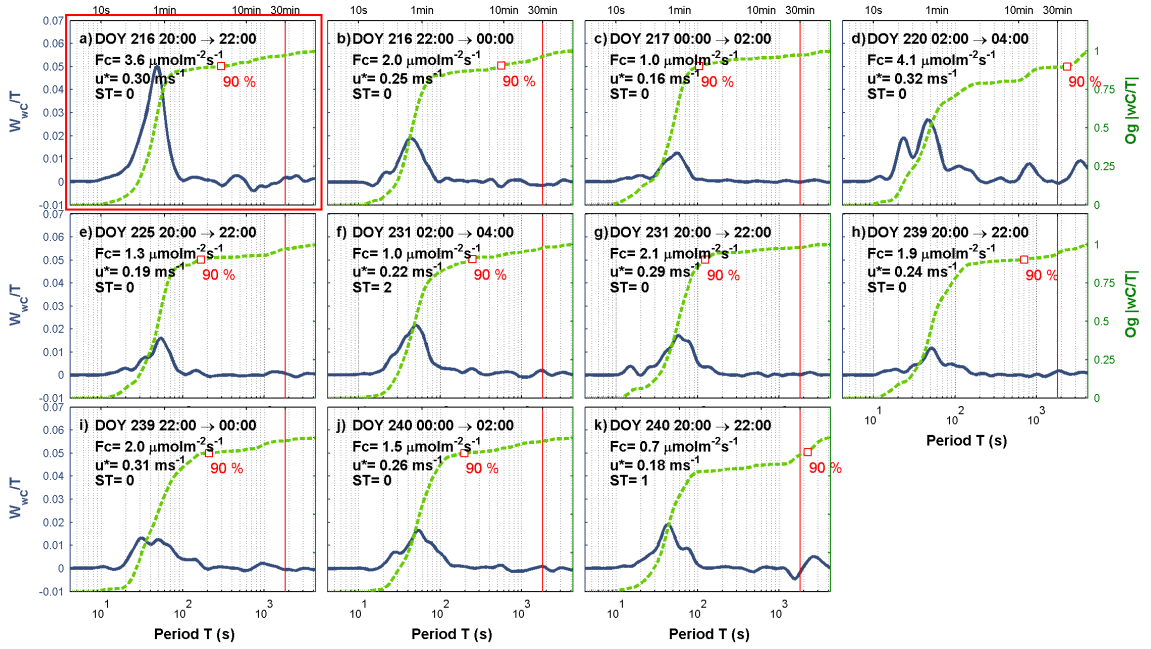

Figure 4.5: Same as Figure 4.4, for nighttime periods when $u^* \leqslant 0.35$ ms^{-1}. The highlighted cospectrum corresponds to the periodogram in Figure 4.2.

4.4 Discussion

Organized motions dominate the high nighttime fluxes of CO_2 at the Wetzstein site. The time scales observed were typically associated with coherent structures (seconds) and large eddies (several minutes). The results from the cross wavelet analysis have shown that the dominant time scales during a period with high nocturnal CO_2-flux (Figure 4.1) ranged from 20 to $\approx$ 200 s. The turbulent events during this situation were observed to be stronger and more intermittent in time than the events observed during a period characterized by calm conditions (Figure 4.2).

However, the cospectra of several similar turbulent periods presented in general a broad peak, caused by the contribution of different time scales. The usually higher CO_2-fluxes observed at these circumstances are induced by coherent motions with time scales ranging from 20 to $\approx$ 400 s. In contrast, the cospectra for calm nights with lower CO_2-flux were narrower, generally composed of single peaks at $\approx$ 50 s.

These results are in agreement with the typical enhanced turbulent activity during nights characterized by neutral conditions (Vickers and Mahrt, 2003; Cava et al., 2004). However, the source of the CO_2 exchanged vertically by these motions can not be explained by these results. Rather, as discussed in Chapter 3, the modeling work of

Finnigan and Belcher (2004) and Katul et al. (2006) supports that the flow over the hill induce sub-canopy flows.

These transport processes carry CO_2 and other scalars across the ridge. The tower footprint is then enriched with CO_2 brought from the valleys by the up-slope flows from the upwind and downwind sides of the hill. This additional CO_2 is then exchanged vertically by coherent motions of the turbulent flow.

The typical weather conditions at the site frequently induce cloudy nighttime situations, as indicate by the frequent occurrence of neutrally stratified nights (Stull, 1988). The clouds absorb and emit back the heat lost by the surface. The surface then is kept warmer than in clear sky nights. As a result, the stable stratification that is usually dominant during nighttime is weakened, due to the reduced cooling of the surface, and the atmospheric surface layer becomes neutral. The dumping of turbulence activity by stability is then avoided and motions of several sizes and time scales dominate the vertical exchanges of energy and scalars.

Neutral stratification is typically observed during the transition periods from daytime to nighttime at the atmospheric surface layer (Stull, 1988). At the Wetzstein site, though, this stratification regime is additionally observed for long periods at nighttime and daytime, induced by the overcast conditions.

Additionally, for strong wind speeds and neutral stability the flow is known to pass over the hill causing a speed-up of the wind velocity at the top and sub-canopy flows of scalars as CO_2 (Stull, 1988; Finnigan and Belcher, 2004; Katul et al., 2006). According to the results presented above, the micrometeorological tower is influenced by a combination of high availability of CO_2 at the tower footprint caused by sub-canopy transport and enhanced turbulent activity during nighttime.

In section 5.5 the nocturnal fluxes of CO_2 will be related to meteorological variables such as stability, friction velocity, and wind direction. An example of the evolution of the CO_2-fluxes in two heights above the canopy will be given. Based on these findings, a solution will be proposed regarding the calculation of annual sums of CO_2-flux.

Chapter 5

Micrometeorological Characterization

Some characteristics of the Wetzstein site are described in the following sections. Initially, the energy balance closure is compared for typical and very turbulent situations as well as for situations with different values of nighttime fluxes of CO_2 (Section 5.1). The results from the footprint analysis are presented in Section 5.2. Finally, the coupling between the wind field below and above the canopy is analyzed in Section 5.3, where the influence of different stratification regimes, wind direction, and friction velocity was assessed.

5.1 Energy balance

The energy balance closure is regarded as a test of the eddy covariance technique concerning the correct accounting of all energy sources and sinks (Mahrt, 1998; Wilson et al., 2002; Foken et al., 2004; Oncley et al., 2007). It is performed by comparing the sum of the turbulent fluxes H and LE with the available energy R_a:

$$H + LE = R_a \tag{5.1}$$

where H and LE are the sensible and latent heat fluxes, respectively. The available energy is composed of the net radiation R_n, the storage of sensible, latent, and canopy heat below the measurement height (S) and the soil heat flux G. Thus, Equation 5.1 is rewritten as:

$$H + LE = R_n - G - S \tag{5.2}$$

The storage components were neglected in this study as they generally account for a small part of the available energy (Rebmann, 2004; Foken et al., 2006; Foken, 2007). Moreover, as will be discussed next, an imbalance of $\approx$ 20 % in Equation 5.2 is commonly observed for a variety of experiments and ecosystems. This unexplained part of the available energy is called the residual, i.e., the sum of all imbalances in the terms of Equation 5.2.

Wilson et al. (2002) compared the energy balance closure for 22 sites from the FLUXNET network and found an imbalance of approximately 20 % regardless of the vegetation, topography, latitude or gas analyzer (closed or open path). The imbalances found were associated with different sensor footprints, advection of scalars, and contribution from frequencies not accounted for in the standard averaging procedures.

Oncley et al. (2007) discussed several studies that associated the energy imbalance to factors as surface heterogeneities, soil heat storage, and the choice of the coordinate system. The authors also described the results from the Energy Balance Experiment EBEX-2000, when instruments were compared side-by-side and different techniques for processing the data were evaluated (Mauder et al., 2007). A lack of closure in the energy balance in the order of 10 % was found and the horizontal advection was associated with the late afternoon imbalance.

The energy balance closure for the Wetzstein site between July and September, 2005, is shown in Figure 5.1. The linear regression analysis was applied first to all half-hourly values (left figure) and then only for situations when the friction velocity u* was higher than 0.5 m s^{-1} (right figure). For a matter of comparison the regression line was forced to cross zero in both cases. The resulting equation is seen at the top-left corner of the figures. If all situations are considered the closure is 72 %, as indicated by the slope parameter; if only turbulent conditions are selected the closure increases to 75 % (right figure).

The increase in the energy balance closure is caused by the filtering for high u* conditions, that eliminates nights with calm winds and poorly mixed surface layers. These situations are not suitable for the eddy covariance technique, as the turbulent exchange of energy and scalars is small. Still, the lack of closure lies inside the commonly reported range of 10-30 % (Wilson et al., 2002; Lee and Hu, 2002; Foken et al., 2006; Foken, 2007).

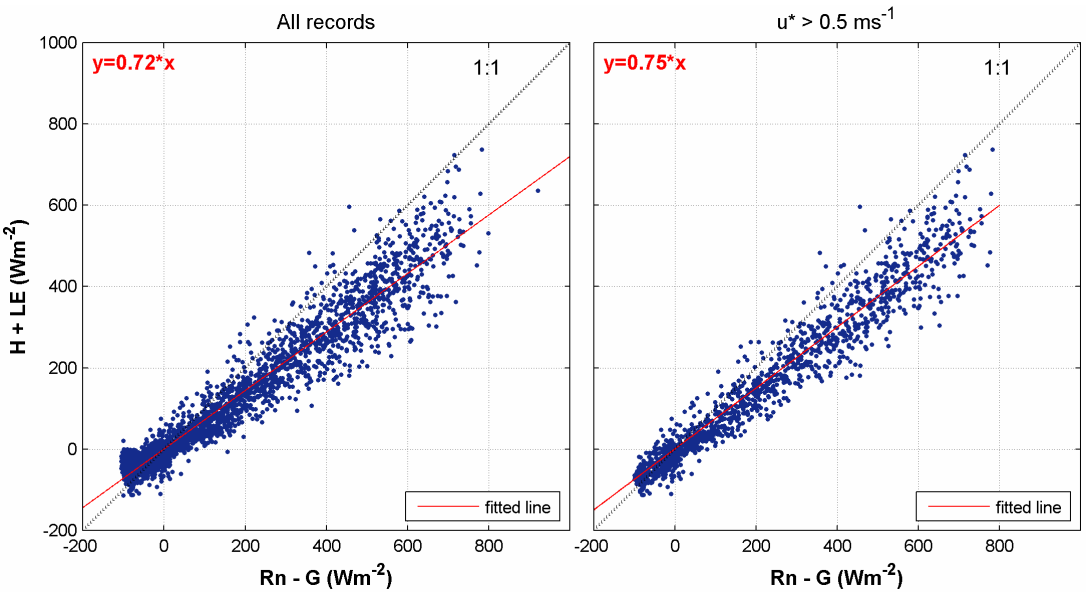

Figure 5.1: Regression analysis for the energy components between July and September 2005. Left figure: all situations; right figure: only situations with u* > 0.5 ms^{-1}. The regression line was forced to cross zero and the resulting equation is shown at the top-left corner of each figure.

The same comparative analysis was performed for nighttime situations only, as shown in Figure 5.2. The symbols in this figure are colored according to the NEE value in the respective half hour, and the color scale is shown at the bottom of the figures. The energy balance for nocturnal periods could not be assessed with confidence (Figure 5.2-left), as the large dispersion around the adjusted line indicates that there is no statistically relevant relation between the turbulent fluxes (H and LE) and the available energy (R_n - G).

In contrast, the removal of half-hourly values for u* < 0.5 m s^{-1} improved the adjustment around the fitted line and increased the significance of the energy balance closure, that summed up to 85 % (Figure 5.2-right).

The inspection of the NEE color scale in Figure 5.2-left shows that the majority of the half-hourly values with lower fluxes are grouped approximately where the sum of H + LE ranges from -75 to -20 Wm^{-2}. They are also distant from the 1:1 line, contributing strongly to the imbalance of energy. Additionally, these situations presented lower values of u*, as they were almost completely removed by the filtering of turbulent periods at the right figure.

The drainage of cold air, or gravitational flow, (Massman and Lee, 2002; Froelich and Schmid, 2006; Sun et al., 2006a) can be the mechanism that relates the imbalance of

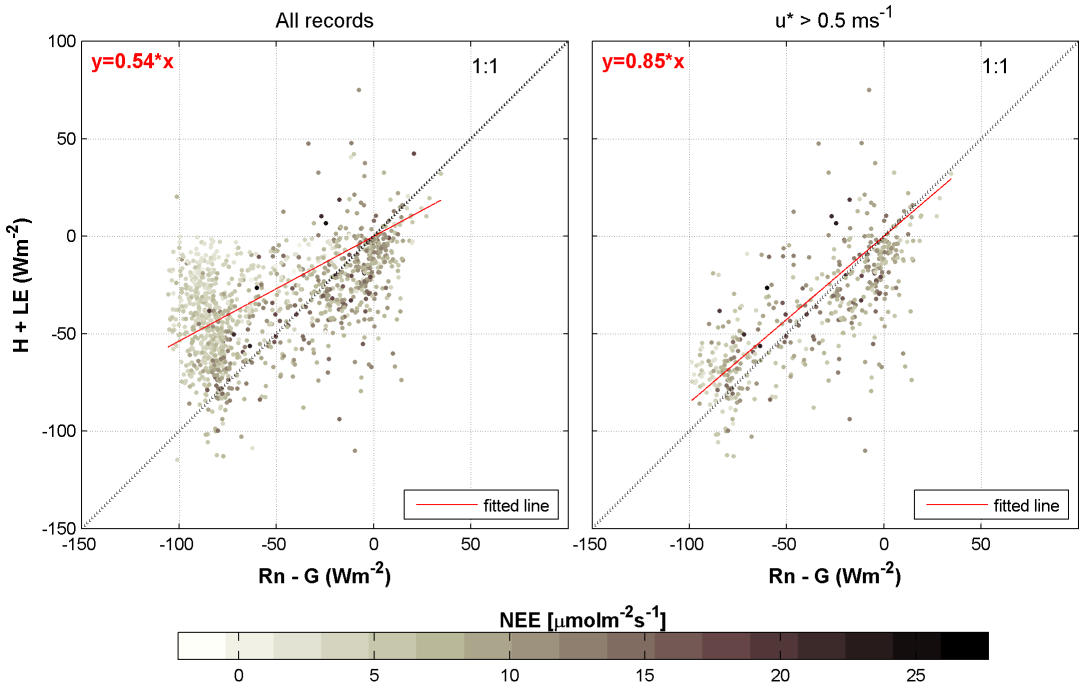

Figure 5.2: Same as Figure 5.1, but for nighttime conditions only (shortwave incident radiation, S↓, < 20 Wm^{-2}). The color scale at the bottom indicates the NEE value.

energy with the low turbulent values of nocturnal respiration. Indeed, as seen in Figure 5.2-left, the cases with lower CO_2-flux are grouped around large negative values of R_n - G and H - LE, approximately -75 and -50 Wm^{-2} respectively.

Given that LE is negligible at night, these values indicate that the surface is colder (negative H) than the air above the measurement height of 30 m. Therefore, the air close to the soil surface is cooled down and transported downhill. As a consequence, the CO_2 that would be otherwise accounted for in the storage term or in the turbulent fluxes is removed from the volume around the tower.

5.2 Footprint Analysis

The footprint is the region upwind the sensor location that influences the measurements. It is also called the source area of the turbulent fluxes measured at a given micrometeorological tower. Its calculation is dependent on the measurement height, terrain roughness, and atmospheric stability (Baldocchi, 1997; Schmid, 1997; Hsieh et al., 2000; Markkanen et al., 2003; Göckede et al., 2004, 2006). The footprint is regarded as a good measure of the area influencing tower fluxes, as confirmed

by several validation studies (Foken and Leclerc, 2004; Göckede et al., 2005). The implications for sites with complex topography will be discussed later.

The footprint analysis was applied to the turbulent fluxes measured at 30 m at the Wetzstein site. The calculations were performed using a forward Lagrangian stochastic footprint model (Göckede et al., 2006; Tiina Markkanen, personal communication). The model was originally developed by Göckede et al. (2004, and references therein) and applied by Rebmann et al. (2005) to a database of 18 CARBOEUROFLUX sites.

Data measured from April to June of 2006 were used for the current analysis. Results for periods of unstable and neutral stratification are shown in Figures 5.3 and 5.4, respectively, where the tower position is marked with a red dot. The fraction of neutral and unstable conditions was respectively 26 and 37 %, what gives a good representativity for each stratification regime.

The area that influences the measurements during *unstable* stratification ($\xi < -0.0625$) is approximately contained inside a square of 300 m enclosing the tower, as seen in Figure 5.3-a. However, the center of the area with the highest contribution is located at $\approx$ 100 m to the southwest (Figure 5.3-b), the dominant wind direction at the site. The east sector also contributes significantly during unstable conditions. The footprint lines in Figure 5.3-a cover almost 90 % of forested areas.

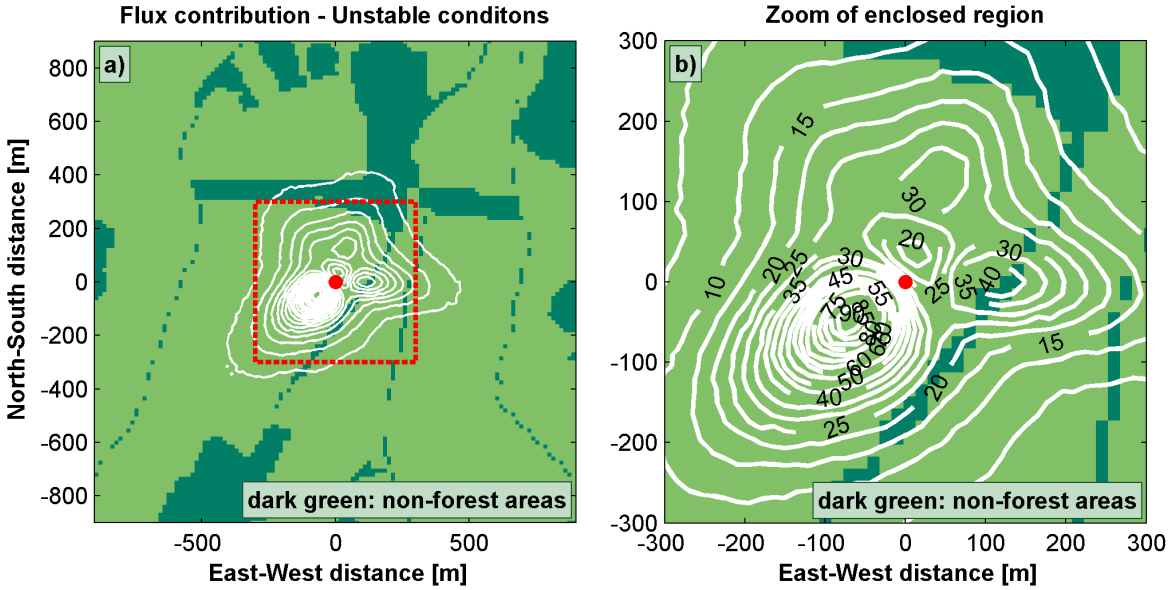

Figure 5.3: Cumulative flux footprint for unstable conditions. Tower at the red mark. Data measured from April to June, 2006.

For *neutral* stratification ($-0.0625 \leqslant \xi \leqslant 0.0625$, Figure 5.4) the footprint lines extend more strongly to the southwest in comparison with unstable situations. The east

and northeast sectors do not contribute frequently to the footprint during neutral conditions. This is explained by the fact that during these situations the site is mostly influenced by the strong southwesterly winds imposed by the local weather. The center of the area with the most frequent contribution to the turbulent fluxes is located approximately at 100 m to the southwest, the same location in comparison with unstable conditions (Figure 5.3). In Figure 5.4-a, the region enclosed by the footprint lines cover more than 90 % of forested areas.

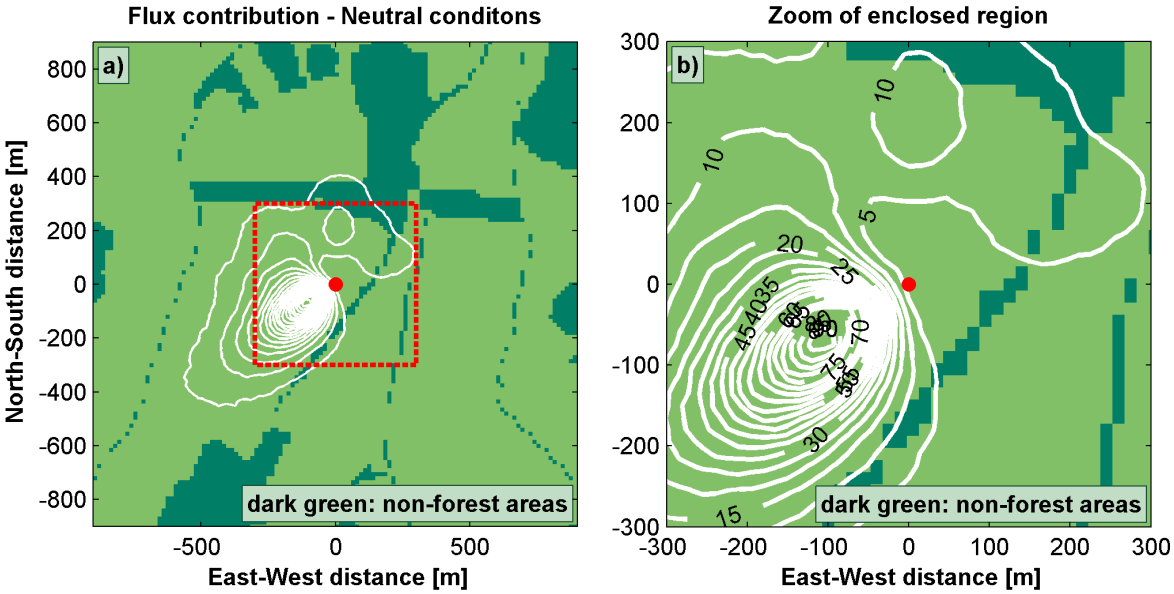

Figure 5.4: Same as Figure 5.3, for neutral conditions.

For *stable* stratification (figure not shown) the footprint region increases considerably, as stability is a main factor influencing its determination. At these situations the footprint of the tower includes more than 15 % of non-forested sectors and covers a much larger area, decreasing the representativity of the measurements regarding the local ecosystem. Anyhow, as done in general, data measured during very stable conditions are excluded and replaced by modeled values in the calculations of annual balances, due to the lack of turbulent activity during these cases (Moncrieff et al., 1997; Aubinet et al., 2000; Baldocchi et al., 2001).

The different conditions at the site were well exemplified by the results presented above since the distinct atmospheric stratifications compared were well represented. The similarities between neutral and unstable conditions were larger than the differences. For both situations the southwest sector contributed to the majority of the fluxes. However, for neutral stratifications the southwest sector contributed almost exclusively to the source area, while for unstable stratifications the east sector was also important.

It should be noted, however, that footprint models assume that the flow is horizontally homogeneous (Göckede et al., 2006), what may not be true for measurement towers over complex topography. Additionally, profiles of wind velocity components used by footprint models are approximated and generalized and do not account for site specific features. For instance, the results from Section 5.3 show that the flow above and below the canopy are decoupled during specific conditions, what weakens the validity of footprint model assumptions.

Furthermore, the wind decoupling and advective fluxes below the canopy affect the assumptions of footprint models regarding the vertical distribution of sources and sinks in the canopy space (Göckede et al., 2007). Consequently, care must be taken when interpreting the predictions from footprint models for sites over complex topography, as the model results may not be as reliable as the predictions for flat and homogeneous terrains (Finnigan, 2004).

5.3 Coupling of the flow above and below the canopy

5.3.1 Wind decoupling at the main tower

Measurements of turbulent fluxes in forests require a vertical mixing between the flow below and above the vegetation, so that the exchanges of CO_2 and other scalars are fully measured by the eddy covariance system at the top of the tower. Decoupling of the flow below and above the canopy cause the scalars to leave the ecosystem unaccounted, what leads to underestimation of turbulent fluxes.

Decoupling between the flow below and above the canopy has been reported in several studies and it is regarded as a serious problem concerning the interpretation of turbulent fluxes of CO_2, the validity of the storage correction and advective fluxes based on above-canopy measurements alone (Knohl et al., 2003; Cook et al., 2004; Iwata et al., 2005; Froelich and Schmid, 2006; Thomas and Foken, 2007a).

The coupling between the wind direction below and above the canopy for different classes of friction velocity, u*, and stratification regimes, from July to September of 2005 is shown in Figure 5.5. The two heights are poorly coupled during calm conditions (u* < 0.3 m s^{-1}, the three top figures), as also observed in other studies (Knohl et al., 2003; Froelich et al., 2005; Marcolla et al., 2005; Ruppert et al., 2006).

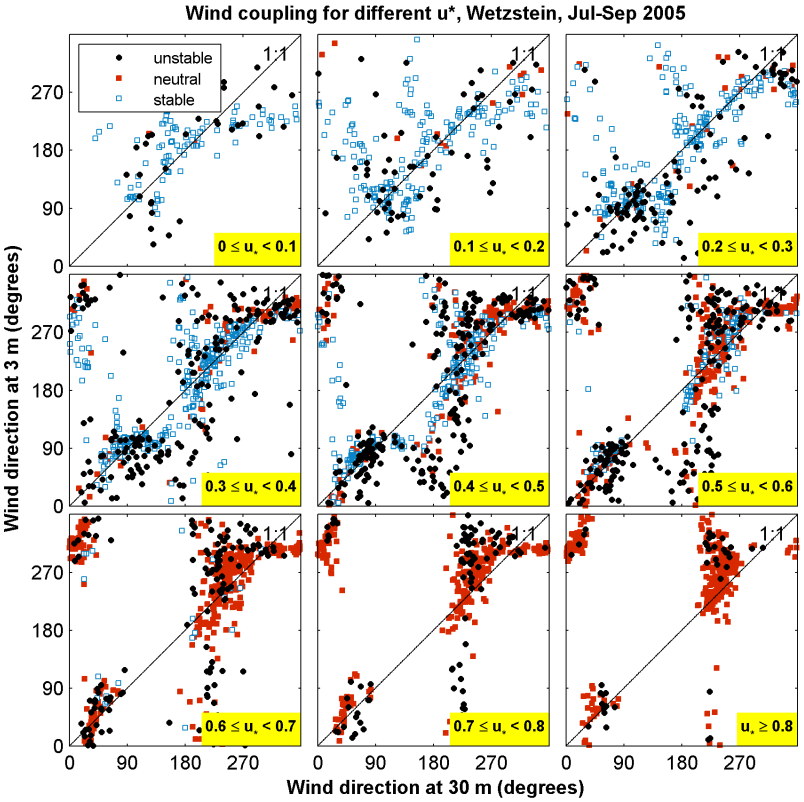

Figure 5.5: Coupling of the flow above (x axis) and below the canopy (y axis). Different symbols and colors used for different stability conditions: black circles for unstable, red squares for neutral, and blue open squares for stable stratification.

For turbulent situations a good coupling exists for wind directions between 45 and 90°, when $0.3 \leqslant u^* < 0.6$ m s^{-1} (the three middle figures). However, for the same range of u*, the flows above and below the canopy are not well coupled for wind directions between 180 and 270°. This coupling pattern is rotated counter-clockwise; also, it is dominant for higher values of u*, when neutral stratification conditions prevail (red squares).

5.3.2 Wind decoupling and reverse flow at the slope tower

Decoupling between the flows above and below the canopy was observed at the lee side of the hill, for situations with strong easterly winds. During these situations the wind direction below the canopy was reversed in comparison to the top level, implying up-slope flows. This result is supported by the general theory of flow over hills and by recent modeling works (Stull, 1988; Finnigan and Belcher, 2004; Katul et al., 2006; Sun et al., 2006a,b).

Data measured at the slope tower from April to June of 2006 were used in this analysis. The wind direction at 2 m was plotted against the wind direction at 35 m (Figure 5.6). The data were separated in classes of u* and different colors were used according to the atmospheric stratification at the top level.

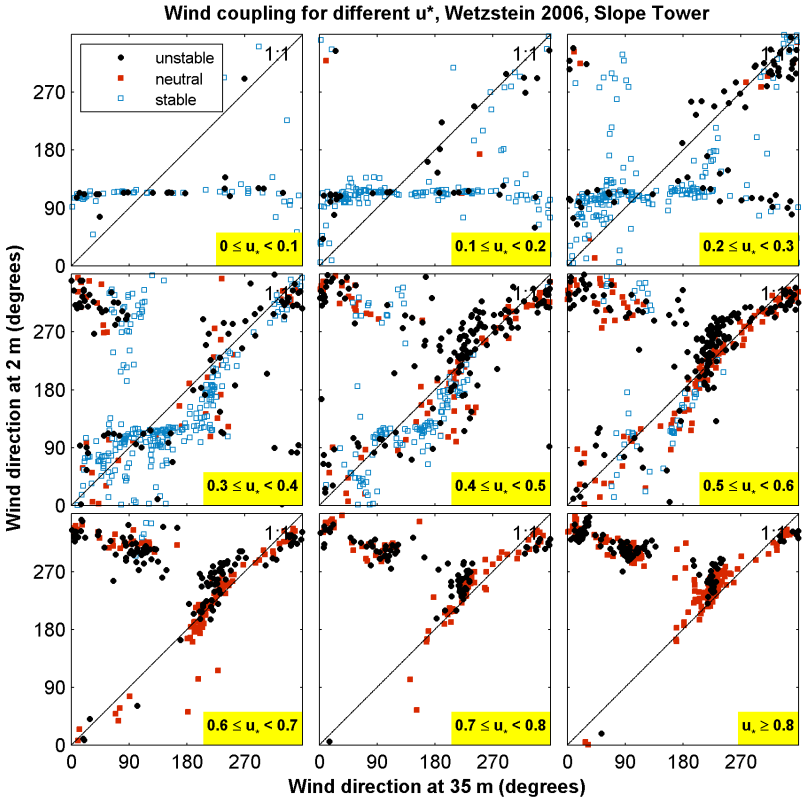

Figure 5.6: Coupling of the wind direction above and below the canopy for the slope tower. Different symbols and colors used for different stability conditions: black circles for unstable, red squares for neutral, and blue open squares for stable stratification.

The results in Figure 5.6 show that for low values of u* ($0 \leqslant u^* < 0.3$ ms^{-1} , upper panels) stable stratification dominates and a clear decoupling pattern occurs, caused by the drainage of cold air following the slope. At these situations, regardless of the wind direction at 35 m, the sub-canopy flow always blows from $\approx 120°$, the approximate orientation of the slope at this location. For intermediate values of u* (middle panels) this decoupling pattern disappears and the strong winds from southwest at the top create a shifted coupling between both levels, especially around 240°, as already observed in Section 5.3 for the main tower at the crest.

For increasing values of the friction velocity ($u^* \geqslant 0.6$ ms^{-1} , lower panels) a strong decoupling pattern appears when easterly winds blow at the top level. As the wind direction at 35 m is $\approx 90°$ the flow at 2 m is coming from $\approx 300°$ (northwest), the opposite direction. The orientation of the slope at this tower is indicated by the

topography lines of Figure 3.2 as well as by the direction at which drainage flow occurs at the top panels ($u^* < 0.3$ ms^{-1}). This result reveals the existence of a reverse flow, with an approximately opposed direction in comparison with the top level, implying the existence of up-slope flows at the lee side of the hill.

5.3.3 Discussion

The results in Figures 5.5 and 5.6 have shown that the flows below and above the canopy are not well coupled during very turbulent conditions. Low coupling between levels indicates the existence of sub-canopy flows, i.e., advection of scalars such as CO_2 below the measurement height. As a consequence, care should be taken with CO_2-fluxes measured under these conditions, if annual sum of net ecosystem exchange have to be determined.

The transport of CO_2 below the canopy and the lack of coupling with the above-canopy level leads to a lower representativity of the measurements performed above the vegetation, suggesting that the situations with high values of friction velocity should also be removed and gap filled if annual sums of CO_2 are calculated for this site. In Section 5.5 the high flux situations will be screened and an alternative filtering that includes the friction velocity, wind direction, and stratification information will be detailed.

5.4 Horizontal and vertical advection of CO_2

In flat and homogeneous terrain the net CO_2 ecosystem exchange (NEE) is estimated by accounting the turbulent fluxes and the storage below the measuring height, as expressed in Equation 2.8 (Moncrieff et al., 1997; Aubinet et al., 2000; Baldocchi et al., 2001). However, over terrain in complex topography or subjected to local circulations, the assumptions of homogeneity of the flow are not valid anymore (Stull, 1988; Kaimal and Finnigan, 1994). As a consequence, some neglected terms in the mass conservation equation become important and may be responsible to a considerable part of the exchange of scalars and energy between the surface and the atmosphere (Lee, 1998; Finnigan, 1999; Lee, 1999; Paw U et al., 2000; Aubinet et al., 2003; Feigenwinter et al., 2004; Staebler and Fitzjarrald, 2004; Marcolla et al., 2005).

In recent years some of the simplifications and approximations that led to Equation 2.5

were questioned by several studies. It has been shown that factors as local circulations, synoptic scale subsidence, and surface heterogeneity can be responsible for non zero $\overline{w}$, resulting in previously neglected advective contributions to the vertical fluxes of CO_2 (Lee, 1998; Finnigan, 1999; Aubinet et al., 2003; Kutsch et al., 2007).

The best method for $\overline{w}$ calculation, though, is still an open question in the micrometeorology community (Vickers and Mahrt, 2006). The horizontal advection, the product of the horizontal CO_2 gradient versus the mean horizontal velocity, was also found to be significant in some studies (Feigenwinter et al., 2004; Staebler and Fitzjarrald, 2004; Feigenwinter et al., 2007).

The vertical and horizontal advection terms were not included in the calculations of NEE in this work. It was expected that during the turbulent conditions associated with the high nighttime fluxes the vertical and horizontal gradients of CO_2 would be small, resulting in low values for the advection terms. Indeed, the results from the ADVEX Experiment described in Feigenwinter et al. (2007) show that the daily averaged vertical advection is small, due to a low vertical gradient of CO_2.

However, the horizontal advection was comparable to the results from the other sites, although with a lower absolute value. On average, the horizontal advection was found to be positive, being higher during nighttime. According to the convention, a positive value of horizontal advection is caused by a positive horizontal gradient of CO_2 in the direction of the blowing wind. Physically it implies that CO_2 is leaving the volume that encloses the tower.

This result contradicts the expectation of CO_2 being brought inside the volume by advection and then being measured by the eddy covariance system at the top of the tower. In this case the horizontal advection would be negative and, when summed to the other terms (the turbulent flux and the storage), would reduce the usually high nighttime value of NEE measured at the Wetzstein site.

Nevertheless, the results of Feigenwinter et al. (2007) may not be representative of the typical situation of nights with high turbulent fluxes observed at the Wetzstein site, as these conditions were not frequent during the experiment. Additionally, the scatter plot of horizontal advection versus wind direction (Feigenwinter et al., 2007) shows a maximum around 270°, a wind direction sector with relative low frequency of occurrence of high nighttime fluxes, as will be detailed in Section 5.5.

5.5 Screening of high nighttime fluxes of CO_2

High nighttime fluxes of CO_2 derived from the eddy covariance technique were already reported by Anthoni et al. (2004) for the Wetzstein site. Such unusually high respiration rates lead to reduced annual uptake of carbon dioxide (-4 $gC m^{-2} y^{-1}$, for 2002 - Anthoni et al., 2004), when compared to similar ecosystems like, for example, the Waldstein-Weidenbrunnen site, near Bayreuth, Germany (average of -91 $gC m^{-2} y^{-1}$, for 1999 - Rebmann et al., 2004).

Besides, Anthoni et al. (2004) reported that the annual NEE (CO_2-flux plus CO_2 storage) was highly dependent on the friction velocity threshold used in the gap-filling procedure and also that such high ecosystem respiration was not detected by soil chamber measurements. Additionally, the spruce stand at the Tharandt site (at 380 m a.s.l., near Dresden - Bernhofer et al., 2003) has a higher annual uptake of CO_2 (-400 to -700 $gC m^{-2} y^{-1}$, from 1996 to 2005 - Grünwald and Bernhofer, 2007), although the higher uptake may be attributed to a longer growing season at the lower elevation and differences in stand age and structure.

In the following sections the nocturnal values of CO_2-flux were considered high when they exceeded 5 $\mu molm^{-2} s^{-1}$. This threshold is supported by the modeled soil respiration and by measurements at the site. These measurements indicated that the soil respiration accounts for $\approx$ 50 % of nighttime CO_2-fluxes (F. Moyano, personal communication). Thus, as the average value of the modeled respiration between July and September of 2005 was $\approx$ 2.8 $\mu molm^{-2} s^{-1}$, the threshold of 5 $\mu molm^{-2} s^{-1}$ was a reasonable measure of the "normal" nocturnal values of CO_2-flux at the site.

The high nighttime fluxes of CO_2 measured during the summer of 2005 at the Wetzstein site were related to some meteorological variables in Section 5.5.1. Next, the nocturnal fluxes and the storage of CO_2 below the measurement height were plotted against the friction velocity u*, so that the influence of turbulence conditions on measured CO_2-fluxes could be assessed (Section 5.5.2). In Section 5.5.3 the CO_2 flux and the modeled soil respiration were examined during a period with changing weather conditions. Finally, in Section 5.5.4 the meteorological variables described in Section 5.5.1 were used to remove situations with high nocturnal fluxes that were later modeled by a gap-filling tool; the resulting annual sums of CO_2-fluxes between 2003 and 2005 were compared with the annual sums derived from the standard gap-filling approach (e.g. removal of situations with low friction velocity).

5.5.1 High nighttime fluxes of CO_2 versus micrometeorological variables

Histograms of the stability parameter ξ, the friction velocity u*, and wind direction θ were shown in Figures 5.7, 5.8, and 5.9, respectively. The histograms were calculated for three classes of nighttime NEE, as indicated by the legends in the figures, using data from July to September, 2005.

According to Figure 5.7, the situations with NEE higher than 5 µmolm^{-2}s^{-1} occur mainly during neutral stratification (-0.0625 $\leqslant \xi \leqslant$ 0.0625, delimited by the vertical red lines). These situations contribute to the majority of the nocturnal fluxes inside this range.

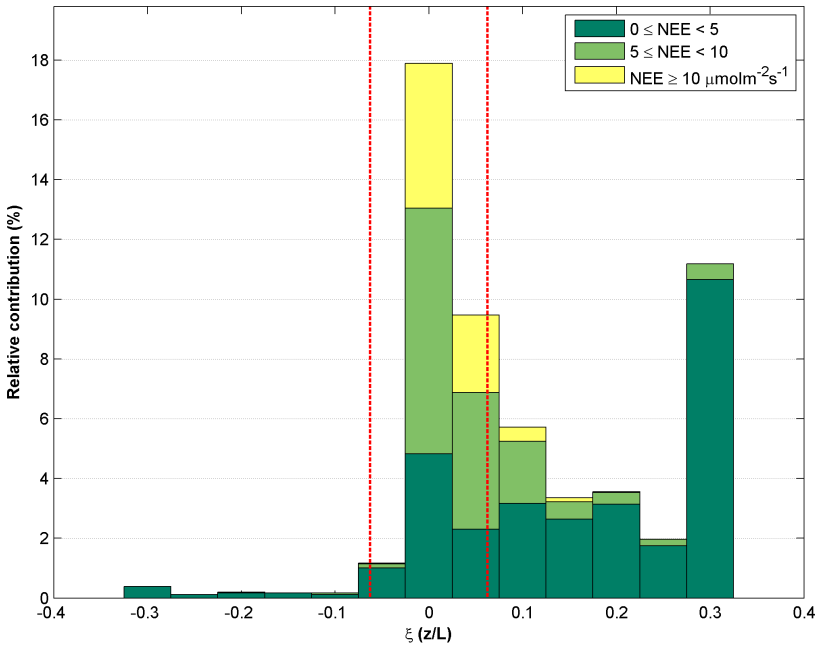

Figure 5.7: Histograms for the stability parameter ξ, for different classes of nighttime NEE. Neutral range (-0.0625 $\leqslant \xi \leqslant$ 0.0625) delimited by the red dotted line.

The histogram of the friction velocity for three classes of NEE is shown in Figure 5.8. The average for u* over all situations is marked by the vertical red line. Values of NEE higher than 5 µmolm^{-2}s^{-1} are dominant when the friction velocity is higher than the average ($\overline{u}* \approx 0.5$ ms^{-1}). On the other hand, situations with NEE lower than 5 µmolm^{-2}s^{-1} are normally distributed around u* ≈ 0.35 ms^{-1}.

Finally, according to the histogram in Figure 5.9, high nocturnal values of NEE are related to specific sectors of wind direction. The highest fluxes at the site occur

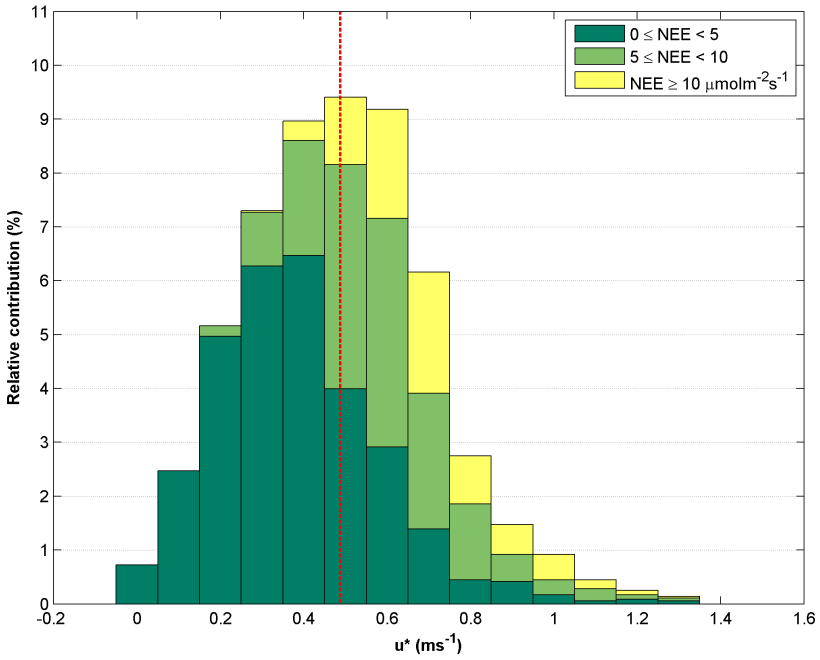

Figure 5.8: Histograms for the friction velocity u*, for different classes of nighttime (positive) NEE. Average for u* over all the points marked with the red dotted line.

in general for winds blowing from northeast and southwest. The situations with NEE higher than 5 µmolm^{-2}s^{-1} contribute to the majority of the cases when the wind direction is $\approx$ 30 or 240°.

The results presented above have shown the specific meteorological conditions associated with high nighttime fluxes at the Wetzstein site. The unexpectedly high nocturnal turbulent fluxes were found to be mainly associated with neutrally stratified surface layers, high values of friction velocity, and specific wind directions. These results are important for the Wetzstein site as they provide additional criteria for the exclusion of unrealistic situations if annual sums of net CO_2 exchange have to be determined. In general, only calm nights with low levels of turbulence are eliminated in these calculations (Moncrieff et al., 1997; Aubinet et al., 2000; Baldocchi et al., 2001). The findings from the current section were used to remove the situations with the highest CO_2-fluxes. These cases were later modeled by a gap-filling tool. The resulting annual sums are shown in Section 5.5.4.

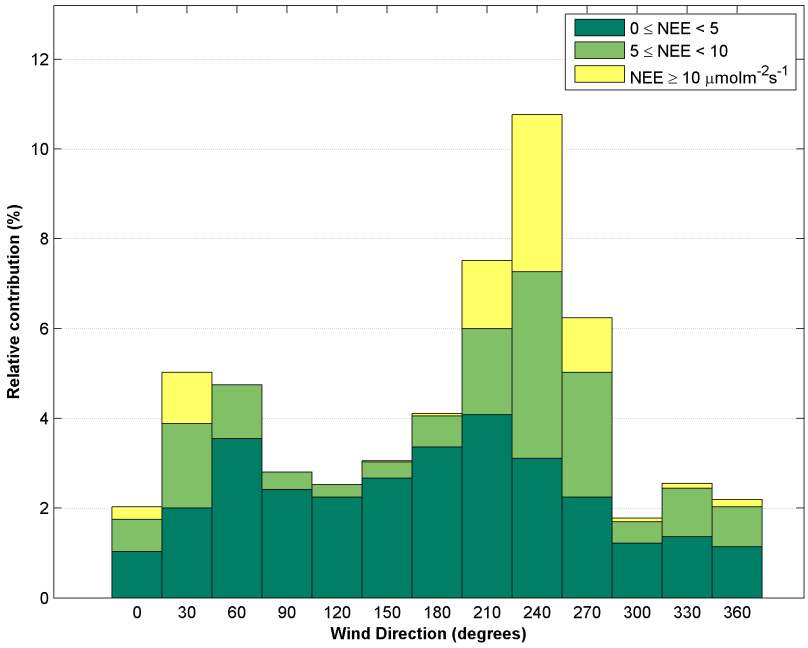

Figure 5.9: Wind direction histograms for different classes of NEE.

5.5.2 Nighttime fluxes versus friction velocity

Nocturnal CO_2-fluxes were plotted against the friction velocity u* in order to check for a possible relation between these variables. Goulden et al. (1997) reported that independent measurements of nighttime soil respiration (a large fraction of nocturnal fluxes) are in better agreement with eddy covariance data for high values of u*. As observed in other studies, the measured nighttime fluxes of CO_2 generally increase for increasing values of u* up to a site specific threshold.

Above this value of u*, the nocturnal CO_2-flux increases at a lower rate or reaches a constant level (Wilson et al., 2002). This threshold is used then as a high pass filter for values of friction velocity: turbulent fluxes of CO_2 associated with u* below the threshold are excluded and replaced by modeled values if annual sums of NEE are calculated (Gu et al., 2005).

However, some studies have reported an ever increasing nighttime CO_2-flux as the friction velocity intensifies (Massman and Lee, 2002; Anthoni et al., 2004). In this case, the threshold of friction velocity can not be objectively determined, compromising the confidence of annual sums of CO_2-fluxes, as they become highly dependent of the threshold arbitrarily chosen.

Nighttime NEE and the storage of CO_2 below the measurement height for July,

August, and September of 2005 were plotted against sorted values of u* (Figure 5.10). The CO_2 storage becomes negligible, on average, as the friction velocity decreases below 0.3 ms^{-1}. This result indicates that during these calm situations the CO_2 stored below the measurement height is probably removed from the system by non-turbulent transport such as the drainage of cold air (Aubinet et al., 2005).

In fact, the drainage of cold air during nights with low u* is evident in the weak coupling between wind directions below and above the canopy, as presented in Chapter 5.3 (top panels in Figure 5.5). These results confirm that situations with low values of friction velocity have to be removed from the calculations of annual sums, as the transport of energy and scalars are not captured by the eddy covariance system at the top of the tower.

For the filtering of low levels of turbulence activity one needs to know the threshold at which the turbulent transport is dominant. The turbulent fluxes of CO_2 at the Wetzstein site do not reach a constant level for moderate values of u*, as already reported by Anthoni et al. (2004). Indeed, a persistent enhancement of turbulent fluxes for increasing values of friction velocity is obvious in Figure 5.10. This kind of relation between the nocturnal fluxes and u* introduces an uncertainty in the gap-filling procedure, as the threshold for calm conditions is not obvious.

Measurements performed during situations with high values of u* are not representative of the local ecosystem at the Wetzstein site. The turbulent fluxes measured during these conditions are strongly affected by the mechanical turbulence that is induced by the flow passing over the hill (discussed in Chapters 3 and 4). Consequently, these situations were also considered in a gap-filling tool, resulting in annual sums of NEE that are in better agreement with the ones obtained in similar ecosystems (Section 5.5.4).

Similar results for the increase of CO_2-flux with u* were found in other studies. It was hypothesized that the high values of nocturnal fluxes of CO_2 could be caused by the "pressure pumping" effect. By this mechanism, CO_2 is released from the soil by changes in the pressure field in the canopy air-space (Massman and Lee, 2002; Staebler and Fitzjarrald, 2004; Gu et al., 2005; Wohlfahrt et al., 2005; Ruppert et al., 2006). Such changes would be originated by the penetration of strong turbulent events below the canopy.

Actually, Shaw and Zhang (1992) observed the turbulence intensity to be related to pressure changes at the ground surface. The occurrence of such effect at the Wetzstein

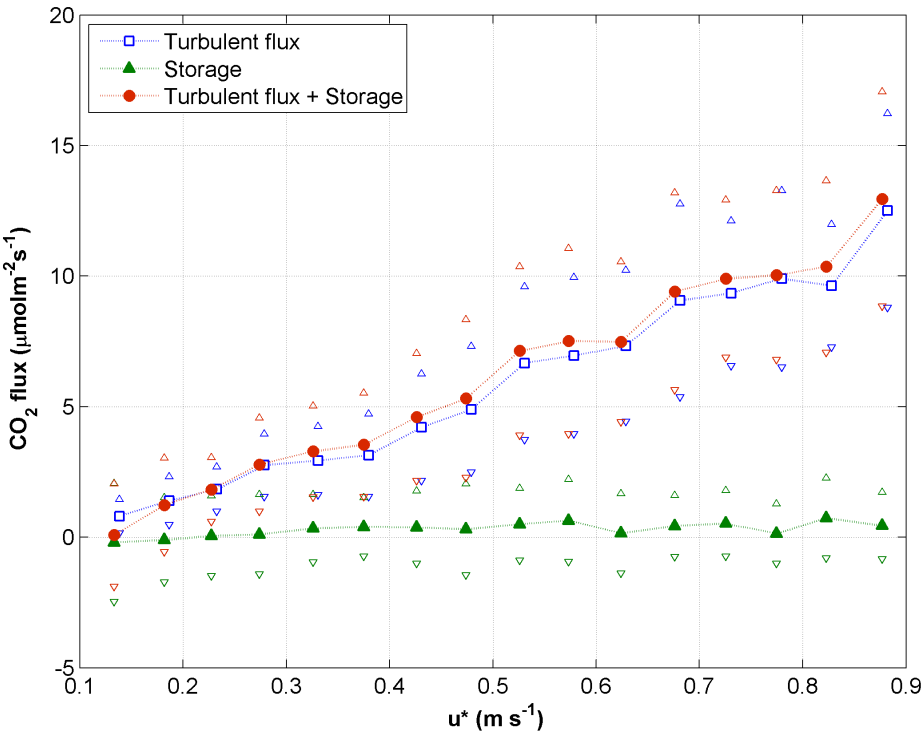

Figure 5.10: Turbulent flux and storage of CO_2 versus u*, for night-time periods in July, August, and September 2005. Night-time defined when the incident shortwave radiation is lower than 20 Wm^{-2}. Half-hourly values sorted according to u* and averaged every 0.05 ms^{-1}. Turbulent flux points displaced horizontally for clarity; standard deviation range marked by open triangles.

site was not confirmed, as it requires detailed measurements of the pressure field below the canopy. Nevertheless, as shown in Chapters 3 and 4, the unusually high nocturnal fluxes of CO_2 are most probably caused by turbulent exchanges originating from above and below the canopy as the flow passes over the hill.

5.5.3 CO_2-fluxes during changing weather conditions

The evolution of the CO_2-flux plus the storage below the measurement height during several days in August of 2005 is shown in Figures 5.11-b (DOY 223.5 to 228) and 5.12-b (DOY 228 to 232.5). The influence of the meteorological variables on the CO_2-flux, as described in Section 5.5.1, is evident during this continuous period of 8 days, as the high nocturnal fluxes are associated with southwesterly winds, neutral stratification, and high values of friction velocity (further discussed next).

Additionally, the estimated soil respiration R_e was plotted for a matter of comparison.

The soil respiration is a large fraction of the nocturnal ecosystem respiration and was used as a standard for nighttime fluxes of CO_2 during the whole period. R_e was calculated as:

$$R_e = R_{10}\, Q_{10}^{\ \frac{T_s-10}{10}}, \tag{5.3}$$

where T_s is the soil temperature in 2 cm depth, R_{10} is the soil respiration at 10 °C, and Q_{10} is the difference in soil respiration rates over a 10 °C interval. R_{10} and Q_{10} were estimated to be 2.27 $\mu molm^{-2}s^{-1}$ and 2.54 in 2005, respectively (F. Moyano, personal communication).

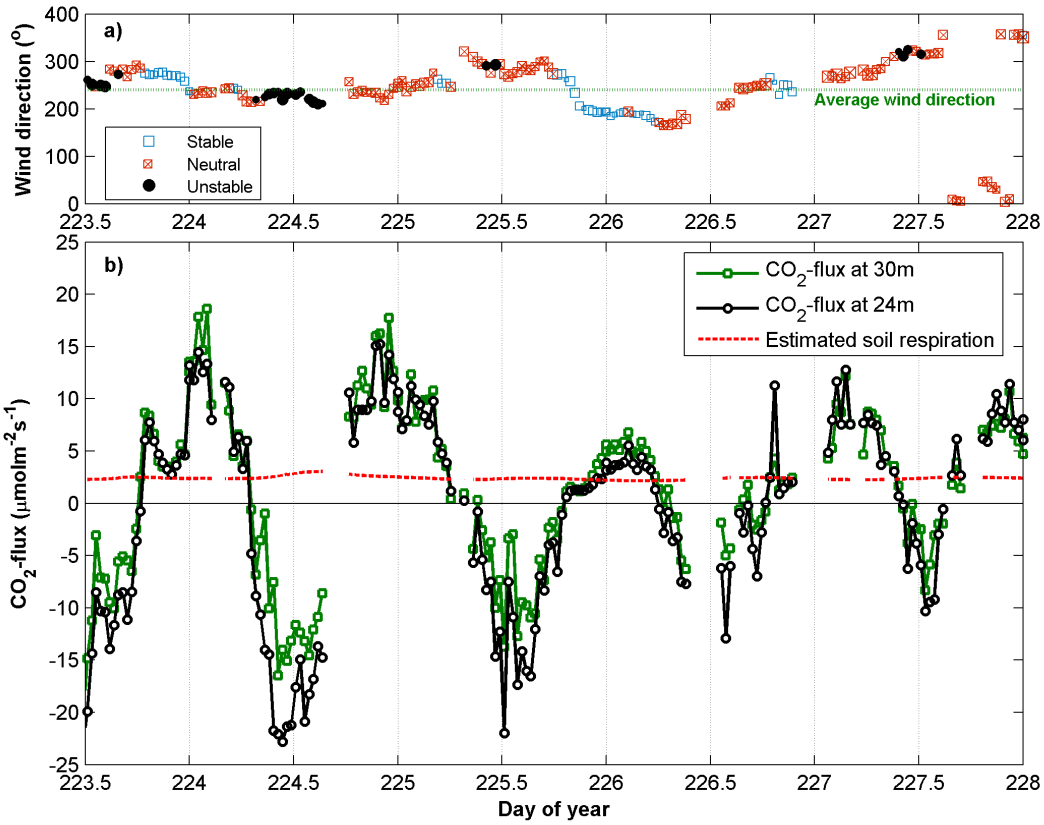

Figure 5.11: Top: wind direction at 30 m at the main tower. Different symbols were used for different stratification regimes. The symbol size is proportional to the friction velocity value. The green dotted line refers to the main wind direction. **bottom:** CO_2-fluxes at 24 and 30 m, and modeled soil respiration. The gaps in the time series indicate periods with none or bad quality data. The labels of day of year in the x axis denote midnight.

The wind direction is shown in Figures 5.11-a and 5.12-a, where the green dotted line indicates the main wind direction (southwest). Different symbols were used according

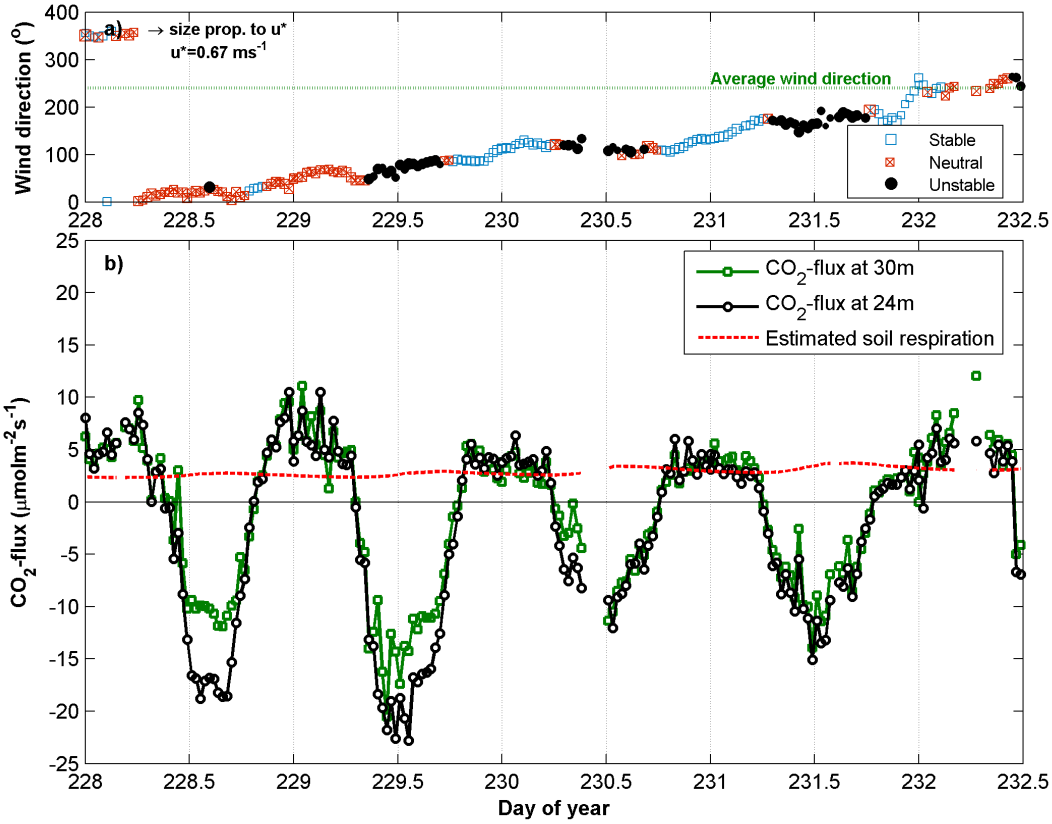

Figure 5.12: Same as Figure 5.11, for days of year 228 to 232.

to the stratification regime, as indicated in the legend of the figure. Additionally, the symbol size is proportional to the friction velocity (an example of the relation size/u* is given in Figure 5.12-a). The gaps in the time series indicate periods with none or bad quality data (according to Foken and Wichura, 1996). The labels of day of year in the x axis denote midnight.

The CO_2-fluxes at 30 m were provided by C. Rebmann (personal communication). The fluxes at 24 m were calculated using the corrections described in Section 2.3.2. The difference between the CO_2-fluxes in both heights for July, August, and September was of $\approx$ 5 %, with an offset of 0.4 µmolm^{-2}s^{-1}. However, the two levels were not significantly different during nighttime situations (positive values).

The nocturnal CO_2-fluxes presented the highest values compared to the estimated soil respiration during the nights of DOY 224 - 225, and from 227 - 229. As seen at the top-figures, these periods were characterized by neutral stratification (red squares), large values of friction velocity (large symbols), and wind directions corresponding to the southwest or northeast sectors.

The fluxes of CO_2 at both levels respond quickly to changes in the nighttime stratification regime. This was observed during the nights of DOY 223 to 224 and from 231 to 232. As seen in the top-figures, the first half of these nights were characterized by stable stratification (blue squares) and lower fluxes while the second half was characterized by neutral conditions and higher fluxes.

Neutral stability is typical during overcast conditions with strong winds and little vertical gradient of temperature across the atmospheric surface layer ASL (Stull, 1988). This was observed during the DOY 225 and 228, when neutral stratification was dominant for long periods of day and night. The association of these periods with the main wind directions at the site (SW and NE) suggests that they are probably influenced by the overcast conditions created by the passage of weather motions as cold fronts.

Conversely, neutral stratification regimes are also common in the ASL during the transition periods, i.e., at early morning and early night. This is observed in Figure 5.12-a during days of the year 229, 230, and 231. During these days neutrally stratified half-hours (red squares) are only seen between long periods of unstable (daytime, black dots) and stable (nighttime, blue squares) situations.

Finally, the CO_2-fluxes were more consistent with the modeled soil respiration during the nights of DOY 230 and 231. The CO_2-fluxes measured by the eddy covariance system during these two nights were $\leqslant$ 5 $\mu molm^{-2}s^{-1}$ while the average modeled soil respiration was $\approx$ 2.8 $\mu molm^{-2}s^{-1}$. Therefore, the turbulent fluxes during these nights were in good agreement with the expected ecosystem respiration R_{eco}, assuming that the modeled soil respiration accounts for 50 % of R_{eco}.

Measurements of soil respiration using automatic chambers were not available during the periods in Figures 5.11 and 5.12 due to technical problems. However, soil chamber measurements performed in 2003 did not confirm the high nocturnal values of CO_2-flux registered by the eddy covariance system (Anthoni et al., 2004). Further analysis should be performed using soil chamber measurements at the site in order to have an independent measure of soil respiration that can support the nocturnal eddy covariance fluxes of CO_2.

5.5.4 Annual sums of NEE

The values of u*, ξ, and wind direction associated with high nighttime CO_2-fluxes were used to remove these situations in the annual sums of NEE (Rebmann et al., in preparation). A gap-filling technique (Reichstein et al., 2005) was used to model the excluded values, resulting in the annual courses of NEE shown in Figure 5.13.

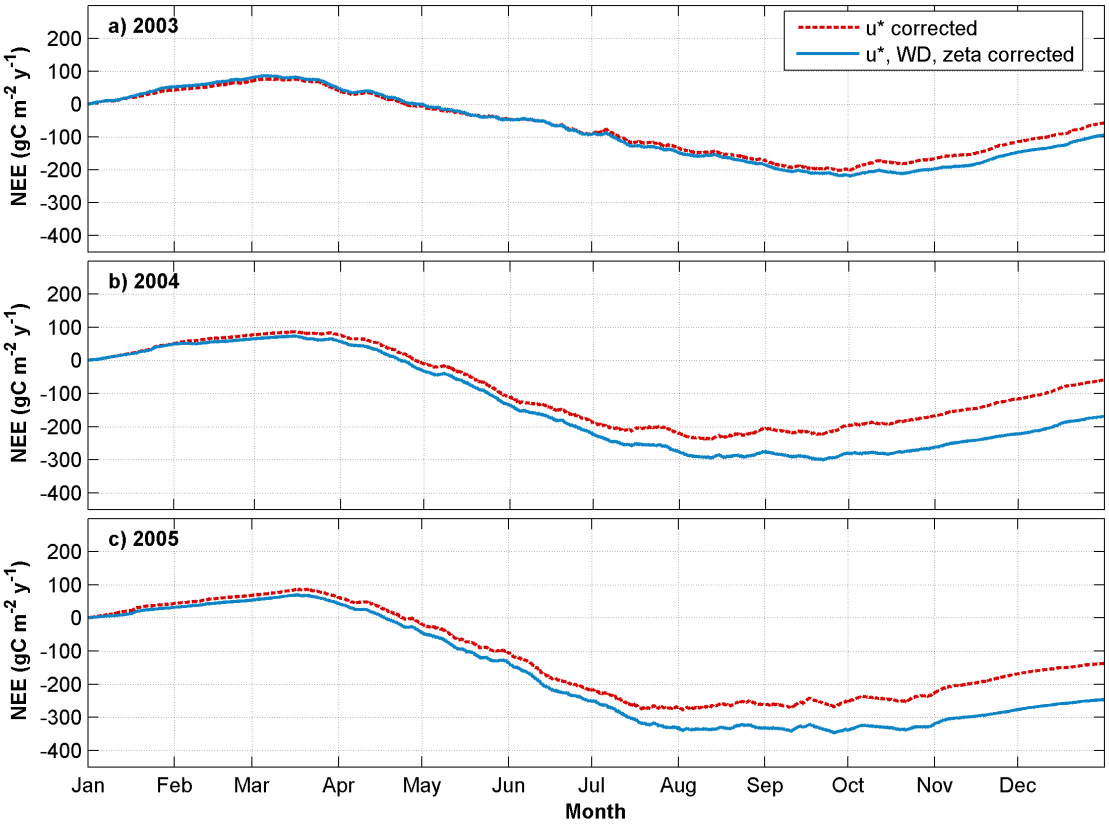

Figure 5.13: Annual courses of gap-filled NEE for 2003, 2004, and 2005. "u* corrected" stands for the annual sums derived from the standard gap-filling approach (exclusion of low u* situations only); "u*, WD, zeta corrected" stands for the further filtering for situations associated with high nocturnal fluxes of CO_2 detailed in Section 5.5.1.

The annual sums derived from the standard gap-filling approach (exclusion of low u* situations only) are plotted as red dashed lines, marked as *u* corrected*. The result from the additional exclusion of high CO_2-fluxes based on the variables described in Section 5.5.1 is plotted as a continuous blue line. It was expected that the annual uptake of CO_2 would increase, given the removal of high (positive) nocturnal fluxes. Indeed, as a result of the new approach, the annual uptake increased for the three years shown, going from -57 to -94 $gC m^{-2} y^{-1}$ in 2003, from -59 to -169 $gC m^{-2} y^{-1}$ in 2004, and from -137 to -246 $gC m^{-2} y^{-1}$ in 2005.

Anthoni et al. (2004) reported that the Wetzstein site was almost carbon neutral, as the annual uptake of CO_2 for 2002 was -4 gCm^{-2}y^{-1}. However, the authors reported relatively large uncertainties in the annual balances of CO_2-flux. These uncertainties were highly dependent on the friction velocity threshold used in the gap-filling procedure.

The annual uptake of CO_2 obtained in the current section for 2003, 2004, and 2005 represent better the Wetzstein site, as the extreme situations related to the unusually high nighttime fluxes were excluded for the determination of the sums. Although the inclusion of additional criteria in the gap-filling procedure may increase its uncertainties, the removal of these extremely turbulent conditions is justified as they most probably do not represent the local ecosystem.

Nevertheless, bottom-up results of the carbon balance led to higher values for the uptake of CO_2. NEE should be equivalent to NPP - R_h, where NPP stands for the Net Primary Production and R_h is the heterotropic respiration. NPP was estimated to be 791 gCm^{-2}y^{-1} in 2001-2002 (FORCAST Project; M. Mund, personal communication); R_h ranged from 260 to 356 gCm^{-2}y^{-1}, according to soil samplings performed at the site in 2001 (T. Persson, personal communication). Thus, the annual uptake would vary between 531 and 435 gCm^{-2}y^{-1}, much higher than the values for NEE shown above.

However, as can be seen in Figure 5.14, the annual uptake of CO_2 has been increasing since 2003, if the proposed gap-filling approach is considered. The new approach for gap-filling the time series of NEE is certainly capturing the increase in the uptake of CO_2 caused by two factors: (1) the improved growth rate of the vegetation after the thinning operation (after snow damage) that was performed at the site in 2002; (2) the recovering of the stand after the drought of 2003. Thus, this new approach should be further applied in order to compare the annual sums of NEE with the updated biomass inventory data that are soon to be released by the CARBOEUROPE-IP database.

Anthoni et al. (2004) also related the low annual uptake of CO_2 at the Wetzstein site to its high *ecosystem* respiration at 10 °C, R_{eco10}, twice as much as two beech sites compared in their study, but this was due to unrealistic nighttime fluxes. R_{eco10} for the Wetzstein site was the highest found in their study (7.8 µmolm^{-2}s^{-1}) being also much higher than the value reported by Rebmann (2004) for the nearby spruce site of Waldstein/Weidenbrunnen (R_{eco10} = 3-5.3 µmolm^{-2}s^{-1}).

Recent measurements at the Wetzstein site registered a *soil* respiration at 10 °C R_{10} of 2.27 µmolm^{-2}s^{-1} (F. Moyano, personal communication). However, this value

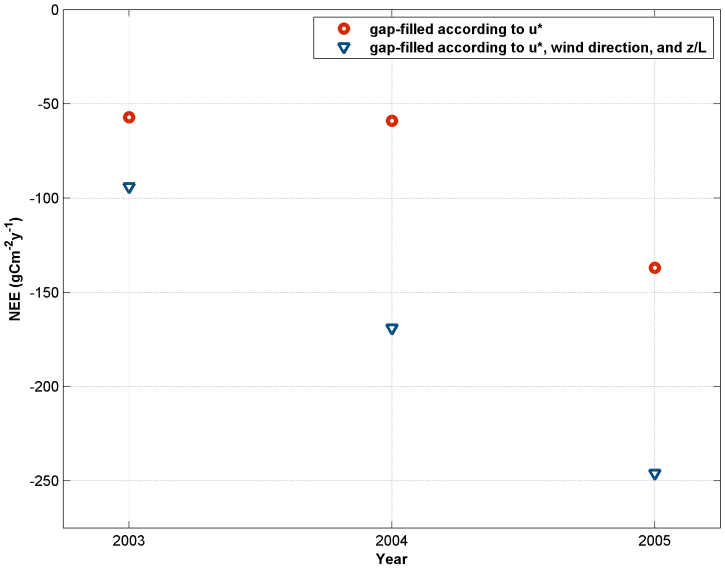

Figure 5.14: Evolution of the annual sums of NEE from 2003 to 2005.

corresponds to the soil respiration only, which is a component of the total ecosystem respiration R_{eco} (that includes contributions from soil, wood, and foliage). Thus, as the soil respiration was estimated to be $\approx$ 50 % of R_{eco}, the value of R_{10} obtained leads to a R_{eco} for the Wetzstein site ($\approx$ 5 µmolm^{-2}s^{-1}) that is comparable to the R_{eco} at the similar site of Waldstein/Weidenbrunnen.

Consequently, the high nighttime values of CO_2-flux measured at the Wetzstein site are not caused by extreme values of soil respiration. Rather, typical weather conditions at the site impose strong winds that flow over the hill, creating gradients of pressure between the crest and the slopes. These gradients induce the transport of scalars as CO_2 across the ridge. Then, the large availability of CO_2 at the crest and the high level of turbulence associated with these weather conditions create high turbulent fluxes of CO_2. These turbulent fluxes do not represent the local ecosystem, as evident in the resulting unrealistic annual sums of NEE.

Chapter 6

Conclusions

Micrometeorological characteristics associated with high nocturnal fluxes of CO_2 at the Wetzstein site were investigated in this work. The site is a spruce ecosystem located on a hill that is frequently subjected to extremely turbulent conditions. The site is subjected to strong winds and high values of friction velocity during long periods of neutral stratification. Unusually high values of nighttime fluxes of CO_2 are often associated with these situations.

As a result, the annual balance of CO_2-flux for this site is unrealistic when compared to the similar spruce ecosystem of Waldstein-Weidenbrunnen (Anthoni et al., 2004; Rebmann, 2004). Additionally, the high ecosystem respiration measured by the eddy covariance system was not confirmed by independent soil respiration measurements performed in 2003 (Anthoni et al., 2004).

The high nocturnal CO_2-fluxes were found to be caused by a combination of sub-canopy flows across the hill and high turbulent activity during neutrally stratified nights. Such stratification regimes are frequent at the site given the characteristics of the local weather. During long periods of neutral stratification, caused by overcast conditions, the atmospheric flow is forced to pass over the hill (Stull, 1988), generating sub-canopy transports of scalars as CO_2 (Finnigan and Belcher, 2004; Katul et al., 2006).

Neutral stratifications are characterized by an intense turbulent activity (Vickers and Mahrt, 2003; Cava et al., 2004). The turbulent fluxes of CO_2 at the Wetzstein site are overestimated during neutral conditions as they are related to the CO_2 brought from outside of the local ecosystem. Next, the results that led to these conclusions will

be summarized, as well as some results that helped to characterize the site during situations of high CO_2-flux.

Influence of the flow passing over the hill was found after the analysis of the wind speed and advection. The wind speed was compared for levels above and below the canopy at the main tower and at a tower installed at the slope. As a result, the wind speed under the canopy at the upwind part of the ridge was observed to be consistently higher. This result is supported by the modeling work of Finnigan and Belcher (2004). This is the first time that the predictions from this model have been confirmed by measurements.

According to the model of Finnigan and Belcher (2004), the flow below the canopy at the upwind side of the hill is accelerated by the pressure gradient forces that are created by the flow passing over the hill. As a consequence, advective fluxes of scalars as CO_2 are induced below the canopy at the upwind and lee sides of the hill, converging at the top, close to the micrometeorological tower (Katul et al., 2006).

Another important result regarding the influence of the flow over the hill on the wind speeds measured below the canopy was presented in Section 3.3. Linear regression analysis was applied to the wind speed measured at the sub-canopy spaces at the top of the hill and at the slope tower. This analysis indicated that a significant correlation exists between these levels during periods of strong winds and neutral stratification. This result revealed that the southwest component of the wind vector at the lower part of the canopy is correlated across the hill, induced by the strong inertial forces that generate sub-canopy flows.

Spectral analysis was applied to the high frequency data of vertical velocity and CO_2 concentration, in order to check for the time scales associated with high nighttime fluxes of CO_2 at the site. Several continuous periods of two hours were selected for situations with high nocturnal fluxes of CO_2. It was found that time scales ranging from 20 to $\approx$ 200 s dominate the turbulent exchanges during these nights. These events were also observed to be more intermittent than the ones at nights with stable stratification.

High levels of turbulent activity and the presence of organized motions (coherent structures) are a common feature of neutral stratification regimes (Vickers and Mahrt, 2003; Cava et al., 2004). The high nocturnal fluxes of CO_2 at the Wetzstein site are associated with coherent structures, as indicated by the dominant time scales found in the wavelet spectral analysis (Thomas and Foken, 2007b). However, recent

measurements of soil respiration did not support the high values of CO_2-fluxes measured at the site during these turbulent periods. Most probably, the CO_2 is transported by the sub-canopy flows across the hill, as indicated by the results in Chapter 3, and then exchanged vertically by coherent structures. Air parcels enriched with CO_2 from the valleys are brought to the source area of the tower and then transported upwards by the intense turbulent motions found in the spectral analysis.

Results from the energy balance closure have shown that a residual of approximately 25-28 % exists for the site, a value commonly observed in other studies of tower flux measurements. The direct influence of situations with high nighttime values of CO_2 on the energy balance was not conclusive. Instead, the removal of cases with low values of both friction velocity and CO_2-flux improved the energy balance closure for nighttime periods, as observed in other studies (Goulden et al., 1997; Wilson et al., 2002).

Calculations regarding the source area of *daytime* fluxes measured at 30 m (Chapter 5.2) have confirmed that the majority of the turbulent fluxes are influenced by forested areas located at a maximum distance of 500 m, mainly to the southwest. Neutrally stratified nights presented almost the same pattern, with a slightly stronger influence from the southwest sector. Neutrally stratified conditions, associated with high nighttime fluxes of CO_2, have a source area close to the tower, with the center of the contribution located at approximately 100 m to the southwest.

Contributions from more distant areas and different sectors of wind direction were observed for stable situations. The large source area for these cases were not relevant for the current study, as the CO_2-fluxes measured at stable nights with low levels of turbulence are generally not taken into account in the determination of annual sums. This filtering is especially important for sloping terrains, where the drainage of cold air below the measurement level cause the flow below and above-canopy spaces to decouple (Marcolla et al., 2005; Ruppert et al., 2006).

Eddy covariance measurements of turbulent fluxes of CO_2 and other scalars require that the flows below and above the canopy are coupled. At the Wetzstein site, the sub-canopy flow is not well coupled with the level at the top of the tower during very turbulent and neutrally stratified conditions. Increasing values of u* worsened the coupling between these levels. This result supports the removal of these situations if annual sums of NEE are determined, as they do not represent the surrounding ecosystem and compromise the calculation of the storage of CO_2 below the measurement height.

Low values of the friction velocity u* were associated with a weak coupling of wind direction between the levels above and below the canopy at the main tower. At the slope tower the decoupling between these levels was even stronger for situations with low values of u*. This result indicates the existence of drainage of cold air below the canopy for calm conditions. This finding support the removal and consequent gap-filling of these cases (Falge et al., 2001; Foken et al., 2004), as the lack of turbulent activity during stably stratified nights compromises the eddy covariance assumptions (Kaimal and Finnigan, 1994; Arya, 2001).

The inspection of the coupling between the wind speed below and above the canopy for the slope tower revealed a strong decoupling pattern for low levels of turbulence. This is an evidence of drainage of cold air during these periods. For high levels of turbulence, easterly winds blowing at the top of the slope tower are associated with reverse flow below the canopy, as predicted by the theory of flow over hills and by recent modeling works (Stull, 1988; Finnigan and Belcher, 2004; Katul et al., 2006).

The existence of sub-canopy flows created by the interaction between the atmospheric flow and the topography highlights that care should be taken when interpreting eddy covariance fluxes measured over complex terrains. Advective fluxes are generated by the air blowing across the hill below and above the canopy, transporting CO_2 and other scalars into the source area of the micrometeorological tower.

Sub-canopy flow generates horizontal advection of CO_2 under the canopy, as observed by Feigenwinter et al. (2007). These authors used data measured at the Wetzstein site during the ADVEX Experiment, an experiment designed to measure vertical and horizontal advective fluxes of CO_2 (Lee, 1998; Finnigan, 1999; Aubinet et al., 2003). The vertical advection of CO_2 found was not significant while the horizontal component was important during nighttime. The horizontal advection was found to be positive when averaged for all the campaign. According to the convention, the positive sign means that air enriched with CO_2 leaves the system. This result contradicts the expectation of CO_2 being transported up the hill by sub-canopy flows.

However, these results may not represent the typical situation of high nocturnal CO_2-fluxes turbulent fluxes, as such periods were rarely observed during the experiment. Some limitations of this experiment were discussed in Section 5.4. Nevertheless, the results from Feigenwinter et al. (2007) confirm the existence of sub-canopy flows at the Wetzstein site, as indicated by the results of wind coupling and wind speed under the canopy.

Finally, the screening of high nocturnal fluxes of CO_2 has shown that they occur for special sectors of wind direction, besides the neutrally stratified conditions and high values of friction velocity. These findings were used to remove the high nighttime fluxes that were then replaced by modeled values by a gap-filling tool (Reichstein et al., 2005). The annual sums obtained for 2003, 2004, and 2005 revealed a stronger uptake of CO_2, when compared with the standard approach that removes only situations with low u* (C. Rebmann, personal communication). This analysis resulted in annual sums of CO_2 that are more comparable to results from similar ecosystems (Waldstein/Weidenbrunnen – Rebmann; 2004, Tharandt – Bernhofer et al., 2003).

It is strongly recommended that the situations of high CO_2-flux described above be replaced by modeled values if annual sums of CO_2-fluxes are performed for this site. Besides the u*-filtering commonly used for replacing calm nighttime periods, it is suggested that the fluxes measured during conditions of neutral stratification and high values of u* be substituted by modeled values, as they clearly do not represent the local ecosystem. This screening should also be applied to data from previous years in order to estimate annual sums of CO_2 that would be more realistic.

Chapter 7

Summary

Nighttime fluxes of CO_2 are uncommonly high at the Wetzstein spruce site, in Thuringia, Germany (Anthoni et al., 2004). As a result, the annual sums of CO_2-flux obtained for this site are not comparable with the ones obtained at similar spruce ecosystems (Rebmann, 2004; Grünwald and Bernhofer, 2007). The site is located on a hill and subject to strong winds and high levels of turbulence for continuous periods. The unusual high fluxes of CO_2 are predominantly associated with these situations.

As reported by Anthoni et al. (2004), measurements of soil respiration performed with automatic chambers in 2003 did not explain such high ecosystem respiration. Also, recent results of soil respiration have revealed that the ecosystem respiration R_{eco} should be comparable to the value obtained for the similar spruce site of Waldstein/Weidenbrunnen (Rebmann, 2004).

According to the modeling work of Finnigan and Belcher (2004), the flow over low hills as the Wetzstein site disturbs the wind field at the sub-canopy space across the ridge. As a consequence, advective fluxes of scalars as CO_2 are generated at the upwind and lee sides of the hill. Two results from the model were confirmed for the first time in an experiment, namely (1) higher wind speeds below the canopy at the slope, when compared with the same level at the crest, and (2) the flows above and below the canopy in opposite direction at the lee side of the hill.

Besides the agreement of the measured wind field with the model results, the existence of horizontal advection was confirmed by Feigenwinter et al. (2007), using data from the advection experiment ADVEX. However, the sign of the advective flux was positive on average, meaning that CO_2 was flushed out of the control volume enclosed by the

additional towers. This result was not directly related to the high nighttime fluxes of CO_2, as these situations were rarely observed during the experiment. However, it has shown that sub-canopy flows exist at the site and should be further investigated.

The analysis of several cospectra of the vertical flux of CO_2 have shown that the frequencies, or time scales, associated with the high nocturnal fluxes are mainly the turbulent ones, typically observed for nighttime turbulent regimes. The high turbulent activity observed during neutral situations leads then to enhanced turbulent fluxes of CO_2.

High nocturnal fluxes of CO_2 were related to specific micrometeorological conditions, namely high values of friction velocity, southwesterly and northeasterly winds, and neutral stratification. These conclusions were used in a gap-filling approach as annual sums of CO_2 were calculated (Rebmann et al., in preparation). As a result of this new approach the site presented a higher uptake of CO_2 by the vegetation. Additionally, the newly found results have shown that the uptake of CO_2 has been increasing since 2003, caused by factors as the improved growth rate induced by a thinning operation (after snow damage) in 2002, and the recovery from the drought of 2003.

The tendency observed in the annual sums of CO_2-flux indicates that the site may be in a transition period after the disturbances described above. The proposed removal of unusually high values of CO_2-fluxes (with objective criteria) for the determination of annual sums should be also applied in future analysis, in order to capture changes in uptake rates. In this case the CO_2 balance for the Wetzstein site would be more comparable to similar ecosystems as Waldstein/Weidenbrunnen (Rebmann, 2004) and Tharandt (Bernhofer et al., 2003; Grünwald and Bernhofer, 2007).

Chapter 8

Zusammenfassung

Die mit der Kovarianzmethode gemessenen nächtlichen CO_2-Flüsse über einem Fichtenbestand am Wetzstein in Thüringen, Deutschland sind ungewöhnlich hoch (Anthoni et al., 2004). Die daraus resultierenden Jahressummen der CO_2-Flüsse sind deshalb nicht vergleichbar mit denen über vergleichbaren Ökosystemen (Rebmann, 2004; Grünwald and Bernhofer, 2007). Die Messstation befindet sich auf einem Berg, wo sie häufig starkem Wind und damit verbunden anhaltend hoher Turbulenz ausgesetzt ist.

Wie bereits von Anthoni et al. (2004) berichtet, können Bodenatmungsmessungen, die mit automatischen Kammern durchgeführt wurden, eine derartig hohe Ökosystematmung nicht erklären. Auch haben neuere Ergebnisse gezeigt, dass die Gesamtatmung des Ökosystems R_{eco} mit einem ähnlichen Fichtenbestand am Waldstein / Weidenbrunnen vergleichbar sein müsste (Rebmann, 2004).

Modellergebnisse von Finnigan and Belcher (2004) zeigten, dass Überströmungen von kleineren Bergen, wie dem Wetzstein zu Störungen des Windfeldes im Stammraum führen können. Daraus folgt, dass advektive Flüsse von skalaren Grössen, wie z.B. CO_2 luv- und leeseitig entstehen können. Zwei Modellergebnisse konnten zunächst experimentell bestätigt werden: erhöhte Windgeschwindigkeiten in Bodennähe am Hang im Vergleich zum Bergkamm und entgegengesetzte Strömungen über und unter dem Bestand im Lee.

Neben der Übereinstimmung des Windfeldes aus Messungen und Modellierungen, wurde durch Feigenwinter et al. (2007) in einem Advektionsexperiment (ADVEX) bestätigt, dass an der Messstation Wetzstein horizontale Advektion auftritt. Jedoch

ist das Vorzeichen der advektiven Flüsse im Mittel positiv, was bedeutet, dass CO_2 aus dem Kontrollvolumen hinaus transportiert wird. Dieses Ergebnis kann jedoch nicht direkt mit den hohen nächtlichen CO_2-Flüssen in Verbindung gebracht werden, da solche während des Experiments kaum auftraten. Trotzdem konnte gezeigt werden, dass entkoppelte Strömungen im Stammraum existieren, die weiter untersucht werden müssen.

Die Analyse verschiedener Cospektren des vertikalen CO_2-Flusses hat gezeigt, dass die Frequenzen, bzw. Zeitskalen, die den hohen nächtlichen Flüssen zugeordnet werden können im turbulenten Regime auftreten. Hohe Turbulenzaktivität bei neutralen atmosphärischen Bedingungen führt damit zu erhöhten turbulenten Flüssen von CO_2.

Die unerwartet hohen nächtliche CO_2-Flüsse konnten eindeutig bestimmten mikrometeorologischen Bedingen zugeordnet werden: hohe Werte der Schubspannungsgeschwindigkeit u*, Windrichtung aus Südwest oder Nordost und neutrale atmosphärische Schichtung. Diese Bedingungen wurden bei der Bestimmung von Jahressummen des Netto-Ökosystemaustauschs berücksichtigt, wobei die Zeitreihen mit parametrisierten Werten aufgefüllt wurden (Rebmann et al., in preparation). Damit ergeben sich höhere sich jährliche Kohlenstoffaufnahmen durch die Vegetation am Standort Wetzstein. In den Jahren 2003 bis 2005 hat die jährliche Netto-Kohlenstoffaufnahme stetig zugenommen, was einerseits durch erhöhte Wachstumsraten nach einer Durchforstung (nach Schneebruch) im Jahr 2002, jedoch auch auf eine Erholung des Bestandes nach der Dürre im Jahr 2003 zurückzuführen sein kann.

Die zunehmende Tendenz der Jahressummen des Netto-CO_2-Austauschs deutet eine mögliche Übergangsphase des Bestandes nach Störungen an. Die vorgeschlagene Entfernung unrealistisch hoher positiver CO_2-Flüsse mit objektiven Kriterien bei der Bestimmung von Jahressummen sollte auch in Zukunft angewandt werden, um mögliche Änderungen der Aufnahmeraten quantifizieren zu können. Damit wird die Vergleichbarkeit mit ähnlichen Ökosystemen wie z.B. Waldstein / Weidenbrunnen (Rebmann, 2004) oder Tharandt (Bernhofer et al., 2003; Grünwald and Bernhofer, 2007) besser gewährleistet sein.

References

Alvala, R. C. S., R. Gielow, H. R. da Rocha, H. C. Freitas, J. M. Lopes, A. O. Manzi, C. Von Randow, M. A. F. S. Dias, O. M. R. Cabral, and M. J. Waterloo. "Intradiurnal and seasonal variability of soil temperature, heat flux, soil moisture content, and thermal properties under forest and pasture in Rondonia." *Journal of Geophysical Research-Atmospheres* 107, D20: (2002) , doi:10.1029/2001JD000,599.

Anthoni, P. M., A. Knohl, C. Rebmann, A. Freibauer, M. Mund, W. Ziegler, O. Kolle, and E. D. Schulze. "Forest and agricultural land-use-dependent CO2 exchange in Thuringia, Germany." *Global Change Biology* 10, 12: (2004) 2005–2019.

Araujo, A. C., A. D. Nobre, B. Kruijt, J. A. Elbers, R. Dallarosa, P. Stefani, C. von Randow, A. O. Manzi, A. D. Culf, J. H. C. Gash, R. Valentini, and P. Kabat. "Comparative measurements of carbon dioxide fluxes from two nearby towers in a central Amazonian rainforest: The Manaus LBA site." *Journal of Geophysical Research-Atmospheres* 107, D20: (2002) , doi:10.1029/2001JD000,676.

Arya, S. P. *Introduction to Micrometeorology*. San Diego: Academic Press, 2001. 420 pp.

Aubinet, M., P. Berbigier, C. H. Bernhofer, A. Cescatti, C. Feigenwinter, A. Granier, T. H. Grünwald, K. Havrankova, B. Heinesch, B. Longdoz, B. Marcolla, L. Montagnani, and P. Sedlak. "Comparing CO2 storage and advection conditions at night at different carboeuroflux sites." *Boundary-Layer Meteorology* 116, 1: (2005) 63–94.

Aubinet, M., A. Grelle, A. Ibrom, U. Rannik, J. Moncrieff, T. Foken, A. S. Kowalski, P. H. Martin, P. Berbigier, C. Bernhofer, R. Clement, J. Elbers, A. Granier, T. Grünwald, K. Morgenstern, K. Pilegaard, C. Rebmann, W. Snijders, R. Valentini, and T. Vesala. "Estimates of the annual net carbon and water exchange of forests: The EUROFLUX methodology." *Advances in Ecological Research* 30: (2000) 113–175.

Aubinet, M., B. Heinesch, and M. Yernaux. "Horizontal and vertical CO2 advection in a sloping forest." *Boundary-Layer Meteorology* 108, 3: (2003) 397–417.

Baas, A. C. W. "Wavelet power spectra of aeolian sand transport by boundary layer turbulence." *Geophysical Research Letters* 33, L05403: (2006) , doi:10.1029/2005GL025,547.

Baldocchi, D. "Flux footprints within and over forest canopies." *Boundary-Layer Meteorology* 85, 2: (1997) 273–292.

Baldocchi, D., E. Falge, L. H. Gu, R. Olson, D. Hollinger, S. Running, P. Anthoni, C. Bernhofer, K. Davis, R. Evans, J. Fuentes, A. Goldstein, G. Katul, B. Law, X. H. Lee, Y. Malhi, T. Meyers, W. Munger, W. Oechel, K. T. P. U, K. Pilegaard, H. P. Schmid, R. Valentini, S. Verma, T. Vesala, K. Wilson, and S. Wofsy. "FLUXNET: A new tool to study the temporal and spatial variability of ecosystem-scale carbon dioxide, water vapor, and energy flux densities." *Bulletin of the American Meteorological Society* 82, 11: (2001) 2415–2434.

Baldocchi, D. D. "Assessing the eddy covariance technique for evaluating carbon dioxide exchange rates of ecosystems: past, present and future." *Global Change Biology* 9, 4: (2003) 479–492.

Bernhofer, C., M. Aubinet, R. Clement, A. Grelle, T. Grünwald, A. Ibrom, P. G. Jarvis, C. Rebmann, E.-D. Schulze, and J. D. Tenhunen. "Spruce forests (Norway and sitka spruce, including douglas fir): carbon and water fluxes and balances, ecological and ecophysiological determinants." In *Ecological Studies 163. Fluxes of Carbon, Water and Energy of European Forests*, edited by R. Valentini, Berlin: Springer Verlag, 2003, 99–123.

Cava, D., U. Giostra, M. Siqueira, and G. Katul. "Organised motion and radiative perturbations in the nocturnal canopy sublayer above an even-aged pine forest." *Boundary-Layer Meteorology* 112, 1: (2004) 129–157.

Chen, H., J. Chen, F. Hu, and Q. Zeng. "The Coherent Structure of Water Vapour Transfer in the Unstable Atmospheric Surface Layer." *Boundary-Layer Meteorology* 111, 3: (2004) 543–552.

Ciais, P., M. Reichstein, N. Viovy, A. Granier, J. Ogee, V. Allard, M. Aubinet, N. Buchmann, Chr. Bernhofer, A. Carrara, F. Chevallier, N. De Noblet, A. D. Friend, P. Friedlingstein, T. Grünwald, B. Heinesch, P. Keronen, A. Knohl, G. Krinner, D. Loustau, G. Manca, G. Matteucci, F. Miglietta, J. M. Ourcival, D. Papale, K. Pilegaard, S. Rambal, G. Seufert, J. F. Soussana, M. J. Sanz, E. D. Schulze, T. Vesala, and R. Valentini. "Europe-wide reduction in primary productivity caused by the heat and drought in 2003." *Nature* 437, 7058: (2005) 529–533.

Ciais, P., P. P. Tans, M. Trolier, J. W. C. White, and R. J. Francey. "A Large Northern-Hemisphere Terrestrial Co2 Sink Indicated by the C-13/C-12 Ratio of Atmospheric CO2." *Science* 269, 5227: (1995) 1098–1102.

Collineau, S., and Y. Brunet. "Detection of Turbulent Coherent Motions in a Forest Canopy. Part 2: Time-Scales and Conditional Averages." *Boundary-Layer Meteorology* 66, 1-2: (1993a) 49–73.

———. "Detection of turbulent coherent motions in a forest canopy. Part I: Wavelet Analisys." *Boundary-Layer Meteorology* 65, 4: (1993b) 357–379.

Cook, B. D., K. J. Davis, W. Wang, A. Desai, B. W. Berger, R. M. Teclaw, J. G. Martin, P. V. Bolstad, P. S. Bakwin, C. Yi, and W. Heilman. "Carbon exchange and venting anomalies in an upland deciduous forest in northern Wisconsin, USA." *Agricultural and Forest Meteorology* 126, 3-4: (2004) 271–295.

Cooper, D.I., M.Y. Leclerc, J. Archuleta, R. Coulter, W.E. Eichinger, C.Y.J. Kao, and C.J. Nappo. "Mass exchange in the stable boundary layer by coherent structures." *Agricultural and Forest Meteorology Advances in Surface-Atmosphere Exchange - A Tribute to Marv Wesely* 136, 3-4: (2006) 114–131.

Daubechies, I. *Ten lectures on wavelets*. Philadelphia, PA.: Society for Industrial and Applied Mathematics, 1992. 357 pp.

Druilhet, A., and P. Durand. "Experimental investigation of atmospheric boundary layer turbulence." *Atmospheric Research* 43, 4: (1997) 345–388.

DWD, Deutscher Wetterdienst. "Mean values for the period 1961 to 1990." http://www.dwd.de/en/FundE/Klima/KLIS/daten/online/nat/index_mittelwerte.htm.

Eugster, W., and W. Senn. "A Cospectral Correction Model for Measurement of Turbulent NO_2 Flux." *Boundary-Layer Meteorology* 74, 4: (1995) 321–340.

Falge, E., D. Baldocchi, R. Olson, P. Anthoni, M. Aubinet, C. Bernhofer, G. Burba, R. Ceulemans, R. Clement, H. Dolman, A. Granier, P. Gross, T. Grünwald, D. Hollinger, N. O. Jensen, G. Katul, P. Keronen, A. Kowalski, C. T. Lai, B. E. Law, T. Meyers, H. Moncrieff, E. Moors, J. W. Munger, K. Pilegaard, U. Rannik, C. Rebmann, A. Suyker, J. Tenhunen, K. Tu, S. Verma, T. Vesala, K. Wilson, and S. Wofsy. "Gap filling strategies for defensible annual sums of net ecosystem exchange." *Agricultural and Forest Meteorology* 107, 1: (2001) 43–69.

Farge, M. "The wavelet transform and its aplications to turbulence." *Annual Review of Fluid Mechanics* 24: (1992) 395–457.

Feigenwinter, C., C. Bernhofer, U. Eichelmann, B. Heinesch, M. Hertel, D. Janous, O. Kolle, F. Lagergren, A. Lindroth, S. Minerbi, U. Moderow, M. Mölder, L. Montagnani, R. Queck, C. Rebmann, P. Vestin, M. Yernaux, M. Zeri, W. Ziegler, and M. Aubinet. "The ADVEX advection field campaigns: Comparison of mean horizontal and vertical non turbulent advective fluxes at three CarboEurope forest sites." *Agricultural and Forest Meteorology – accepted*.

Feigenwinter, C., C. Bernhofer, and R. Vogt. "The Influence of Advection on the Short Term CO2-Budget in and Above a Forest Canopy." *Boundary-Layer Meteorology* 113, 2: (2004) 201–224.

Fink, A. H., T. Brucher, A. Kruger, G. C. Leckebusch, J. G. Pinto, and U. Ulbrich. "The 2003 European summer heatwaves and drought - synoptic diagnosis and impacts." *Weather* 59, 8: (2004) 209–216.

Finnigan, J. "A comment on the paper by Lee (1998): On micrometeorological observations of surface-air exchange over tall vegetation." *Agricultural and Forest Meteorology* 97, 1: (1999) 55–64.

———. "Turbulence in plant canopies." *Annual Review of Fluid Mechanics* 32: (2000) 519–571.

———. "The footprint concept in complex terrain." *Agricultural and Forest Meteorology* 127, 3-4: (2004) 117–129.

Finnigan, J., and S. E. Belcher. "Flow over a hill covered with a plant canopy." *Quarterly Journal of the Royal Meteorological Society* 130, 596: (2004) 1–29.

Foken, T. "50 years of the Monin-Obukhov similarity theory." *Boundary-Layer Meteorology* 119, 3: (2006) 431–447.

———. "The energy balance closure problem - An overview." *Ecological Applications* accepted.

Foken, T., M. Göckede, M. Mauder, L. Mahrt, B. D. Amiro, and J. W. Munger. "Post-field data quality control." In *Handbook of micrometeorology: a guide for surface flux measurement and analysis.*, edited by X. Lee, W. J. Massman, and B. Law, Dordrecht: Kluwer Academic Publishers, 2004, pp 181–208.

Foken, T., and M. Y. Leclerc. "Methods and limitations in validation of footprint models." *Agricultural and Forest Meteorology* 127, 3-4: (2004) 223–234.

Foken, T., and B. Wichura. "Tools for quality assessment of surface-based flux measurements." *Agricultural and Forest Meteorology* 78, 1-2: (1996) 83–105.

Foken, T., F. Wimmer, M. Mauder, C. Thomas, and C. Liebethal. "Some aspects of the energy balance closure problem." *Atmospheric Chemistry and Physics* 6: (2006) 4395–4402.

Froelich, N. J., H. P. Schmid, C. S. B. Grimmond, H. B. Su, and A. J. Oliphant. "Flow divergence and density flows above and below a deciduous forest. Part I. Non-zero mean vertical wind above canopy." *Agricultural and Forest Meteorology* 133, 1-4: (2005) 140–152.

Froelich, N.J., and H.P. Schmid. "Flow divergence and density flows above and below a deciduous forest: Part II. Below-canopy thermotopographic flows." *Agricultural and Forest Meteorology* 138, 1-4: (2006) 29–43.

Gao, W., and B. L. Li. "Wavelet Analysis of Coherent Structures at the Atmosphere Forest Interface." *Journal of Applied Meteorology* 32, 11: (1993) 1717–1725.

Garratt, J. R. *The atmospheric boundary layer*. Cambridge; New York: Cambridge University Press, 1992. 316 pp.

Göckede, M., T. Markkanen, C. B. Hasager, and T. Foken. "Update of a footprint-based approach for the characterisation of complex measurement sites." *Boundary-Layer Meteorology* 118, 3: (2006) 635–655.

Göckede, M., T. Markkanen, M. Mauder, K. Arnold, J. Leps, and T. Foken. "Validation of footprint models using natural tracer measurements from a field experiment." *Agricultural and Forest Meteorology* 135, 1-4: (2005) 314–325.

Göckede, M., C. Rebmann, and T. Foken. "A combination of quality assessment tools for eddy covariance measurements with footprint modelling for the characterisation of complex sites." *Agricultural and Forest Meteorology* 127, 3-4: (2004) 175–188.

Göckede, M., C. Thomas, T. Markkanen, M. Mauder, J. Ruppert, and T. Foken. "Sensitivity of Lagrangian Stochastic footprints to turbulence statistics." *Tellus B* 59, 3: (2007) 577–586.

Goulden, M. L., B. C. Daube, S. M. Fan, D. J. Sutton, A. Bazzaz, J. W. Munger, and S. C. Wofsy. "Physiological responses of a black spruce forest to weather." *Journal of Geophysical Research-Atmospheres* 102, D24: (1997) 28,987–28,996.

Goulden, M. L., J. W. Munger, S. M. Fan, B. C. Daube, and S. C. Wofsy. "Measurements of carbon sequestration by long-term eddy covariance: Methods and a critical evaluation of accuracy." *Global Change Biology* 2, 3: (1996) 169–182.

Granier, A., M. Reichstein, N. Breda, I.A. Janssens, E. Falge, P. Ciais, T. Grünwald, M. Aubinet, P. Berbigier, C. Bernhofer, N. Buchmann, O. Facini, G. Grassi, B. Heinesch, H. Ilvesniemi, P. Keronen, A. Knohl, B. Kostner, F. Lagergren, A. Lindroth, B. Longdoz, D. Loustau, J. Mateus, L. Montagnani, C. Nys, E. Moors, D. Papale, M. Peiffer, K. Pilegaard, G. Pita, J. Pumpanen, S. Rambal, C. Rebmann, A. Rodrigues, G. Seufert, J. Tenhunen, T. Vesala, and Q. Wang. "Evidence for soil water control on carbon and water dynamics in European forests during the extremely dry year: 2003." *Agricultural and Forest Meteorology* 143, 1-2: (2007) 123–145.

Grinsted, A., J. C. Moore, and S. Jevrejeva. "Application of the cross wavelet transform and wavelet coherence to geophysical time series." *Nonlinear Processes in Geophysics* 11, 5-6: (2004) 561–566.

Grünwald, T., and C. Bernhofer. "A decade of carbon, water and energy flux measurements of an old spruce forest at the Anchor Station Tharandt." *Tellus B* 59, 3: (2007) 387–396.

Gu, L. H., E. M. Falge, T. Boden, D. D. Baldocchi, T. A. Black, S. R. Saleska, T. Suni, S. B. Verma, T. Vesala, S. C. Wofsy, and L. K. Xu. "Objective threshold determination for nighttime eddy flux filtering." *Agricultural and Forest Meteorology* 128, 3-4: (2005) 179–197.

Hartmann, D. L. *Global Physical Climatology*. San Diego: Academic Press, 1994. 441 pp.

Hogstrom, U., J. C. R. Hunt, and A. S. Smedman. "Theory and measurements for turbulence spectra and variances in the atmospheric neutral surface layer." *Boundary-Layer Meteorology* 103, 1: (2002) 101–124.

Hsieh, C. I., G. Katul, and T. Chi. "An approximate analytical model for footprint estimation of scaler fluxes in thermally stratified atmospheric flows." *Advances in Water Resources* 23, 7: (2000) 765–772.

Hunt, J. C. R., S. Leibovich, and K. J. Richards. "Turbulent Shear Flows over Low Hills." *Quarterly Journal of the Royal Meteorological Society* 114, 484: (1988) 1435–1470.

IPCC. *Climate Change 2001: The Scientific Basis. Contribution of Working Group I to the Third Assessment Report of the Intergovernmental Panel on Climate Change*. Cambridge, United Kingdom and New York, NY, USA: Cambridge University Press, 2001. 881 pp.

Iwata, H., Y. Malhi, and C. Von Randow. "Gap-filling measurements of carbon dioxide storage in tropical rainforest canopy airspace." *Agricultural and Forest Meteorology* 132, 3-4: (2005) 305–314.

Kaimal, J. C., and J. J. Finnigan. *Atmospheric boundary layer flows : their structure and measurement*. New York: Oxford University Press, 1994. 289 pp.

Katul, G., J. Finnigan, D. Poggi, R. Leuning, and S. Belcher. "The Influence of Hilly Terrain on Canopy-Atmosphere Carbon Dioxide Exchange." *Boundary-Layer Meteorology* 118, 1: (2006) 189–216.

Katul, G. G., A. Porporato, E. Daly, A. C. Oishi, H. S. Kim, P. C. Stoy, J. Y. Juang, and M. B. Siqueira. "On the spectrum of soil moisture from hourly to interannual scales." *Water Resources Research* 43, W05428: (2007) , doi:10.1029/2006WR005,356.

Knohl, A., E. D. Schulze, O. Kolle, and N. Buchmann. "Large carbon uptake by an unmanaged 250-year-old deciduous forest in Central Germany." *Agricultural and Forest Meteorology* 118, 3-4: (2003) 151–167.

Koch, H. G. *Wetterheimatkunde von Thüringen*. Jena: VEB Gustav Fischer Verlag, 1953. 190 pp.

Kolle, O., and C. Rebmann. "Eddysoft - Documentation of a Software Package to Acquire and Process Eddy Covariance Data." Technical report, Technical Reports - Max-Planck-Institut für Biogeochemie 10, 2007.

Kowalski, A. "Comment on "An Alternative Approach for CO2 Flux Correction Caused by Heat and Water Vapour Transfer" by Liu." *Boundary-Layer Meteorology* 120, 2: (2006) 353–355.

Krusche, N., and A. P. De Oliveira. "Characterization of coherent structures in the atmospheric surface layer." *Boundary-Layer Meteorology* 110, 2: (2004) 191–211.

Kutsch, W., O. Kolle, C. Rebmann, A. Knohl, W. Ziegler, and E. D. Schulze. "Process modelling and direct measurements reveal uncertainties in flux measurements above a tall forest." *Ecological Applications* accepted.

Lee, X. "On micrometeorological observations of surface-air exchange over tall vegetation." *Agricultural and Forest Meteorology* 91, 1-2: (1998) 39–49.

———. "Reply to comment by Finnigan on On micrometeorological observations of surface-air exchange over tall vegetation." *Agricultural and Forest Meteorology* 97, 1: (1999) 65–67.

Lee, X., W. J. Massman, and B. E. Law. *Handbook of micrometeorology : a guide for surface flux measurement and analysis*. Atmospheric and oceanographic sciences library; v. 29. Dordrecht; Boston; London: Kluwer Academic, 2004. 250 pp.

Lee, X. H., and X. Z. Hu. "Forest-air fluxes of carbon, water and energy over non-flat terrain." *Boundary-Layer Meteorology* 103, 2: (2002) 277–301.

Leuning, R. "Measurements of trace gas fluxes in the atmosphere using the eddy covariance: WPL corrections revisited." In *Handbook of micrometeorology: a guide for surface flux measurement and analysis*, edited by X. Lee, W. J. Massman, and B. Law, Dordrecht: Kluwer Academic Publishers, 2004, pp. 119–132.

———. "The correct form of the Webb, Pearman and Leuning equation for eddy fluxes of trace gases in steady and non-steady state, horizontally homogeneous flows." *Boundary-Layer Meteorology* 123, 2: (2007) 263–267.

Liebethal, C., and T. Foken. "On the significance of the Webb correction to fluxes." *Boundary-Layer Meteorology* 109, 1: (2003) 99–106.

———. "On the significance of the Webb correction to fluxes. Corrigendum (vol 109, pg 99, 2003)." *Boundary-Layer Meteorology* 113, 2: (2004) 301–301.

Liu, H. P. "An alternative approach for CO2 flux correction caused by heat and water vapour transfer." *Boundary-Layer Meteorology* 115, 1: (2005) 151–168.

Lloyd, J., and J. A. Taylor. "On the Temperature-Dependence of Soil Respiration." *Functional Ecology* 8, 3: (1994) 315–323.

Mahrt, L. "Flux Sampling Errors for Aircraft and Towers." *Journal of Atmospheric and Oceanic Technology* 15, 2: (1998) 416–429.

Marcolla, B., A. Cescatti, L. Montagnani, G. Manca, G. Kerschbaumer, and S. Minerbi. "Importance of advection in the atmospheric CO2 exchanges of an alpine forest." *Agricultural and Forest Meteorology* 130, 3-4: (2005) 193–206.

Markkanen, T., U. Rannik, B. Marcolla, A. Cescatti, and T. Vesala. "Footprints and fetches for fluxes over forest canopies with varying structure and density." *Boundary-Layer Meteorology* 106, 3: (2003) 437–459.

Massman, W. J., and X. Lee. "Eddy covariance flux corrections and uncertainties in long-term studies of carbon and energy exchanges." *Agricultural and Forest Meteorology* 113, 1-4: (2002) 121–144.

Mauder, M., S. P. Oncley, R. Vogt, T. Weidinger, L. Ribeiro, C. Bernhofer, T. Foken, W. Kohsiek, H. A. R. DeBruin, and H. Liu. "The energy balance experiment EBEX-2000. Part II: Intercomparison of eddy-covariance sensors and post-field data processing methods." *Boundary-Layer Meteorology* 123, 1: (2007) 29–54.

McNaughton, K. G., and Y. Brunet. "Townsend's hypothesis, coherent structures and Monin-Obukhov similarity." *Boundary-Layer Meteorology* 102, 2: (2002) 161–175.

Moeng, C. H., and P. P. Sullivan. "A Comparison of Shear-Driven and Buoyancy-Driven Planetary Boundary-Layer Flows." *Journal of the Atmospheric Sciences* 51, 7: (1994) 999–1022.

van der Molen, M. K., J. H. C. Gash, and J. A. Elbers. "Sonic anemometer (co)sine response and flux measurement - II. The effect of introducing an angle of attack dependent calibration." *Agricultural and Forest Meteorology* 122, 1-2: (2004) 95–109.

Moncrieff, J. B., J. M. Massheder, H. deBruin, J. Elbers, T. Friborg, B. Heusinkveld, P. Kabat, S. Scott, H. Soegaard, and A. Verhoef. "A system to measure surface fluxes of momentum, sensible heat, water vapour and carbon dioxide." *Journal of Hydrology* 189, 1-4: (1997) 589–611.

Oncley, S. P., T. Foken, R. Vogt, W. Kohsiek, H. A. R. DeBruin, C. Bernhofer, A. Christen, E. Gorsel, D. Grantz, C. Feigenwinter, I. Lehner, C. Liebethal, H. Liu, M. Mauder, A. Pitacco, L. Ribeiro, and T. Weidinger. "The Energy Balance Experiment EBEX-2000. Part I: overview and energy balance." *Boundary-Layer Meteorology* 123, 1: (2007) 1–28.

Panofsky, H. A. "Spectra of Atmospheric Variables in Boundary Layer." *Radio Science* 4, 12: (1969) 1101–1109.

Panofsky, H. A., and J. A. Dutton. *Atmospheric turbulence: models and methods for engineering applications*. New York: Wiley, 1984. 397 pp.

Paw U, K. T., D. D. Baldocchi, T. P. Meyers, and K. B. Wilson. "Correction of eddy-covariance measurements incorporating both advective effects and density fluxes." *Boundary-Layer Meteorology* 97, 3: (2000) 487–511.

Raupach, M. R., and J. J. Finnigan. "The influence of topography on meteorological variables and surface-atmosphere interactions." *Journal of Hydrology* 190, 3-4: (1997) 182–213.

Raupach, M. R., J. J. Finnigan, and Y. Brunet. "Coherent eddies and turbulence in vegetation canopies: The mixing-layer analogy." *Boundary-Layer Meteorology* 78, 3-4: (1996) 351–382.

Raupach, M. R., and A. S. Thom. "Turbulence in and above Plant Canopies." *Annual Review of Fluid Mechanics* 13: (1981) 97–129.

Rebmann, C. *Kohlendioxid-, Wasserdampf- und Energieaustausch eines Fichtenwaldes in Mittelgebirgslage in Nordostbayern*, volume 106. Bayreuther Forum Ökologie, 2004.

Rebmann, C., P. Anthoni, E. Falge, M. Göckede, A. Mangold, J-A Subke, C. Thomas, B. Wichura, E-D. Schulze, J. D. Tenhunen, and T. Foken. "Carbon budget of a spruce forest ecosystem." In *Biogeochemistry of forested catchments in a changing environment: a German case study*, edited by E. Matzner, Berlin: Springer Verlag, 2004, volume 172 of *Ecological Studies*, 143–160.

Rebmann, C., M. Göckede, T. Foken, M. Aubinet, M. Aurela, P. Berbigier, C. Bernhofer, N. Buchmann, A. Carrara, A. Cescatti, R. Ceulemans, R. Clement, J. A. Elbers, A. Granier, T. Grünwald, D. Guyon, K. Havrankova, B. Heinesch, A. Knohl, T. Laurila, B. Longdoz, B. Marcolla, T. Markkanen, F. Miglietta, J. Moncrieff, L. Montagnani, E. Moors, M. Nardino, J. M. Ourcival, S. Rambal, U. Rannik, E. Rotenberg, P. Sedlak, G. Unterhuber, T. Vesala, and D. Yakir. "Quality analysis applied on eddy covariance measurements at complex forest sites using footprint modelling." *Theoretical and Applied Climatology* 80, 2-4: (2005) 121–141.

Rebmann, C., M. Zeri, O. Kolle, W. Kutsch, C. Wirth, and E. D. Schulze. "Meso-scale transport processes of CO2 at a complex site in Thuringia - Germany." *in preparation* .

Reichstein, M., E. Falge, D. Baldocchi, D. Papale, M. Aubinet, P. Berbigier, C. Bernhofer, N. Buchmann, T. Gilmanov, A. Granier, T. Grünwald, K. Havrankova, H. Ilvesniemi,

D. Janous, A. Knohl, T. Laurila, A. Lohila, D. Loustau, G. Matteucci, T. Meyers, F Miglietta, J-M. Ourcival, J. Pumpanen, S. Rambal, E. Rotenberg, M. Sanz, J. Tenhunen, G. Seufert, F. Vaccari, T. Vesala, D. Yakir, and R. Valentini. "On the separation of net ecosystem exchange into assimilation and ecosystem respiration: review and improved algorithm." *Global Change Biology* 11, 9: (2005) 1424–1439.

Ruppert, J., M. Mauder, C. Thomas, and J. Luers. "Innovative gap-filling strategy for annual sums of CO2 net ecosystem exchange." *Agricultural and Forest Meteorology* 138, 1-4: (2006) 5–18.

Saito, M., J. Asanuma, and A. Miyata. "Dual-scale transport of sensible heat and water vapor over a short canopy under unstable conditions." *Water Resources Research* 43, W05413: (2007) , doi:10.1029/2006WR005,136.

Sakai, R. K., D. R. Fitzjarrald, and K. E. Moore. "Importance of low-frequency contributions to eddy fluxes observed over rough surfaces." *Journal of Applied Meteorology* 40, 12: (2001) 2178–2192.

Schmid, H. P. "Experimental design for flux measurements: matching scales of observations and fluxes." *Agricultural and Forest Meteorology* 87, 2-3: (1997) 179–200.

Schotanus, P., F. T. M. Nieuwstadt, and H. A. R. Debruin. "Temperature-Measurement with a Sonic Anemometer and Its Application to Heat and Moisture Fluxes." *Boundary-Layer Meteorology* 26, 1: (1983) 81–93.

Schulze, E. D. "Carbon-Dioxide and Water-Vapor Exchange in Response to Drought in the Atmosphere and in the Soil." *Annual Review of Plant Physiology and Plant Molecular Biology* 37: (1986) 247–274.

Schulze, E. D., C. Wirth, and M. Heimann. "Climate change - managing forests after Kyoto." *Science* 289, 5487: (2000) 2058–2059.

Shaw, R.H., and X.J Zhang. "Evidence of pressure-forced turbulent flow in a forest." *Boundary-Layer Meteorology* 58: (1992) 273–288.

Solomon, S., D. Qin, M. Manning, R. B. Alley, T. Berntsen, N. L. Bindoff, Z. Chen, A. Chidthaisong, J. M. Gregory, G. C. Hegerl, M. Heimann, B. Hewitson, B. J. Hoskins, F. Joos, J. Jouzel, V. Kattsov, U. Lohmann, T. Matsuno, M. Molina, N. Nicholls, J. Overpeck, G. Raga, V. Ramaswamy, J. Ren, M. Rusticucci, R. Somerville, T. F. Stocker, P. Whetton, R. A. Wood, and D. Wratt. "Technical Summary." In *Climate Change 2007: The Physical Science Basis. Contribution of Working Group I to the Fourth Assessment Report of the Intergovernmental Panel on Climate Change*,

edited by S. Solomon, D. Qin, M. Manning, Z. Chen, M. Marquis, K. B. Averyt, M. Tignor, and H. L. Miller, Cambridge, United Kingdom and New York, NY, USA: Cambridge University Press, 2007.

Staebler, R. M., and D. R. Fitzjarrald. "Observing subcanopy CO2 advection." *Agricultural and Forest Meteorology* 122, 3-4: (2004) 139–156.

Stull, R. B. *An Introduction to Boundary Layer Meteorology*. Dordrecht, Boston, London: Kluwer Academic Publishers, 1988. 666 pp.

Sun, H., T. L. Clark, R. B. Stull, and T. A. Black. "Two-dimensional simulation of airflow and carbon dioxide transport over a forested mountain: Part I: Interactions between thermally-forced circulations." *Agricultural and Forest Meteorology* 140, 1-4: (2006a) 338–351.

———. "Two-dimensional simulation of airflow and carbon dioxide transport over a forested mountain: Part II. Carbon dioxide budget analysis and advection effects." *Agricultural and Forest Meteorology* 140, 1-4: (2006b) 352–364.

Sun, J. L., J. F. Howell, S. K. Esbensen, L. Mahrt, C. M. Greb, R. Grossman, and M. A. LeMone. "Scale dependence of air-sea fluxes over the Western Equatorial Pacific." *Journal of the Atmospheric Sciences* 53, 21: (1996) 2997–3012.

Sun, X-M., Z-L. Zhu, X-F. Wen, G-F. Yuan, and G-R. Yu. "The impact of averaging period on eddy fluxes observed at ChinaFLUX sites." *Agricultural and Forest Meteorology - Carbon Exchange Research in ChinaFLUX* 137, 3-4: (2006c) 188–193.

Thomas, C., and T. Foken. "Detection of long-term coherent exchange over spruce forest using wavelet analysis." *Theoretical and Applied Climatology* 80, 2-4: (2005) 91–104.

———. "Flux contribution of coherent structures and its implications for the exchange of energy and matter in a tall spruce canopy." *Boundary-Layer Meteorology* 123, 2: (2007a) 317–337.

———. "Organised Motion in a Tall Spruce Canopy: Temporal Scales, Structure Spacing and Terrain Effects." *Boundary-Layer Meteorology* 122, 1: (2007b) 123–147.

Thomas, C., J.-C. Mayer, F. Meixner, and T. Foken. "Analysis of Low-Frequency Turbulence Above Tall Vegetation Using a Doppler Sodar." *Boundary-Layer Meteorology* 119, 3: (2006) 563–587.

Torrence, C., and G. P. Compo. "A practical guide to wavelet analysis." *Bulletin of the American Meteorological Society* 79, 1: (1998) 61–78.

Trebs, I., L. L. Lara, L. M. M. Zeri, L. V. Gatti, P. Artaxo, R. Dlugi, J. Slanina, M. O. Andreae, and F. X. Meixner. "Dry and wet deposition of inorganic nitrogen compounds to a tropical pasture site (Rondonia, Brazil)." *Atmospheric Chemistry and Physics* 6, 2: (2006) 447–469.

Turnipseed, A. A., D. E. Anderson, P. D. Blanken, W. M. Baugh, and R. K. Monson. "Airflows and turbulent flux measurements in mountainous terrain Part 1. Canopy and local effects." *Agricultural and Forest Meteorology* 119, 1-2: (2003) 1–21.

Turnipseed, A. A., D. E. Anderson, S. Burns, P. D. Blanken, and R. K. Monson. "Airflows and turbulent flux measurements in mountainous terrain: Part 2: Mesoscale effects." *Agricultural and Forest Meteorology* 125, 3-4: (2004) 187–205.

Vickers, D., and L. Mahrt. "Quality control and flux sampling problems for tower and aircraft data." *Journal of Atmospheric and Oceanic Technology* 14, 3: (1997) 512–526.

———. "The cospectral gap and turbulent flux calculations." *Journal of Atmospheric and Oceanic Technology* 20, 5: (2003) 660–672.

———. "Contrasting mean vertical motion from tilt correction methods and mass continuity." *Agricultural and Forest Meteorology* 138, 1-4: (2006) 93–103.

Von Randow, C., L. D. A. Sa, P. S. S. D. Gannabathula, A. O. Manzi, P. R. A. Arlino, and B. Kruijt. "Scale variability of atmospheric surface layer fluxes of energy and carbon over a tropical rain forest in southwest Amazonia - 1. Diurnal conditions." *Journal of Geophysical Research-Atmospheres* 107, D20: (2002) , doi:10.1029/2001JD000,379.

Webb, E. K., G. I. Pearman, and R. Leuning. "Correction of Flux Measurements for Density Effects Due to Heat and Water-Vapor Transfer." *Quarterly Journal of the Royal Meteorological Society* 106, 447: (1980) 85–100.

Wilczak, J. M., S. P. Oncley, and S. A. Stage. "Sonic anemometer tilt correction algorithms." *Boundary-Layer Meteorology* 99, 1: (2001) 127–150.

Wilks, D. S. *Statistical methods in the atmospheric sciences : an introduction*. International geophysics series; v. 59. San Diego: Academic Press, 1995. 467 pp.

Wilson, K., A. Goldstein, E. Falge, M. Aubinet, D. Baldocchi, P. Berbigier, C. Bernhofer, R. Ceulemans, H. Dolman, C. Field, A. Grelle, A. Ibrom, B. E. Law, A. Kowalski, T. Meyers, J. Moncrieff, R. Monson, W. Oechel, J. Tenhunen, R. Valentini, and

S. Verma. "Energy balance closure at FLUXNET sites." *Agricultural and Forest Meteorology* 113, 1-4: (2002) 223–243.

Wohlfahrt, G., C. Anfang, M. Bahn, A. Haslwanter, C. Newesely, M. Schmitt, M. Drosler, J. Pfadenhauer, and A. Cernusca. "Quantifying nighttime ecosystem respiration of a meadow using eddy covariance, chambers and modelling." *Agricultural and Forest Meteorology* 128, 3-4: (2005) 141–162.

Zeri, L. M. M. *Estudo comparativo da estrutura da turbulência atmosférica na camada limite superficial acima do Pantanal Matogrossensse nos períodos úmido e seco*. Master's degree, Instituto Nacional de Pesquisas Espaciais, São José dos Campos, SP, Brazil, 2002.

Zhang, G., C. Thomas, M. Y. Leclerc, A. Karipot, H. L. Gholz, M. Binford, and T. Foken. "On the effect of clearcuts on turbulence structure above a forest canopy." *Theoretical and Applied Climatology* 88, 1: (2007) 133–137.

List of Symbols

ρ_c	Concentrantion of a scalar *c* [mol$^{3-1}$m]
σ_w	Vertical velocity standard deviation [ms^{-1}]
τ	Vertical flux of momentum [kgm^{-1}s^{-2}]
θ	Wind direction [°]
ξ	Stability parameter z/L, where L is the Obukhov lenght
e	Vapor pressure [hPa]
e_{sat}	Saturation vapor pressure [hPa]
F_c	Vertical flux of a scalar *c* [molm^{-2}s^{-1}]
R_{eco}	Total ecosystem respiration [µmolm^{-2}s^{-1}]
R_e	Soil respiration [µmolm^{-2}s^{-1}]
R_{net}	Net radiation [Wm^{-2}]
T_s	Air temperature provided by the sonic anemometer [°C]
T_{air}	Air temperature [°C]
T_{soil}	Soil temperature [°C]
w	Vertical velocity [ms^{-1}]
ABL	Atmospheric Boundary Layer
ASL	Atmospheric Surface Layer
F_C	CO_2-flux [µmolm^{-2}s^{-1}]
Fc_H	Horizontal advection of CO_2 [µmolm^{-2}s^{-1}]

H	Sensible heat flux [Wm^{-2}]
IRGA	Infra-red gas analyzer
L↓	Longwave incident radiation [Wm^{-2}]
L↑	Longwave radiation emitted by the surface [Wm^{-2}]
NEE	Net CO_2 ecosystem exchange [$\mu molm^{-2}s^{-1}$]
S↓	Shortwave incident radiation [Wm^{-2}]
S↑	Shortwave reflected radiation [Wm^{-2}]
U_{30}	Wind speed at 30 m, at the main tower [ms^{-1}]
U_{SW}	Southwest component of wind velocity [ms^{-1}]
u*	Friction velocity [ms^{-1}]

Appendix A

Additional meteorological variables

Time series of soil temperature, snow cover, soil moisture, and precipitation from 2003 to 2006 are described next. The evolution of such variables helped in the characterization of the weather conditions at the site.

Soil Temperature

Soil temperature (T_s) influences several biological processes as soil respiration and seed germination. T_s is used to model the soil or ecosystem respiration in non-turbulent nights when eddy covariance fluxes are rejected (Lloyd and Taylor, 1994; Baldocchi, 2003; Gu et al., 2005; Iwata et al., 2005). The rejected nocturnal fluxes are then replaced by modeled values of respiration if annual sums of CO_2-fluxes are calculated. T_s was measured at the Wetzstein site at 2, 4, 8, 16, 32, and 64 cm depth; the annual courses from 2003 to 2006, for the 16 cm depth, are shown in Figure A.1.

A rough estimative of the snow cover is presented in the same figure, related to the right axis. Measurements of snow heights were carried out weekly close to the tower. Daily values were obtained interpolating the weekly measurements, using the day-to-day mean air temperature and precipitation in the interpolation procedure (C. Rebmann, personal communication). Despite the apparent similar annual courses of T_s in Figure A.1, some differences were found:

the variability between March and April: The soil at 16 cm in March of 2004 was on average 0.85 °C warmer than in 2003. Such difference is explained by the

insulation effect caused by the snow cover (Hartmann, 1994): in March of 2003 the layer of snow was shallower and lasted for a shorter period, reducing the insulation effect and keeping the soil cooler than the same period in 2004; in March of 2005 the snow cover lasted for a longer period and kept T_s slightly lower (≈ 0.2 °C) than in 2004.

Additionally, the standard deviation of T_s in March of 2004 was the highest in comparison with 2003, 2005, and 2006 (Table A.1), caused by a sharp increase in temperature and snow melting (reaching 3.6 °C in March 21st, 2004). T_s was almost constant during March and the first half of April in 2006, a rather different variability in comparison with the 3 previous years. However, the period of time at which the temperature reaches 5 °C was approximately the same in the four years compared (the second half of April).

the variability in November 2003: T_s in November of 2003 did not decrease steadily as in 2004 and 2005. This may be explained by the higher T_{air} in the period (Figure 2.7), which kept the soil warmer. The decline in T_s occurred one month later, in December of 2003, when T_{air} also dropped. For November of 2006 T_s remained constant on average, with a similar variability as T_{air}.

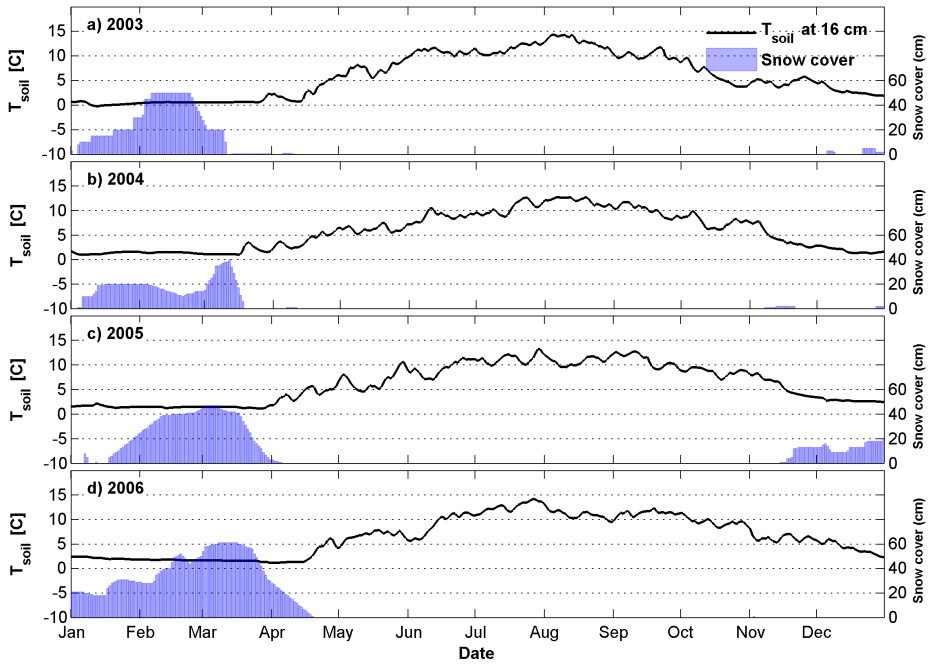

Figure A.1: Soil temperature at 16 cm and snow cover between 2003 and 2006.

Although some differences in T_s were significant between the years compared, they did not explain the occurrence of high nocturnal fluxes of CO_2. The screening of periods

with high nighttime values of NEE was performed for 2003, 2004, and 2006 (results not shown) as well as for 2005 (described in Section 5.5). The occurrence of high values for NEE was similar for all years analyzed. Such high fluxes were associated with the interaction between the weather and the local topography. The disturbance in the flow induced by the hill and intense turbulent transports were the main cause of high fluxes of CO_2 at nighttime (Chapters 3, 4, and 5.5).

Table A.1: Averages of T_s between 2003 and 2006. Units in °C; standard deviations in parenthesis.

	2003	2004	2005	2006
$\overline{T}_{soil}$	5.92 (4.52)	5.81 (3.87)	6.24 (3.89)	6.58 (4.02)
$\overline{T}_{soil}$ (March)	0.75 (0.44)	1.62 (0.75)	1.4 (0.14)	1.56 (0.13)
$\overline{T}_{soil}$ (Jun - Aug)	11.76 (1.25)	10.40 (1.62)	10.42 (1.38)	10.90 (2.03)

Soil Moisture

Soil moisture quantifies the amount of water within a column in an unsaturated soil. It is important for vegetation growth, microbial activity, and transport of nutrients to the roots. The moisture contained in the soil evaporates to the atmosphere and is also transpired by the vegetation (Schulze, 1986; Alvala et al., 2002; Katul et al., 2007).

Time series composed of daily averages of soil moisture at 64 cm depth, from 2003 to 2006, are plotted in Figure A.2. Daily sums of precipitation are plotted in the same figures, related to the right vertical axis. Until 2006, the lowest value for the daily mean of soil moisture was registered in 2003, as a result of the drought that occurred in this year (Ciais et al., 2005; Granier et al., 2007). This low value occurred in the middle of September, when the soil moisture was less than 20 %.

However, two events with even lower values were registered in 2006 (Figure A.2-d). From the four years compared, 2006 presented the most distinct pattern between June and October. During this period soil moisture dropped rapidly to the lowest values in the years analyzed ($\approx$ 15 %), rising quickly after strong rain events.

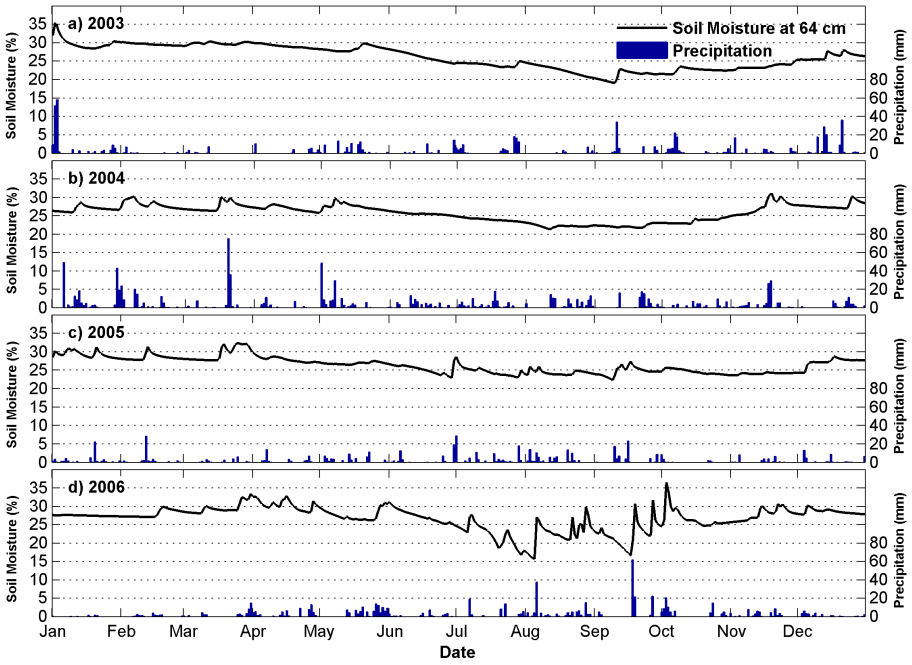

Figure A.2: Soil moisture at 16 cm depth and precipitation from 2003 to 2006.

The soil moisture was on average slightly higher in August of 2005 than in the two previous years. However, such difference did not influenced the occurrence of unusual nocturnal fluxes of CO_2. The frequency of occurrence of such high fluxes was similar between the years analyzed, for weather conditions comparable to the ones described in Section 5.5.

Erklärung

Hiermit erkläre ich eidesstattlich, dass ich die vorliegende Arbeit selbständig angerfertigt habe. Die aus fremden Quellen direkt oder indirekt übernommenen Gedanken sind als solche kenntlich gemacht. Die Arbeit wurde bisher keiner anderen Prüfungsbehörde vorgelegt und auch nicht veröffentlicht. Ich bin mir bewusst, dass eine unwahre Erklärung rechtliche Folgen haben kann.

Jena, October 17, 2007 Luis Marcelo de Mattos Zeri

Statutory Declaration

I confirm by oath that I have prepared the thesis autonomously. All thoughts of other authors which have been adopted directly or indirectly are explicitly cited. The thesis has not been submitted to another examination authority and it is not published. I am aware that a false declaration will have legal consequences.

Jena, October 17, 2007 Luis Marcelo de Mattos Zeri